CONTRIBUTIONS TO THE EXPERIMENTAL STUDY OF THE G-FACTOR ANOMALY OF FREE ELECTRONS

Thesis

submitted by

ALASTAIR G.A. RAE, B.Sc. (Edinburgh)

for the degree of

DOCTOR OF PHILOSOPHY

UNIVERSITY OF EDINBURGH,

May, 1962.

TABLE OF CONTENTS

TABLE OF CONTENTS (Contd.)

CHAPTER I

HISTORICAL INTRODUCTION

(I.1) Inadequacy of the Dirac Theory of the Electron

As early as 1934 it had been suggested by Houston and Hsieh that Dirac's relativistic electron theory did not give a completely satisfactory account of the fine-structure of the spectrum of atomic hydrogen. The measurements of R.C. Williams (1938) on the fine-structure of the H_α line indicated that the component associated with the transition $3^2p_{\frac{1}{2}} \longrightarrow 2^2s_{\frac{1}{2}}$ was not in the predicted position relative to the other components. The alleged discrepancy was, however, on the limit of the precision then attainable in optical spectroscopy and its existence was not generally admitted by the spectroscopists.

With the development of microwave techniques direct measurement became possible of the splitting of sublevels belonging to the same principal quantum number, n. It was shown by Lamb and Retherford (1947, 1950, 1951, 1952) that their observations of the $2^2s_{\frac{1}{2}} - 2^2p_{\frac{1}{2}}$ and $2^2s_{\frac{1}{2}} - 2^2p_{\frac{3}{2}}$ intervals in atomic hydrogen implied an upward shift of the $2^2s_{\frac{1}{2}}$ level relative to the p levels of about 1060 Mc/s ($0.035\ cm^{-1}$). In Dirac theory the first interval is actually zero, of course. Quantitatively, these measurements confirmed the observations of Williams mentioned

above. The subsequent experimental studies of the spectra of hydrogen, deuterium, tritium and singly-ionised helium by the techniques of both optical and radio-frequency spectroscopy have been discussed in detail by Series (1957). It has been found that s-levels are shifted, while p, d, etc., levels are unaffected.

Bethe (1947) was the first to give a theoretical account of the phenomenon leading to a quantitative agreement with the observation of Lamb and Retherford. Although there is a small contribution arising from other causes (e.g. vacuum polarisation), the anomaly is associated mainly with the electron's self-energy. Bethe's calculation took account only of the latter contribution. A full account would be out of place here. Suffice it to say that the calculation was based on the concept of the self-energy as arising from the interaction between the electron charge and the so-called zero-point fluctuations of the electromagnetic field in the surrounding vacuum, and that it involved the subtraction of two divergent integrals representing the self-energies of a bound and a free electron respectively. This technique, as we shall see, was to become an essential feature of the later, more elaborate theories of quantum electrodynamics. Anticipating for a moment the discussion of section (I.2) we note that these theories lead to the idea of "renormalisation" of mass and of charge. That is, in the case of mass, the observed mass

of the electron is supposed to be made up of a "bare mass" together with a divergent contribution from the self-energy.

Now the Dirac theory of the electron makes use of parameters e and M which are of the nature of a "bare charge" and "bare mass", respectively, and it cannot be expected to describe accurately the motion of a real electron, even when the observed values e_o and M_o are used for e and M. This neglect of the effects of the electron's own field on its motion was the reason for the discrepancy between the predictions of Dirac's theory and the results of the experiments referred to above.

(I.2) Quantum Electrodynamic Effects and the g-factor Anomaly

Calculations of the effects on the electron's motion of its own field have been attempted from the earliest days of electron theory. For a point electron in classical theory, however, these effects turn out to be of infinite magnitude. The difficulty could, of course, be avoided by assuming a finite radius for the electron. Such a model is no longer feasible in quantum electrodynamics and indeed in the quantum-theoretic approach the infinities were, at first sight, all-pervasive. One may see already in certain classical relativistic considerations a hint of the approach by means of which these infinities have been eliminated in a self-consistent way, at least in the case of electrodynamics. Classically, if one assumes that the electronic charge is distributed uniformly over the surface of a sphere of radius R, the self-energy of the electrostatic field of the "particle" is $e^2/2R$ (see, for example, Panofsky and Phillips, 1955). This would appear as a contribution to the observed mass. It cannot constitute the whole mass of the electron since this would lead to difficulties when we consider a moving electron. In this case the field possesses momentum as well as energy and the total momentum and total energy of an electromagnetic field transform together like a four-vector under a Lorentz-transformation only if there are no sources present. On the other hand the total energy

(electromagnetic and other) and the total momentum (electromagnetic and other) of a particle (charged or not) together transform like a four-vector. One should, therefore, think of the observed mass, M_o, as made up of two parts, a "bare mass", M, of unknown origin and a contribution, δM, from the interaction of the charge with its own field, such that

$$M_o = M + \delta M ,$$

On this view neither M nor δM need be finite provided that they are separately unobservable.

These hints have been elaborated and systematised in the extensive development of quantum electrodynamics associated principally with the names of Schwinger, Feynman and Dyson, which followed on the experiment of Lamb and Retherford and the work of Bethe. According to this formalism, not only must the mass be "renormalised", as indicated above, but so also must the charge. Thus the observed charge e_o of the electron is to be written

$$e_o = e(1 + A)$$

where e is a "bare charge" and A a (divergent) contribution whose origin actually lies not only in the properties of the electron itself but also in those of the vacuum surrounding it (the "vacuum polarisation").

The achievement of the more recent theory of quantum electrodynamics has been two-fold. First, it describes the various possible modes of interaction of the electron

and photon fields in the language of scattering theory in a way which makes their relativistic transformation properties explicit and by so doing is able to separate out the matrix-elements for each possible type of scattering of one field by another in a relativistically covariant way. Second, when this programme is carried through, it is found that the divergences occur only in certain of the terms in the matrix-elements, and it is possible to interpret these in a completely consistent way as contributions to the mass and charge of the electron, and thus to eliminate them from the expressions for the transition matrix-elements. The remaining terms turn out to be finite and they can be evaluated by substituting the observed values of charge and mass for the "bare" charge and mass wherever these occur. The whole treatment depends on being able to write down the scattering matrix-elements in an expansion of the type characteristic of perturbation theory. If, further, it is desired to evaluate the theory for comparison with experiment it is obviously necessary that the expansion converge. The theory leads naturally to an expansion in powers of the square of the coupling constant, g, and for electrodynamics, where $g^2 = \alpha \simeq 1/137$, this quantity is much less than unity, so that in practice the expansion converges rather rapidly, at least in the sense that the magnitudes of successive terms decrease rapidly over the first few

terms, the ones of practical interest.

As examples of the kinds of term which crop up we shall consider briefly the scattering of an electron by an external electromagnetic field represented by the four-potential A_μ^{ext}. This might represent the Coulomb field of the nucleus in the case of the hydrogen atom. The zero-order approximation to the matrix-element gives the Dirac results. The second-order (in e) and higher terms (after renormalisation) represent small corrections to these results, of the type observed by Lamb and Retherford. The complexity of the virtual processes contributing to each term increases very rapidly with increasing order of the term and, since the second order term always turns out to be much larger than any other, we shall consider it alone. It is convenient to represent each type of virtual process contributing to a term by a Feynman diagram. There are three types of process leading to observable effects in second order, represented by the four graphs of Fig. (I.2.1). Graphs (a) and (b) represent a process which may be thought of as the emission and subsequent reabsorption of a virtual photon. This process is associated with the self-energy of the electron and leads to a mass and charge renormalisation. Graph (c) represents the creation and subsequent annihilation of virtual electron-positron pairs in the vacuum. Polarisation of these charged pairs by the external field

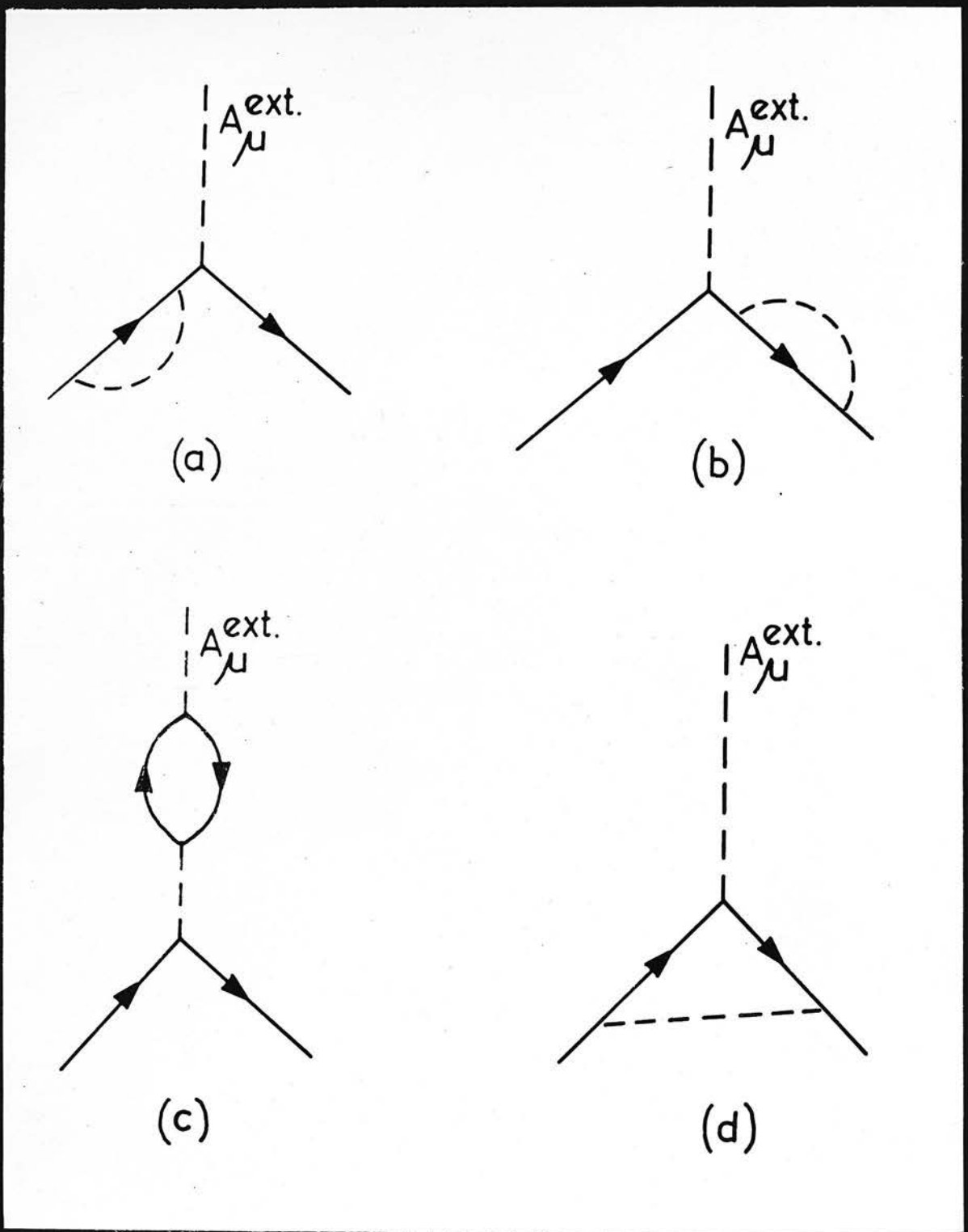

FIG. (I.2.1) Feynman Graphs for second order radiative corrections to Coulomb scattering.

A_μ^{ext} leads to a contribution to the second order term and to a renormalisation of charge. This process is often referred to as the vacuum polarisation. Finally graph (d) represents a process whereby a virtual photon is emitted, the electron is scattered by the external field and the virtual photon is reabsorbed. This is known as a vertex modification and leads to a charge renormalisation. Graph (d) also contributes to the second-order correction to the scattering in a way which will be explained in more detail below.

The phenomenon of the Lamb-shift, where the external field is the Coulomb field of the nucleus, seems to constitute the most comprehensive single test of the theory at present (though certainly not the only test). This is illustrated in Table (I.1).

The Lamb-shift corrections apply to a bound electron but radiative effects are also predicted for a so-called "free electron" in interaction with an external field. By the term "free" is meant, of course, that the electron in question is in a continuous-energy state under the influence of the external field. The radiative effects in this case manifest themselves as a correction, of order $\alpha \simeq 1/137$, to the Dirac magnetic moment of the electron. The correction is often expressed in terms of the free-electron g-factor, when it is known as the g-factor anomaly.

TABLE I.1

Radiative Corrections to $\Delta E(2s - 2p_{\frac{1}{2}})$ in Hydrogen (Lamb-shift)

Order of Term	Graphs	Contribution to Lamb-shift (Mc./sec.)*	Experiment** (Mc./sec.)
2nd	(a) + (b)	1011.45	
	(c)	-27.13	
	(d)	67.82	
4th + proton mass, etc., corrections	All	5.89	
		Total: 1058.03	1057.77 ± 0.10

* Bethe and Salpeter, 1958.

** Dayhoff, Triebwasser and Lamb, 1953.

The g-factor, introduced by Landé (1923), may be defined as the ratio of the magnetic moment in units of the Bohr magneton to the angular momentum in units of $\hbar$. Thus, for a free Dirac electron,

$$g = 2.$$

A small modification is introduced through the value of the magnetic moment, the theoretical expression for which is

$$\mu = \mu_o \left[1 + \alpha/2\pi + C.(\alpha/\pi)^2 + ...\right]$$

where μ and μ_o are, respectively, the observed and the Dirac values of the free-electron magnetic moment and C is a numerical constant. This leads to

$$g/2 - 1 = \alpha/2\pi + C(\alpha/\pi)^2 + ...$$

which is the g-factor anomaly. The factor C was originally calculated to be -2.973 (Karplus and Kroll, 1950) but was later recalculated (Sommerfield, 1957, 1958) and is now believed to be -0.328 (Petermann, 1958). To the accuracy to which the fine-structure constant is known, (Cohen and Dumond, 1958) the g-factor anomaly for the free electron is therefore predicted to be

$$(g/2) - 1 = 0.00115961(4) \quad \text{(to fourth order)}.$$
$$\pm\ 0.000000004$$

It should be remarked that the term $C(\alpha/\pi)^2$ is a fourth-order term and it amounts to slightly less than 0.2% of the g-factor anomaly. It is interesting to note

that whereas the Lamb-shift stems to a greater or lesser degree from the effects of all the possible second order processes represented by the Feynman graphs (a) to (d) ((Fig. I.2.1), the principal term in the expression for the g-factor anomaly stems exclusively from the vertex modification, graph (d); therefore, if the Lamb-shift and the g-factor anomaly are separately verified experimentally (to second order) this will verify the contributions of graphs (a) to (c) and of graph (d) independently.

Finally, it should be remarked that, of course, a magnetic moment anomaly is also predicted for a bound electron (this was first suggested by Breit, 1948) and this will manifest itself, not only as a small contribution to the Lamb-shift, but also, more specifically, in any purely magnetic interaction in which the electron may take part, such as the hyperfine-structure interaction. There arise, therefore, two possible approaches to the experimental verification of the predicted value of the g-factor anomaly, one relying on a study of bound electrons the other on a study of free electrons.

(I.3) Experimental Verification of the Predicted g-factor Anomaly for Bound Electrons.

The earliest measurements to show the effects of the anomalous magnetic moment of the bound electron were those of Nafe, Nelson and Rabi (1947) (see also Nafe and Nelson, 1948) on the hyperfine structure separation, $(\Delta\nu)_H$, in the ground-state of hydrogen. This was a particularly convenient state to choose, first because it is a very pure state where $g_J = g_s$ very closely and second because exact wave-functions can be calculated (for a point nucleus) and a correspondingly exact basic formula for $(\Delta\nu)_H$ obtained. One should note, however, that the measured value of g_J cannot at once be compared with the predicted g-factor for a free electron. A small correction of the form $(1 + \alpha^2/3)$ must be applied (Breit, 1928). In addition, certain reduced-mass, relativistic and small quantum-electrodynamic corrections have to be made to the theoretical value of $(\Delta\nu)_H$, some of which cannot be evaluated exactly. For example, one should take into account the finite size and electromagnetic structure of the proton. Of these corrections only the reduced-mass and relativistic corrections, proportional to $(1 + {}^m/M)^{-3}$ and to $(1 + 3\alpha^2/2)$ (Breit, 1930) respectively, are of importance in a test of the second-order term $\alpha/2\pi$. A summary and discussion of these corrections has been given by Series (1957).

Nafe, Nelson and Rabi (loc. cit.) using the method of

atomic beam magnetic resonance, found a discrepancy between the prediction of Dirac theory and their experimental result, which was not, however, a highly precise result owing to the fact that the value of the proton magnetic moment was not accurately known at that time. It was Breit (1947) who suggested that the discrepancy arose from an anomaly in the electron magnetic moment. The Dirac value of $(\Delta\nu)_H$, with the two main corrections mentioned above is

$$(\Delta\nu)_H = 1418.90 \pm 0.03 \text{ Mc/s.},$$

using the values of the atomic constants given by DuMond and Cohen (1955). Recent experimental values are

$$\left.\begin{array}{l}(\Delta\nu)_H = 1420.40573 \\ \pm 0.00005\end{array}\right\} \text{Mc/s}$$

(Kusch, 1955)

and

$$\left.\begin{array}{l}(\Delta\nu)_H = 1420.40580 \\ \pm\ 0.0006\end{array}\right\} \text{Mc/s}$$

(Wittke and Dicke, 1956).

After the various small corrections mentioned above, amounting to a few parts in 10^5, have been applied to the Dirac value, multiplication by $\mu/\mu_o = 1.0011596$ should lead to a result in agreement with the experimental values. Agreement is indeed obtained to an accuracy of the order of one part in 10^5 in $(\Delta\nu)_H$, representing a verification of the g-factor anomaly itself to the order of 1 % . Because of the uncertain corrections involved the method

is limited to a precision of this order.

Kusch and Foley (1948) attempted to evaluate the g-factor anomaly by comparing the moments of gallium in two different states $P_{\frac{1}{2}}$, $P_{\frac{3}{2}}$ in the same magnetic field. The spin and orbital contributions combine differently for these states and a value of g_s could be isolated. They found

$$g/2 - 1 = 0.00114 \pm 0.00004.$$

Similar measurements on sodium and gallium and on sodium and indium gave essentially the same value, showing that the anomaly was an intrinsic property of the electron and not an effect dependent on the state of binding. The method is not acceptable for a precision determination because one cannot rely on the purity of the states in complex atoms, nor can one calculate the necessary corrections.

Further progress, in fact, has come mainly from studies of the ground-state Zeeman splitting in hydrogen. The central problem in such work was the measurement of the magnetic field. It therefore became customary to refer the measured g-factor anomaly to the free proton g-factor through a determination of the proton resonance frequency in the same magnetic field. Thus in one experiment a value of the ratio g_s/g_p would be obtained by a method involving the measurement of the zero-field and Zeeman splitting frequencies in hydrogen in terms of the nuclear precession frequency for protons in a spherical sample of mineral-oil in the same magnetic field. Then, in an entirely

independent experiment, the ratio, g_ℓ/g_p, of the free electron cyclotron g-factor to the free-proton g-factor would be determined, again in a common magnetic field.

The first type of experiment could be carried out using either of two different experimental techniques. Prodell and Kusch (1952) and Koenig, Prodell and Kusch (1952) used the atomic-beam method and arrived at the result

$$g_s/g_p = 658.2288 \pm 0.0006 ,$$

where the value given has been corrected to refer to the free-electron g-factor and to the protons in a spherical sample of mineral oil.

A somewhat greater precision was achieved by Beringer and Heald (1954) using the electron paramagnetic resonance method for measuring the Zeeman splittings. Their result, referred to the same conditions, was

$$g_s/g_p = 658.2298 \pm .0003 .$$

A third result, obtained with the apparatus used by Beringer and Heald but now referring to deuterium instead of hydrogen, was that of Geiger, Hughes and Radford (1957):

$$g_s/g_p = 658.2286 \pm 0.0009 .$$

Finally, a redetermination of g_s/g_p by E. Lambe using the method of paramagnetic resonance has been reported (DuMond, 1959). A precision some ten times better than that achieved by Beringer and Heald is said to have been

obtained. The quoted experimental result was referred to the protons in a sample of distilled water and unfortunately the geometry of the sample was not stated. Assuming that it was spherical and making the necessary diamagnetic correction (Ramsey, 1950), we find

$$g_s/g_p = 658.22983 \pm 0.00004 ,$$

where g_p now refers to protons in a spherical mineral oil sample. It will be observed that this agrees completely with the Beringer and Heald value. Again the Geiger, Hughes and Radford result agrees well with that of Koenig, Prodell and Kusch. The two pairs of values, however, are only in marginal agreement. It is suggested that, in arriving at a best value for g_s/g_p, we should ignore the Geiger, Hughes and Radford result. Firstly its poorer stated accuracy would in any case lead to its being assigned a small relative weight. Secondly, a deuterium result may not be strictly comparable with those for hydrogen. With regard to the Koenig, Prodell and Kusch result, it should not lightly be discarded since it was obtained by an independent technique which, even at that relatively early date, had reached an advanced state of development. It is felt, therefore, that it should be accorded the full weight corresponding to its stated precision. The result of combining the three values is

$$g_s/g_p = 658.22982 \pm 0.00004 .$$

It is seen that, in practice, the Koenig, Prodell and Kusch result might as well have been neglected.

Coming now to the second type of experiment, the earliest determination of g_ℓ/g_p was carried out by Gardner and Purcell (1949) (see also Gardner, 1952).

The cyclotron resonance frequency of free low energy electrons passing across a 3 cm. waveguide was compared with the spin precession frequency of protons in a spherical sample of mineral oil in the same field. The result was

$$2g_\ell/g_p = 657.475 \pm 0.008,$$

where the quoted error was twice the standard deviation.

A second determination was undertaken by Franken and Liebes (1956), in which much greater care was taken to eliminate the effects of stray electric fields in the cavity. Their result was

$$2g_\ell/g_p = 657.463 \pm 0.007 .$$

The stated error, however, included 95% of the data and it would seem that a more suitable figure for a standard deviation would be $\pm$ 0.003. The result did not agree well with that of Gardner and Purcell and this led Hardy and Purcell (1959) to repeat the earlier experiment more carefully with the result that

$$2g_\ell/g_p = 657.4676 \pm 0.0010 .$$

It is understood that a redetermination of g_ℓ/g_p has recently been carried out by Sanders and Woodgate at the

Clarendon Laboratory, Oxford, in which special care has been taken to eliminate stray electric field effects, and that the result is in agreement with that of Hardy and Purcell.

It seems clear, then, that the result of Gardner and Purcell may safely be ignored and, taking a weighted mean of the two later results, we find

$$2g_\ell/g_p = 657.4671 \pm 0.0010.$$

Combining the results of the two types of experiment, we find

$$g/2 - 1 = 0.001160(0), \pm 0.000001(5)$$

in excellent agreement with the theoretical prediction. Although this outcome is satisfactory, it cannot be said to be completely convincing. Quite apart from the lack of full published accounts of the Hardy and Purcell and of the Lambe experiments, the whole approach to the determination of the g-factor anomaly through measurements on bound electrons suffers from two serious drawbacks. Firstly, the result is obtained as a difference of the order of one part in a thousand between the actual measured quantities. Secondly, and because of this, the several corrections which need to be made to the values of g_s/g_p, mainly for the diamagnetism and geometry of the proton sample, and some uncertainties regarding the elimination of stray electric field

effects in the determinations of g_ℓ/g_p assume a disproportionate degree of importance.

(I.4) Experimental Determinations of the g-factor anomaly for Free Electrons

The whole problem of eliminating the effects of binding and the nuclear g-value can be avoided by studying free rather than bound electrons. The possible types of experiment fall into two classes;

(1) experiments which measure the g-factor of the free electron directly,

(2) experiments which measure the anomaly $(g/2) - 1$ directly.

Into class (1) would fall, for example, the proposed "macroscopic atom" experiment of Bloch (1953). Very low-energy electrons were to be trapped in a shallow potential well in the presence of a homogeneous magnetic field. By application of a radio-frequency field and suitable manipulation of the effective barrier heights in the trap it was hoped to determine the spin precession frequency and the cyclotron resonance frequency in the same magnetic field. Because of practical difficulties this experiment has not borne fruit and no detailed discussion of it will be given here.*

Also into class (1) falls the interesting experiment of Dehmelt (1958). Partially polarised free thermal electrons (energy $\sim 400^{\circ}K$) were produced by exchange collisions between unpolarised electrons and optically oriented sodium atoms in the presence of a buffer gas (argon + helium) at 50-100 m.m. pressure. The initial

* see Gardiner, 1961.

flux of unpolarised electrons was obtained either by radio-frequency pulse ionisation or by photo-ionisation of a rubidium-cesium wall-coating using mercury light.

The polarised electrons, if undisturbed, could then transfer some of their polarisation back to unoriented sodium atoms by a second exchange collision. The overall degree of orientation of the sodium vapour was monitored by detecting the absorption of a beam of suitably polarised sodium light. If a radio-frequency field was applied such that its frequency was in resonance with the spin precession frequency of the free electrons, the overall orientation was found to decrease, the resonance condition being detected as a decrease in transmission of the polarised beam. Then, if ν_s was the observed resonance frequency,

$$\nu_s = g_s(\mu_o B_o/h)$$

where g_s is the free-electron g-factor and B_o was the value of the steady homogeneous magnetic field applied to the sample. The quantity in brackets is half the electron cyclotron-resonance frequency, but unfortunately the latter could not be observed in Dehmelt's apparatus, apparently because the relaxation time, τ_a, associated with electron-argon collisions was much shorter than the cyclotron period, τ_c, in the field used ($B_o \simeq 20$ gauss). One finds

$$\tau_c = 2\pi m/eB_o$$

$$\simeq 15 \text{ m}\mu\text{sec.},$$

while Dehmelt assumes

$$\tau_a \simeq 0.05 \text{ m}\mu\text{sec.}$$

Neither could a direct comparison with the proton resonance frequency be made because of the low value of the magnetic field. Instead, Dehmelt made a direct comparison of ν_s with the sodium hyperfine splitting frequencies, $\nu_1 \longrightarrow \nu_4$, shown in Figure (I.4.1), in the same magnetic field, B_o. Then using a value of g_J/g_I from atomic beam work, where g_J is the bound electron g-factor in the ground state of sodium (an s-state) and g_I is the g-factor for the sodium nucleus, he found

$$g_J/g_s = 1.00002(6) \pm 0.00003 .$$

Although this result was not in itself sufficiently precise to lead to an accurate determination of the free-electron g-factor anomaly, the experiment was potentially important. If the effect could be observed with a filling of hydrogen and alkali vapour a direct comparison would become possible between the free-electron g-factor and the g-factor for the electron bound in hydrogen. Alternatively, if an effect could be observed at very low pressures of buffer gas, it might become possible to compare directly the spin and cyclotron resonance frequencies of the free electrons. Unfortunately it is essential that the electron energy be kept very low, otherwise the spin-

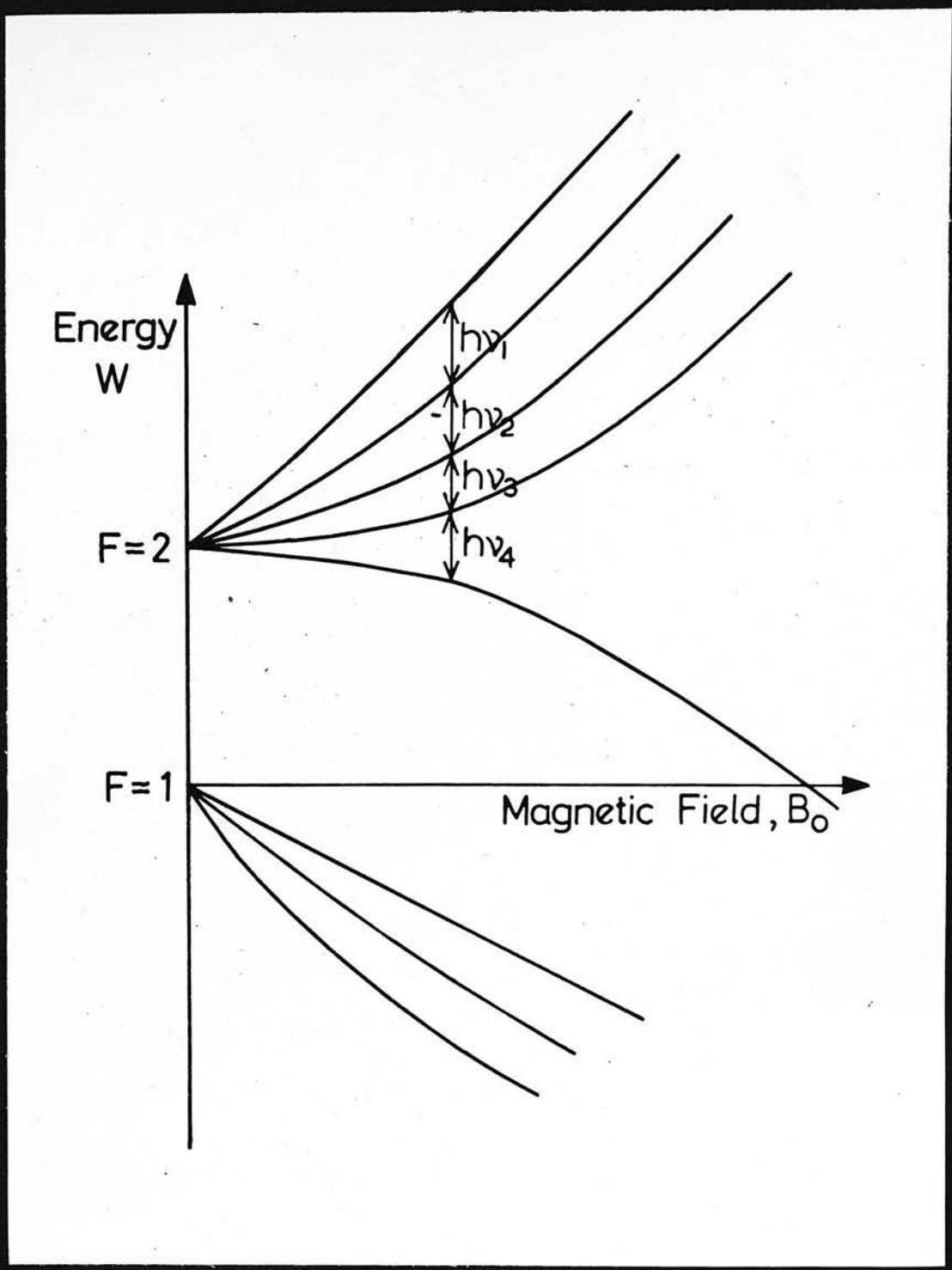

FIG. (I.4.1) Hyperfine Splitting Diagram for sodium.

exchange cross-section becomes small, and this could lead to difficulties when the thermal relaxation time is increased, as it would be at low pressures, owing to the "heating" effect of the radio-frequency field. In fact it is clear that the two requirements of low electron temperature and appreciable cyclotron resonance absorption militate against one another, although this could probably be overcome by alternating the two forms of absorption in time, at the expense of slight loss in accuracy. No experiments along these lines have been reported so far.

A quite different kind of experiment also falling into class (1) was that of Louisell, Pidd and Crane (1954). A partially polarised beam of 420 Kev electrons, obtained by Mott scattering at a thin gold foil, was directed parallel to the magnetic field of a long solenoid and the rotation of the plane of polarisation of the beam was measured after a known distance had been traversed in the field. The plane of polarisation was determined by observing the azimuthal asymmetry in a second Mott scattering. The frequency of precession of the plane of polarisation is linearly related to the g-factor in this experiment and only five rotations of the plane of polarisation could be observed with the solenoid used. Hence the accuracy of the final result was rather poor. The value obtained was

$$g = 2.00 \pm 0.01.$$

However, the experiment showed what was not generally

admitted at the time (see Section (II.1)) that one could perfectly well carry out experiments using quasi-homogeneous fields to determine the magnetic moment of a free electron, provided that the electron is polarised and its polarisation detected by strictly quantum-mechanical means.

From this work was developed the only experiment in class (2) whose completion has so far been reported in the literature, that of Schupp, Pidd and Crane (1961). A detailed description of this masterly, but complex, experiment cannot be given here from considerations of space, but there follows an outline of the more important features.

A pulsed beam of 100 Kev electrons from an electron gun was incident on a gold scattering foil and, under the influence of the magnetic field of a long solenoid, the partially polarised beam scattered at $\sim 89^{\circ}$ followed the helical path indicated in Figure (I.4.2). Part of the beam was trapped for a measured time by the weak auxiliary field of the trapping coil. The resulting precession of the polarisation could be detected by measuring the azimuthal asymmetry in a second Mott scattering (see Figure (I.4.3)). The central feature of the experiment was the trapping of the beam and this was brought about by means of the pairs of cylinders A and B, the inner and outer members of which were connected together. The following was the sequence of operations, repeated 1000 times per second:

(i) with A at earth potential, a negative potential of 100 v. was applied to B:

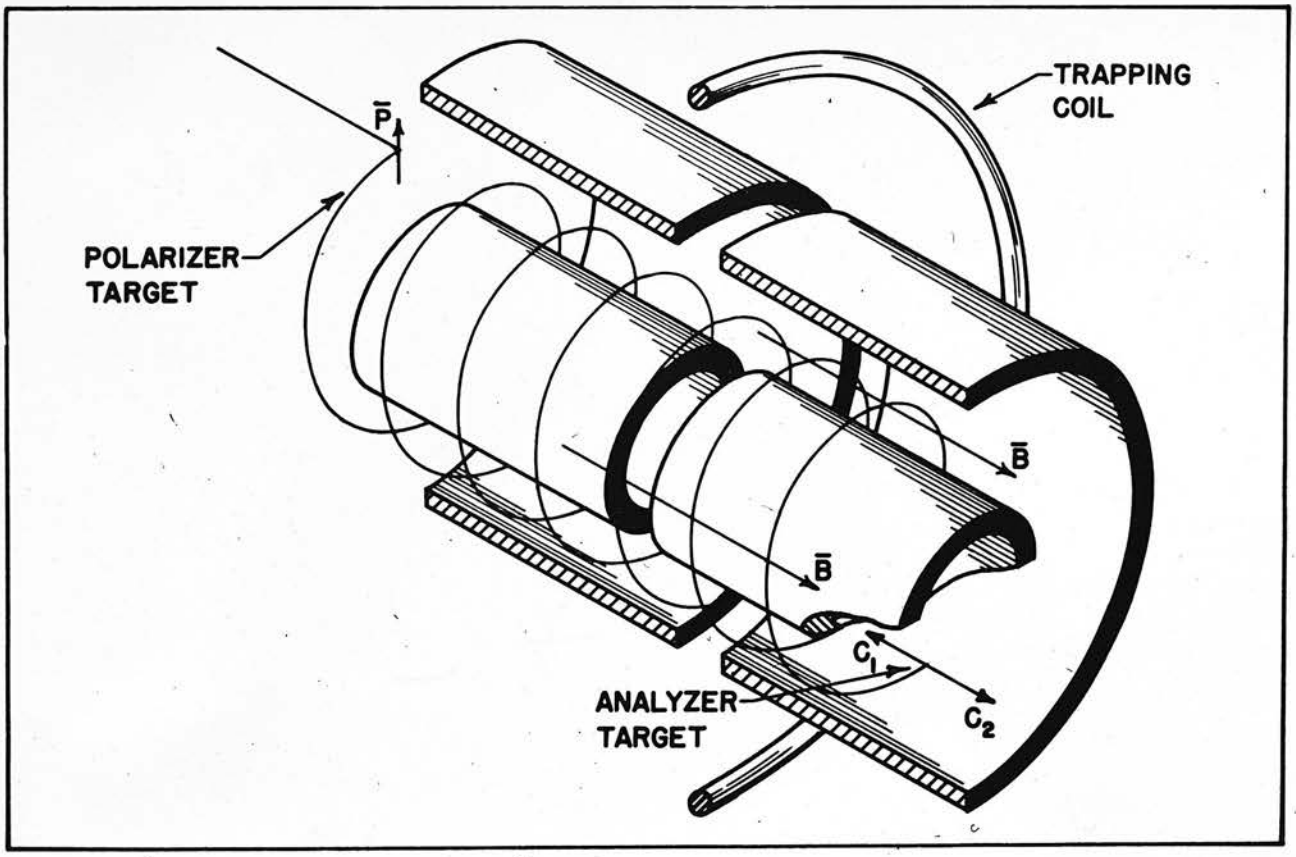

FIG. (I.4.2). Schematic diagram of the experiment of Schupp, Pidd and Crane. (From Schupp, Thesis, 1960).

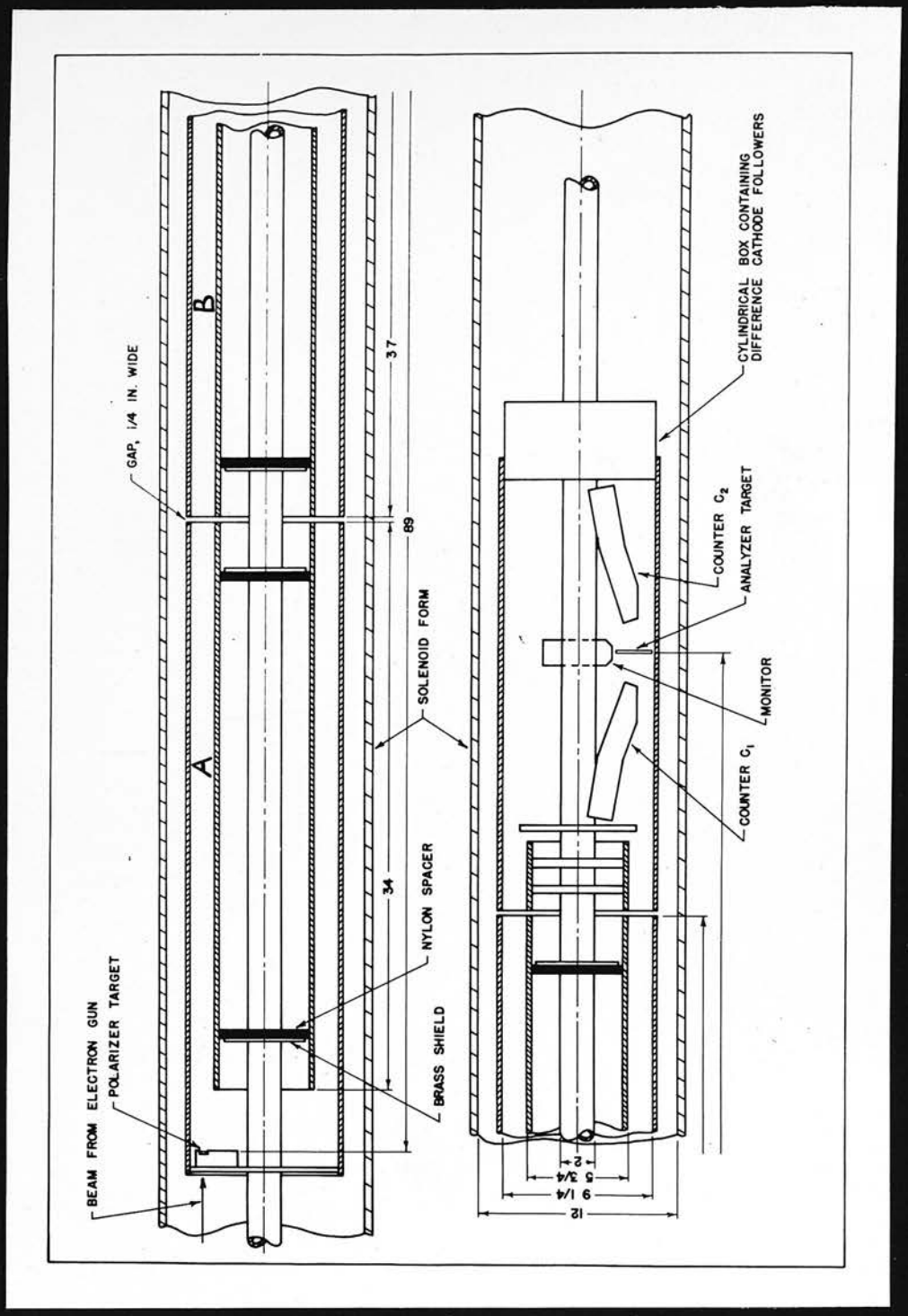

FIG. (I.4.3). Trapping assembly in the experiment of Schupp, Pidd and Crane. (From Schupp, Thesis, 1960).

(ii) the electron-gun was pulsed on, emitting a 0.13 μsec. bunch of electrons:

(iii) the potential of B was reduced to ground in about 30 mμsec., thus capturing some electrons in the betatron-shaped field of the auxiliary coil;

(iv) The operating voltage was applied to the Geiger counters;

(v) A pulse of -100 v. was applied to A to eject the electrons from the trap;

(vi) The counting circuits were gated on;

(vii) Cylinders A were returned to ground potential, completing the cycle.

It was found to be possible to trap electrons for over 300 μsec. while still retaining a measurable asymmetry in the second Mott scattering.

Calculations carried out in connection with this experiment by Mendlowitz and Case (1955), using quantum-mechanical methods, showed that the cyclotron and spin precession frequencies are given by

$$\omega_c = \omega_o(1 - \beta^2)^{\frac{1}{2}} \quad \ldots\ldots \qquad (I.4.1)$$

$$\omega_s = \omega_o(1 - \beta^2)^{\frac{1}{2}} \left[1 + (g/2 - 1)(1 - \beta^2)^{-\frac{1}{2}}\right] \qquad (I.4.2)$$

$$= \omega_c + \omega_o(g/2 - 1),$$

respectively, where

$$\omega_o = eB_{axial}/m_o c \ , \quad \beta = v/c,$$

and therefore that

$$g/2 - 1 = (\omega_s - \omega_c)/\omega_o = \omega_D/\omega_o \qquad (I.4.3)$$

Equation (I.4.2) may also be derived directly from the more general equation (II.4.5) by substituting E = 0; $\underline{v}.(\underline{B} \times \hat{\underline{n}}) = vB_{axial}$. Here B_{axial} is the axial component of the magnetic field in the solenoid, $\underline{v}$ is the velocity of the electrons (v = constant), and $\hat{\underline{n}}$ is a unit vector directed along the outward radius of the solenoid. The aximuthal asymmetry, as a function of the time spent by the electrons in the field, was expected to vary sinusoidally at the "beat frequency" ω_D, which was the difference between the cyclotron- and spin-precession frequencies.

An important advantage of the pulsed method of working was that counting and injection were done at different times and background was therefore largely eliminated. On the other hand a feature which detracted from the simplicity of the experiment was the need to measure ω_o, which was proportional to the mean axial field, $\bar{B}_{axial}$. The latter was not uniform in the trapping region and therefore had to be estimated by an indirect procedure assuming a calculated value of the radial field. The radial field was derived from a calculated total field which was fitted to a series of values measured by the proton magnetic resonance method in the trapping region. The uncertainty introduced by this procedure was estimated as 0.1 gauss ($\sim$0.1% of the total field) which must certainly be

considered a generous allowance since the total range of values of the axial field over the trap was only 0.3 gauss. The uncertainty associated with counting statistics was reduced to comparable proportions by fitting cosine curves at several points over the range 30-300 μsec. trapping-time.

An aspect of this experiment which is, perhaps, open to criticism is the interpretation of the results. Measurements were carried out over a range of electron energies from 50-100 Kev (implying a range of magnetic fields from 82-117 gauss) and unfortunately the values of ω_D/ω_o were found to depend to a small extent on magnetic field. Figure (I.4.4) shows a plot of the results against $1/\bar{B}_{axial}$. The authors were unable to demonstrate directly any definite cause of this trend and they chose to deal with the problem by assuming that a constant radial electric field was present in the trapping region, giving rise to a variation of ω_D/ω_o according to the law

$$\omega_D/\omega_o = a + (\bar{E}_r/c\bar{B}_{axial})\left[(\beta^2 - 1)/\beta + a\beta\right] \quad (I.4.4)$$

$$\simeq a - \bar{E}_r/cB^2k$$

where $a = (g/2) - 1$,

$k = er/m_oc^2$,

r = radius of orbit ,

and B is written for $\bar{B}_{axial}$.

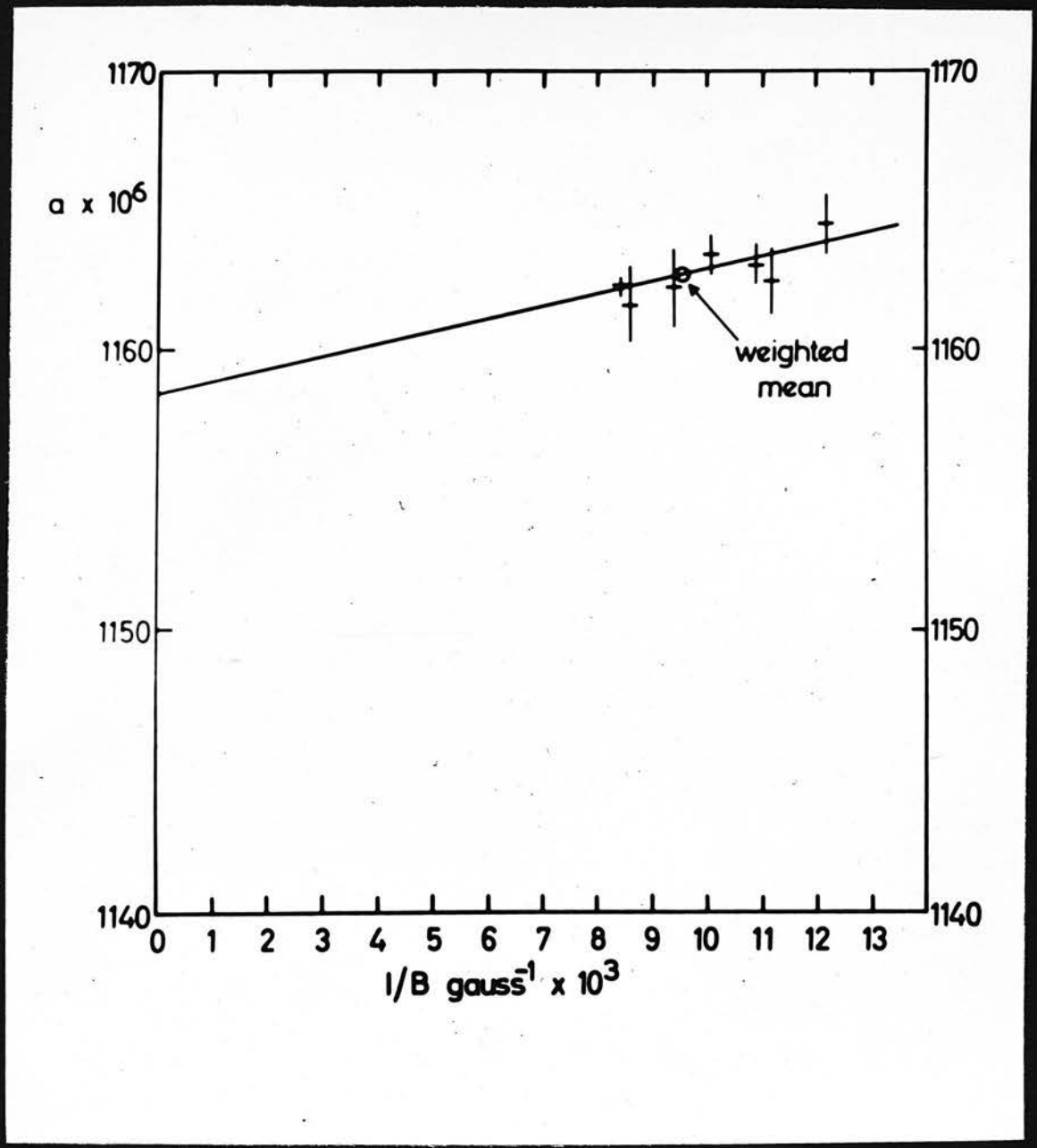

FIG. (I.4.4) Results of Schupp, Pidd and Crane plotted against 1/B.

A plot of ω_D/ω_o against $1/B^2$ should then give approximately a straight line. By extrapolation to $1/B^2 = 0$ of a straight line fitted to the experimental points by the least squares method, the authors obtained the value,

$$\omega_D/\omega_o \text{ (extrapolated)} = (1160.6 \pm 1.2) \times 10^{-6} .$$

The more exact form of the chosen law, equation (I.4.4), was then fitted to the experimental points by choosing the parameters $\bar{E}_r$ and "a" so as to make the curve pass through the weighted mean point and have the slope of the best straight line at that point. The value of "a" found in this way was

$$a = (1160.9 \pm 2.0) \times 10^{-6}$$

where the error was chosen to be great enough to include the weighted average value, 1162.75×10^{-6}. With the addition of a small allowance for systematic error, the final result was given as

$$a = (1160.9 \pm 2.4) \times 10^{-6} ,$$

showing no disagreement with theory.

Such evidence as they were able to obtain from independent experimental checks, however, so far from supporting the hypothesis of a radial electric field effect, actually opposed it. If one approaches the data with an open mind, that is without any preconceived ideas of the cause of the admitted trend, one is led to analyse them in

the following way (Farago, private communication).

One asks the question whether or not an equation of the second order in 1/B (a parabola on Fig. I.4.4) is a significantly better fit to the data by the least squares criterion than a first order equation (a straight line on Fig. I.4.4). Such an analysis carried out by the writer (Appendix C) shows that this is not the case and therefore that, on the evidence of the data themselves, one is entitled only to draw a best straight line through the points on Fig. (I.4.4). Extrapolating such a line to 1/B = 0, one finds

$$\omega_D/\omega_o \text{ (extrapolated)} = (1158.4 \pm 0.8) \times 10^{-6}.$$

In order to be able to equate this to the g-factor anomaly one must assume that the equation of the straight line is of the form

$$\omega_D/\omega_o = a + \text{const.}/B,$$

an assumption which is at least as difficult to justify as that made by Schupp, Pidd and Crane.

The choice between the two approaches, neither of which leads to a result in disagreement with theory, must be a matter for personal judgement as the authors themselves admit. The present writer inclines to favour the choice of the straight line extrapolation on the grounds that what little evidence there was tended to discredit the electric field hypothesis. It is perhaps worth remarking that if one does assume a law of the form

$$\omega_D/\omega_o = a + \text{const.}/B$$

one is immediately led to consider equation (I.4.3) again. Clearly, since $\omega_o \propto \bar{B}_{axial}$, a constant error in measurement of ω_D would lead to precisely the law just mentioned. Now ω_D was obtained from the relation

$$\omega_D = 2\pi N/(M - t_o)$$

where M was the trapping-time required for an integral number, N, of cycles of polarisation asymmetry and t_o was a small zero-error in the time-scale. However, detailed analysis of the figures given by the authors reveals no indication of a constant timing-error, and the authors give convincing evidence that N cannot be in error. The calculated values of magnetic field have also been examined and, with the exception of one value in which there appears to be a small arithmetical slip, all the given data appear to be consistent.

Some of the assumptions made in evaluating the experiment can be questioned, for example that the polarisation immediately after the first scattering is strictly radial and that it remains in a plane normal to the solenoid axis throughout the motion, that the trapped beam oscillates symmetrically about the magnetic centre of the trap, and so on. But such effects as these do not appear to be large enough to explain the observed trend.

In spite of the difficulty of interpretation it must be concluded that this experiment constitutes a striking

verification of the predictions of the renormalised theory of quantum electrodynamics and provides one of the most reliable values of the free-electron g-factor anomaly yet measured. It is the only method which shows definite promise of being able to verify the fourth-order term, $-0.328\ (\alpha/\pi)^2$.

CHAPTER II

SPIN DYNAMICS AND MOTT SCATTERING

(II.1) Electron Spin

Before 1925 the quantum theory of the atom had been based on a study of the classically allowed types of motion of a charged point-particle in the field of a nucleus, the quantisation being carried out by restricting the classical orbits rather than by generalising the laws of motion. Attempts to construct a realistic classical model of a rotating electron had, however, met with serious difficulties especially when the requirements of relativity theory were taken into account (Kramers, 1957).

It would not have been surprising, therefore, if the concept of electron spin (Uhlenbeck and Goudsmit, 1925) had been received with some scepticism, the more so as Uhlenbeck's and Goudsmit's calculation of the splitting of certain atomic energy-levels by the spin-orbit interaction was in disagreement with experiment by a factor of two, an effect which was later explained as being due to the so-called Thomas precession (Thomas, 1926). That the new concept found immediate acceptance was due largely, of course, to the striking manner in which it clarified certain hitherto obscure problems of spectroscopy, notably the anomalous Zeeman effect and the doublet structure of many X-ray and optical levels. Even this might not have been enough had it not been for the fortunate

circumstance that at the very time when the proposal was made, the groundwork of the new theory into which the spin angular momentum could be fitted in a natural way was in process of being laid. It is an interesting coincidence that the first identification of a dynamical variable having no classical analogue should have been made independently in the field of experimental physics at the same time that the first truly quantum-mechanical laws of motion were being formulated. Spin was early incorporated into the new matrix-mechanics (Heisenberg and Jordan, 1926) and soon afterwards Pauli developed what has now become the best-known form of spin-theory, in terms of non-relativistic wave-mechanics (Pauli, 1927).

Quite apart from any difficulties there may be in setting up a classical model of the spinning electron, it is easy to see that the spin angular momentum can have no classical analogue. According to the Correspondence Principle the classical analogue must be obtained from the quantum-mechanical variable in the limit of large quantum numbers, as $h \to 0$. Since the spin angular momentum is postulated to be observable only as a half-quantum, $\pm \frac{1}{2}h$, it follows that it must be unobservable in the classical limit.

An interesting consequence of this fact was pointed out by N. Bohr (1928), following the success of the Stern-Gerlach experiment with silver-atoms, namely that it is impossible to distinguish between the two spin-states of

a free electron by means of any macroscopic experiment of the Stern-Gerlach type. In more general terms, one cannot separate electrons which are initially in opposite spin-states by any device in which their orbits can be described in purely classical terms. A detailed discussion of Bohr's argument can be found in Mott and Massey (1949), where two different types of hypothetical experiment are analysed. Unfortunately, a somewhat misleading conclusion became widely accepted among physicists, including Mott and Massey who wrote "From these arguments we must conclude that it is meaningless to assign to the free electron a magnetic moment." Presumably what they intended to convey was that, as long as the electron is free in the sense that its orbit can be correctly described in classical approximation, the magnetic moment is unobservable (not because it does not exist, but because any Stern-Gerlach splitting of an electron beam produced by quasi-homogeneous electric and magnetic fields would be small compared to the spreading of the beam by diffraction).

If, however, we are allowed first to prepare the electron in a definite spin-state then to send it through our quasi-homogeneous electric and magnetic fields and finally to measure the components of the spin along definite axes, we shall find that the results of our experiment will depend in a perfectly definite and, as we shall see in the following sections, theoretically predictable way on the initial spin-state and the electromagnetic fields.

Furthermore, the theory shows that in an experiment of this type the effect of the fields is just such as would be experienced by a classical charged point-particle endowed with a magnetic dipole moment very closely equal to that postulated for the electron by Uhlenbeck and Goudsmit, namely one Bohr magneton. It should be remarked that if we consider such an experiment conducted with a single electron there is, as is well-known, no possibility of measuring the final spin-direction in the sense implied above. In practice a beam of electrons would be used, not all the members of which will be in the same spin state in general. The theory is then developed in terms of the "polarisation" of the beam rather than of the spin itself.

Before discussing the concept of polarisation, it will be convenient to summarise the relevant conclusions of the Pauli non-relativistic spin-theory. For fuller details see, for example, Rose (1961). Here, and throughout this chapter, we use units such that $\hbar = m_o = c = 1$. The vector spin operator is

$$\underline{s} = \tfrac{1}{2}\underline{\sigma}$$

where the components of $\underline{\sigma}$, the Pauli spin operator, can be written (in the "standard" representation)

$$\sigma_x = \begin{bmatrix} 0 & 1 \\ 1 & 0 \end{bmatrix}, \quad \sigma_y = \begin{bmatrix} 0 & -i \\ i & 0 \end{bmatrix}, \quad \sigma_z = \begin{bmatrix} 1 & 0 \\ 0 & -1 \end{bmatrix}$$

The commutation relations satisfied by these operators

may be written

$$\sigma_j \sigma_k = i\varepsilon_{jkl}\sigma_l + \delta_{jk} \qquad (j, k, l = 1, 2, 3)$$

where $\varepsilon_{jkl} = \begin{cases} 0; & j, k, l \text{ not all different} \\ \pm 1; & (j,k,l) \text{ a cyclic/non-cyclic permutation of } (1,2,3) \end{cases}$

and δ_{jk} is the Kronecker-δ. The actual direction of the spin at any time is inherently unobservable, for the contrary would imply the vector eigenvalue equation

$$\underline{\sigma}\psi = \hat{\underline{n}}\,\psi$$

where $\hat{\underline{n}}$ is some unit vector, and this can easily be shown to be incompatible with the commutation rules of the σ_j. However, the component of $\underline{\sigma}$ along one definite direction $\hat{\underline{n}}$ is observable and so

$$\underline{\sigma}.\underline{n}\,\psi = \lambda\psi, \quad \text{where } \lambda = \pm 1$$

since $(\underline{\sigma}.\hat{\underline{n}})^2 \equiv \hat{\underline{n}}.\hat{\underline{n}} = 1$.

The wave-function is a two-component function, a Pauli spinor. In the standard representation the simplest choice for $\hat{\underline{n}}$ is along the z-axis when the wave-functions which diagonalise σ_z can be written

$$\psi_{\lambda=1} = \chi^{+\frac{1}{2}} = \begin{bmatrix} 1 \\ 0 \end{bmatrix}$$

$$\psi_{\lambda=-1} = \chi^{-\frac{1}{2}} = \begin{bmatrix} 0 \\ 1 \end{bmatrix}$$

The labels $\pm \frac{1}{2}$ refer, of course, to the z-components of the spin, $\underline{s}$. Any other two-component spinor can be written as a

linear superposition of these wave-functions.

$$\chi = a\chi^{\frac{1}{2}} + b\chi^{-\frac{1}{2}} \qquad \text{(II.1.1)}$$

Although we cannot speak of the spin-vector pointing in a definite direction, we can speak of an average spin direction, given by $(\psi, \underline{\sigma}\psi)$. In the case where the wave-functions diagonalise σ_z we have

$$(\chi^{\pm\frac{1}{2}}, \underline{\sigma}\chi^{\pm\frac{1}{2}}) = \pm \hat{\underline{e}}_3$$

where $\hat{\underline{e}}_3$ is the unit vector along the z-axis. Since this relation cannot be affected by the choice of axes, we have in the general case

$$(\chi^{\pm}, \underline{\sigma}\chi^{\pm}) = \pm \hat{\underline{n}} \qquad \text{(II.1.2)}$$

where the $\chi^{\pm}$ are the spinors which diagonalise the component of $\underline{\sigma}$ along the direction $\hat{\underline{n}}$.

(II.2) Electron Polarisation

As we have seen, it is not meaningful to speak in terms of a definite direction for the spin vector-operator, $\underline{\sigma}$. However, confining attention for the moment to an electron whose wave-function is a pure spinor $\chi^{\pm}$ (equation II.1.2), we can see that any such electron is associated with a definite direction, $\hat{\underline{n}}$, in space through equation (II.1.2). We may call the unit vector $\hat{\underline{n}}$ the polarisation of the electron. C.G. Darwin (1928) first suggested that one should define the polarisation of a free electron as the expectation value of the Pauli spin operator, $\underline{\sigma}$, in the rest-frame of the electron. According to this the polarisation can be obtained explicitly by expanding the wave function in terms of the $\chi^{\pm\frac{1}{2}}$ (equation (II.1.1)) and using the expansion coefficients to define the polar and azimuthal angles of $\hat{\underline{n}}$.

It will be explained in due course how the presence of the g-factor anomaly manifests itself through the behaviour of the polarisation of electrons as they pass through electric and magnetic fields. Since, in addition, the electrons used in the present experiment have velocities approximately equal to half that of light, it will clearly be convenient to have a definition of polarisation which will apply to relativistic electrons and which will also be meaningful where electric and magnetic fields are present.

The most recent developments in this subject have been correlated and summarised by Fradkin and Good (1961) whose

review can be recommended as a consistent account of the theory of electron polarisation. Of the three approaches mentioned by these authors only one satisfies both of the requirements set forth above and we shall confine attention here to a brief outline of this approach.

The polarisation is first defined in the absence of fields through a polarisation operator

$$T_\mu = \gamma_5(i\gamma_\mu - p_\mu) \qquad (\mu = 1,2,3,4)$$

where the γ_μ are the 4 x 4 Dirac matrices satisfying

$$\gamma_\mu\gamma_\nu + \gamma_\nu\gamma_\mu = 2\delta_{\mu\nu} \quad ,$$

p_μ is the four-momentum of the electron, and $\gamma_5 = \gamma_1\gamma_2\gamma_3\gamma_4$.

It can be shown (loc. cit.) that the expectation value of T_μ for a plane-wave state is a certain four-vector, s_μ. Thus

$$(\psi(\underline{p}),\ T_\mu\psi(\underline{p})) = s_\mu \qquad \text{(II.2.1)}$$

It can be further shown that s_μ, thus defined, transforms like an axial vector under Lorentz transformation. In fact s_μ is just the Lorentz transform to the laboratory frame (hereafter referred to as the lab-frame) of the four-vector $(\underline{s},\ s_4)$ which reduces to $(\hat{\underline{s}}_o,\ 0)$ in the rest-frame, where $\hat{\underline{s}}_o \equiv \hat{\underline{n}}$. The term "polarisation" is applied indiscriminately by Fradkin and Good to both T_μ and s_μ but we shall reserve it for the latter. It is easily shown that the operator T_μ commutes with the Dirac free-particle Hamiltonian so that the polarisation of an electron in the

absence of fields is a constant of the motion, as it should be.

In the rest-frame of the electron T_μ reduces to the four-vector operator $(\underline{\sigma}, 0)$ where the σ_i are the Pauli spin operators. This is because the four-component plane-wave functions of the Dirac theory reduce to two-component Pauli spinors (only the "large" components being retained) and hence all "odd" Dirac operators such as $\gamma_5 p_\mu$ and $\gamma_5\gamma_4$, which mix large and small components, may be replaced by zero in this limit, while "even" operators such as $i\gamma_5\gamma_k$ are replaced by 2 x 2 Pauli operators σ_k (unity in Dirac space). Thus T_μ constitutes a natural relativistic generalisation of the Pauli spin operator, $\underline{\sigma}$.

Furthermore, the definition of T_μ is capable of immediate generalisation to the case where electromagnetic fields are present. In the usual way, we replace p_μ by

$$\pi_\mu = p_\mu + eA_\mu$$

where $A_\mu \equiv (\underline{A}, i\Phi)$ is the four-potential of the field, in terms of which

$$F_{\mu\nu} = \partial A_\nu/\partial x_\mu - \partial A_\mu/\partial x_\nu ,$$

$F_{\mu\nu}$ being the field components in tensor form. Then we generalise T_μ to

$$T_\mu = \gamma_5(i\gamma_\mu - \pi_\mu) .$$

Of course, the T_μ will no longer commute with the Hamiltonian. For time-independent fields we may write

$$\partial A_\mu/\partial x_4 = 0 \qquad (x_4 = it)$$

and from the equation of motion, which is

$H\psi = -(\partial/\partial x_4)\psi$, with H the Dirac Hamiltonian, we have, after rearrangement of the terms,

$$\gamma_\nu \frac{\partial}{\partial x_\nu} + ie\,\gamma_\nu A_\nu + 1 = 0$$

as an operator relation. Using these relations a straightforward calculation shows that

$$dT_\mu/d\tau = i\left[HT_\mu - T_\mu H\right]$$

$$= ie\gamma_5\gamma_4 F_{\mu\nu}\gamma_\nu$$

where $d\tau = dt/\gamma$, $\gamma = (1 - v^2)^{-\frac{1}{2}}$,

v = electron velocity.

For the polarisation we may therefore write

$$d/d\tau \langle T_\mu \rangle = i\,e \int (\Psi, \gamma_5\gamma_4 F_{\mu\nu}\gamma_\nu \Psi) d^3x \ .$$

This may be regarded as an equation of motion for the four-vector polarisation, s_μ, provided that Ψ is a plane-wave state of definite momentum.

(II.3) Polarisation of Dirac Electrons in Quasi-homogeneous Electric and Magnetic Fields

In order to apply the foregoing result we take note of the fact that in the present experiment the electrons are subject to electric and magnetic fields which are effectively homogeneous. By this is meant the following:
(a) the electron can be represented by a wave-function whose amplitude is negligible except over a very small region corresponding to the classical position of the particle;
(b) the relative change in the fields over the typical dimensions of such a wave-packet is negligible.

Since the apparatus behaves for this purpose like a semicircular β-ray spectrograph with orbit radius ~ 4 cm. and since the fields were homogeneous to a few parts in a thousand over the region of the orbits (Section IV.3), these conditions may be assumed to be satisfied.

If the fields, $F_{\mu\nu}$, do not depend on the space co-ordinates over the region occupied by a wave-packet,

$$d/d\tau \langle T_\mu \rangle = -eF_{\mu\nu} \int (\Psi, \gamma_5\gamma_4\gamma_\nu \Psi) d^3x \qquad (II.3.1)$$

Consider now the expectation value of T_μ evaluated in the rest-frame of the electron, denoted by $\langle T_\mu \rangle^{(r)}$. Using the limiting properties of the Dirac matrices in this frame, one finds from the definition of T_μ

$$\langle T_\mu \rangle^{(r)} \equiv \{ \langle \underline{T} \rangle^{(r)}, \langle T_4 \rangle^{(r)} \} = \{ \langle i\gamma_5 \underline{\gamma} \rangle, 0 \}$$

Hence, expressing equation (II.3.1) in the rest-frame,

$$d/d\tau \langle T_\mu \rangle^{(r)} = eF_{\mu k} \langle i\gamma_5 \gamma_k \rangle = eF_{\mu k} \langle T_k \rangle^{(r)} .$$

We may regard this as the expression in the rest-frame of the covariant equation of motion

$$d/d\tau \langle T_\mu \rangle = e F_{\mu\nu} \langle T_\nu \rangle \qquad \text{(II.3.2)}$$

This derivation (Rose, 1961) is plausible rather than rigorous. For the detailed proof the reader is recommended to consult the paper of Fradkin and Good (1961).

Two remarks need to be made concerning this equation of motion.

(1) In the rest-frame it reduces to

$$d/dt \langle T_j \rangle^{(r)} = e F_{jk} \langle T_k \rangle^{(r)} ,$$

or, since $F_{jk} = \varepsilon_{ijk} B_i$ where $\underline{B}$ is the magnetic flux-density,

$$d/dt \langle \underline{T} \rangle^{(r)} = -e/m_o \langle \underline{T} \rangle^{(r)} \times \underline{B}$$

(in ordinary units) which is of the form of the classical equation of motion for a spinning dipole with angular momentum $\hbar/2$ and magnetic moment equal to one Bohr magneton (cf. Section II.1).

(2) If the wave function, Ψ, can be approximated by a plane-wave function $\Psi(\underline{p})$ of definite momentum $\underline{p}$, then equation (II.2.1) applies and equation (II.3.2) becomes a classical equation of motion for the polarisation four-vector s_μ, namely

$$ds_\mu/d\tau = e F_{\mu\nu} s_\nu \qquad \text{(II.3.3)}$$

This approximation was certainly valid for the purposes of the present experiment, for the radius of curvature of the orbit (~ 4 cm.) was greater by many orders of magnitude than the de Broglie wavelength of the electron ($\sim 3 \times 10^{-10}$ cm.).

Finally, we note that in the classical approximation we can write for the orbital motion of the electron,

$$\pi_\mu \Psi = \langle \pi_\mu \rangle \Psi = u_\mu \Psi$$

(u_μ, the four-velocity $= \gamma \{\underline{v}, ic\}$) ,

and the classical (Lorentz) equation of motion for the orbit can be shown to be valid, namely

$$du_\mu/d\tau = e F_{\mu\nu} u_\nu \qquad \text{(II.3.4)}$$

(II.4) Polarisation of an Electron possessing an Anomalous Magnetic Moment.

We cannot, without more ado, take over equation (II.3.3) to apply to an electron with an anomalous magnetic moment, $\underline{\mu} = (g/2)\mu_o$, merely by substituting ge/2 for e. One reason for this is that ultimately this equation stems from the Dirac equation which, as it were, contains the magnetic moment μ_o within its essential structure and so cannot be a description of any particle having a different value of magnetic moment.

In the original classical treatment of the polarisation of an electron with anomalous magnetic moment (Bargmann, Michel and Telegdi, 1959), the difficulty was avoided and the correct equations of motion obtained. Before considering their treatment in more detail we shall summarise, for purposes of comparison, the quantum mechanical approach to the problem.

This depends on recognising (Pauli, 1958) that the anomaly of the magnetic moment manifests itself only by the small additional magnetic potential energy to which it gives rise in the presence of fields. Therefore the true equation of motion can be written in the form

$$(H_o + H')\Psi = ih\partial\Psi/\partial t,$$

where H_o is the Dirac Hamiltonian and H' is an extra term given by

$$H' = -\tfrac{1}{2}e(g/2 - 1)\{i\,\gamma_5\underline{\gamma}.\underline{B} + \underline{\gamma}.\underline{E}\}$$

which accounts explicitly for the extra magnetic potential

energy due to the anomalous part, $(g/2 - 1)\mu_o$, of the magnetic moment. Using this Hamiltonian together with the resulting operator relation, namely

$$i\gamma_\mu\pi_\mu + \tfrac{1}{4}\, ie(g/2 - 1)F_{\mu\nu}\,\gamma_\mu\gamma_\nu + 1 = 0$$

and defining the polarisation operator, T_μ, in the same way as before, one finds for the equation of motion of the polarisation four-vector, s_μ, in the classical limit (that is under the conditions of section II.3)

$$ds_\mu/d\tau = ge/2.F_{\mu\nu}\, s_\nu + (g/2 - 1)e(u_\nu F_{\nu\lambda} s_\lambda)u_\mu \qquad (II.4.1)$$

The same result was obtained by Bargmann, Michel and Telegdi (1959) from purely classical considerations. They based their argument on three assumptions:

(a) that the expectation value of the spin operator will necessarily follow the same time-dependence as one would obtain from a classical equation of motion, so that to solve the problem of spin precession it is sufficient to produce a consistent set of covariant classical equations of motion;

(b) that the spin-polarisation can be represented by an axial four-vector, s_μ, which reduces in the electron's rest-frame to the three-vector, $\underline{s}_o$, which represents the spin polarisation in that frame;

(c) that the equation of motion for $\underline{s}_o$ is

$$d\underline{s}_o/dt = ge/2.\ \underline{s}_o \times \underline{B} \qquad (II.4.2)$$

They note the following relations;

$$u_\mu s_\mu = 0 \quad ,$$

$$u_\mu u_\mu = -1 \quad .$$

These are direct consequences of the definitions

$$s_\mu = \{\underline{s}, s_4\} = \{\underline{s}_o, 0\} \quad \text{in the rest-frame.}$$

$$u_\mu = \gamma\{\underline{v}, i\} = \{0, i\gamma\} \quad " \quad " \quad " \quad "$$

where $s_o^2 = 1$ and $\gamma^2 = 1/(1 - v^2)$.

Therefore

$$ds_4/d\tau = i\, \underline{s}.d\underline{v}/d\tau \qquad (II.4.3)$$

in any instantaneous rest-frame. They proceed to write down equation (II.4.1) as being the immediate generalisation of (II.4.2) and (II.4.3) to an arbitrary Lorentz frame, under the further (physically reasonable) assumption that the equation of motion for the orbit is

$$du_\mu/d\tau = e\, F_{\mu\nu}\, u_\nu \qquad (II.3.4)$$

In fact, the most general axial vector which can be formed from the available physical quantities, $F_{\mu\nu}$, u_λ, s_λ, g, e, remembering that

$$s_\mu s_\mu = s_o^2 = \text{const.},$$

$$u_\mu s_\mu = 0$$

and $F_{44} = 0$,

is

$$A(g,e)\, F_{\mu\nu}\, s_\nu \;+\; B(g,e) u_\mu (u_\nu F_{\nu\lambda} s_\lambda)$$

where A, B are scalar functions of g and e.

Since s_μ, and therefore $ds_\mu/d\tau$, is an axial vector, we may write

$$ds_\mu/d\tau \;=\; A(g,e)\, F_{\mu\nu} s_\nu \;+\; B(g,e) u_\mu (u_\nu F_{\nu\lambda}\, s_\lambda) \;.$$

By writing down the components of this equation in the rest-frame and comparing with (II.4.2) and (II.4.3) it is easily shown that

$$(A - B) \;=\; e \;,$$

$$A \;=\; ge/2 \;,$$

and this assignment gives equation (II.4.1) correctly.

Assumption (c) might seem to be subject to the criticism mentioned in the first paragraph of this section. However, in the rest-frame the only possible type of motion is a precession and, since the spin angular momentum is not affected by the quantum electrodynamic corrections, it is physically reasonable that if a real electron and a Dirac electron were subject to the same magnetic field, the ratio of their rates of precession would be the same as the ratio of their magnetic moments, namely g/2.

It should be noted that the only term in equation (II.4.1) which is proportional to the anomaly of the g-factor is also dependent on the particle orbit through the four-velocity, u_μ. Thus any direct method of determining the g-factor anomaly using spin-precession in

homogeneous fields must require a knowledge of the electron orbit.

The application of equation (II.4.1) to the present experiment, which will more conveniently be discussed in a separate chapter (see Section III.2)), is facilitated by writing s_μ in the lab-frame in terms of two unit polarisation four-vectors e_l and e_t (following Bargmann et al, loc. cit.), whose space-components are respectively parallel and perpendicular to the velocity in the lab-frame. Thus

$$s_\mu = S(e_l \cos \phi + e_t \sin \phi)\mu \qquad \text{(II.4.4)}$$

where $S = (s_\mu s_\mu)^{\frac{1}{2}}$ is the magnitude of the polarisation and e_l , e_t are defined by

$$e_l = \gamma(\hat{\underline{v}}, i|v|) \; ; \quad e_t = (\hat{\underline{n}}, 0)$$

in the lab-frame, where $\hat{\underline{n}}$ is a unit vector such that

$$\hat{\underline{n}}^2 = 1 \quad \text{and} \quad \hat{\underline{n}}.\hat{\underline{v}} = 0 \; .$$

The rate, Ω , at which the polarisation is transformed from longitudinal to transverse and vice versa in the lab-frame may be written*

$$\Omega = d\phi/dt$$

$$= \gamma^{-1} \, d\phi/d\tau$$

$$= \frac{e}{m_o}\left\{\frac{\underline{E}.\hat{\underline{n}}}{|v|}\left[\frac{g}{2} - 1 - \frac{g}{2\gamma^2}\right] + \hat{\underline{v}}.B \times \hat{\underline{n}}(g/2 - 1)\right\} \qquad \text{(II.4.5)}$$

* for details of the calculation see Gardiner, 1961.

where all quantities are now expressed as ordinary vectors and the mass of the electron has been reintroduced.

So far it has been implicit in the discussion that we are dealing with a single electron. For a beam of electrons which follow the same orbit and which do not interact with one another, the polarisation can be obtained by taking an incoherent average over all members of the beam. Since the formulae describing the behaviour of the polarisation are linear in T_μ they will apply equally well to the polarisation four-vector s_μ of a mono-energetic beam except that now the magnitude $(s_\mu s_\mu)^{\frac{1}{2}} = S$ of the polarisation four-vector will in general be less than unity. Thus, for a single electron, $\langle T_\mu \rangle \langle T_\mu \rangle$ may be evaluated in the rest-frame, choosing the z-axis in the direction which diagonalises the spin-operator, to give

$$\langle T_\mu \rangle \langle T_\mu \rangle = 1 \ .$$

But, employing the same procedure for a mono-energetic beam, we obtain (Fradkin and Good, loc. cit.)

$$\langle T_\mu \rangle \langle T_\mu \rangle = (p_+ - p_-)^2$$

where $p_\pm$ are the probabilities of a particle being observed with spin up/down in its rest-frame.
$100(p_+ - p_-) = 100S$ is the quantity usually referred to as the percentage polarisation of a beam in, for example, β-decay experiments. It is sometimes convenient to be able to regard a beam which is, say, 40% longitudinally

polarised in the forward direction as being composed to the extent of 30% of electrons polarised in the backwards direction and 70% of electrons polarised in the forwards direction.

(II.5) Preparation and Detection of the Electron Polarisation.

As explained in Section (II.1), it is possible to study the behaviour of the electron spin in macroscopic fields provided that one is allowed to prepare the spin state beforehand and detect it afterwards by some purely quantum-mechanical phenomena. In practice one deals with a beam of electrons and prepares it in a state of known polarisation. Methods of doing this have been discussed by Tolhoek (1956). Three methods which have been applied successfully are

(a) Mott scattering of unpolarised relativistic electrons from heavy nuclei,

(b) exchange collisions between free low-energy electrons and oriented atoms (e.g. alkali atoms),

(c) use of the naturally polarised beta-particle given off in beta-decay.

The first method suffers from the disadvantage that the cross-section for scattering into a beam of appreciable polarisation is low. Despite this the method has been successfully employed by Schupp, Pidd and Crane (1961) (see Section I.4). The second method (see Section I.4) cannot be used to produce a beam in the sense that the electrons follow a known classical orbit and therefore, according to a remark of the previous section, cannot be applied in a direct determination of the g-factor anomaly. The third method, chosen for the present experiment, arises

from the fact that the β-decay interaction violates the law of conservation of parity (Lee and Yang, 1957), and this leads to the result that the beta-particles emitted in an allowed transition are longitudinally polarised with $S = v/c$ (in the notation of the previous section) and negative helicity. That is

$$\underline{s}_o \cdot \hat{\underline{v}} = - |v| /c.$$

A discussion of the theory of β-decay would be out of place here and we merely remark that the result just quoted is well-supported experimentally for a wide variety of β-emitters (Grodzins, 1959; Sternheimer, 1959). The particular case of Sulphur-35, which was used in the present experiment, is discussed in Section (III.3).

The detection of the polarisation of a beam after passage through electromagnetic fields can also be carried out by a variety of methods, at least in principle (Tolhoek, 1956). The one which has most frequently been applied and which is most suited to the present experiment is the method of Mott scattering. A full discussion of this phenomenon, first investigated by Mott (1929), has recently been given by Rose (1961) whose treatment, using density-matrix techniques (Fano, 1956), partly follows that of Muhlschlegel and Koppe (1958). We need give only a brief account of those aspects of the general theory which are relevant to the present experiment.

It is assumed that an electron is scattered elastically from an incoming plane-wave state of momentum $\underline{p}$ to

an outgoing spherical wave of momentum $\underline{p}'$. Thus the wave function after scattering is, asymptotically,

$$\Psi = a(\underline{p}) \exp(i\underline{p}.\underline{r}) + b(\underline{p}') \frac{\exp(ipr)}{r}$$

where $a(\underline{p})$, $b\underline{p}')$ are four-component spinors. The Mott cross-section is then given by

$$\sigma = (b, b)$$

A "transition amplitude" $A(\underline{p}', p)$ is defined by

$$\sigma \rho_o(\underline{s}'_o) = A\rho_o(\underline{s}_o)A^\dagger \qquad \text{(II.5.1)}$$

where $\underline{s}_o$, $\underline{s}'_o$ are the polarisations in the rest-frames before and after scattering and the density matrix, ρ_o, is that appropriate to the rest-frame, namely

$$\rho_o(\underline{s}_o) = \tfrac{1}{2}(1 + \underline{s}_o.\underline{\sigma}) \qquad \text{(II.5.2)}$$

The theory then shows that

$$\tfrac{1}{2}(1 + \gamma_4)b = A\,\tfrac{1}{2}(1 + \gamma_4)a \qquad \text{(II.5.3)}$$

which means that the operator A transforms the large components of the incident wave into the large components of the outgoing wave. In other words the scattering is completely described by the manner in which the large components are affected by the scattering field. This is because the initial and final states are taken to be plane-wave states (or nearly so) whose small components are

determined in terms of the large ones in a way independent of the history of the particle.

From (II.5.1) it follows that

$$\sigma = \text{Trace } (\rho_o A^\dagger) \qquad \text{(II.5.4)}$$

since Trace $\rho_o = 1$.

It is clear from (II.5.1), (II.5.2) and (II.5.3) that A is a 2 x 2 matrix and it may therefore be written as a linear combination of the unit matrix and the three Pauli matrices, thus

$$A = \tfrac{1}{2}(\text{Tr } A + \text{Tr } A\underline{\sigma}.\underline{\sigma})$$

or, as it is usually written,

$$A = F + G\,\hat{\underline{n}}.\underline{\sigma}$$

where $\hat{\underline{n}}$ is a unit vector which, as the detailed calculation of A shows, is normal to the plane of the scattering; $\hat{\underline{n}} = (\underline{p} \times \underline{p}')/|(\underline{p} \times \underline{p}')|$. From (II.5.4) and (II.5.2) one finds

$$\sigma(\underline{p}', \underline{p}, \underline{s}_o) = |F|^2 + |G|^2 + (F^*G + G^*F)\underline{s}_o.\hat{\underline{n}} \ .$$

If electrons are scattered "up" and "down" through equal angles θ (see Figure II.5.1), then

$$\frac{\sigma(p'') - \sigma(p')}{\sigma(p'') + \sigma(p')} = \frac{F^*G + FG^*}{|F|^2 + |G|^2}(\underline{s}_o.\underline{n})$$

$$= S(\theta)\,\underline{s}_o.\hat{\underline{n}}, \text{ say} \qquad \text{(II.5.5)}$$

Thus there results an up-down asymmetry in the scattering which is proportional to the component of polarisation transverse to the plane of scattering.

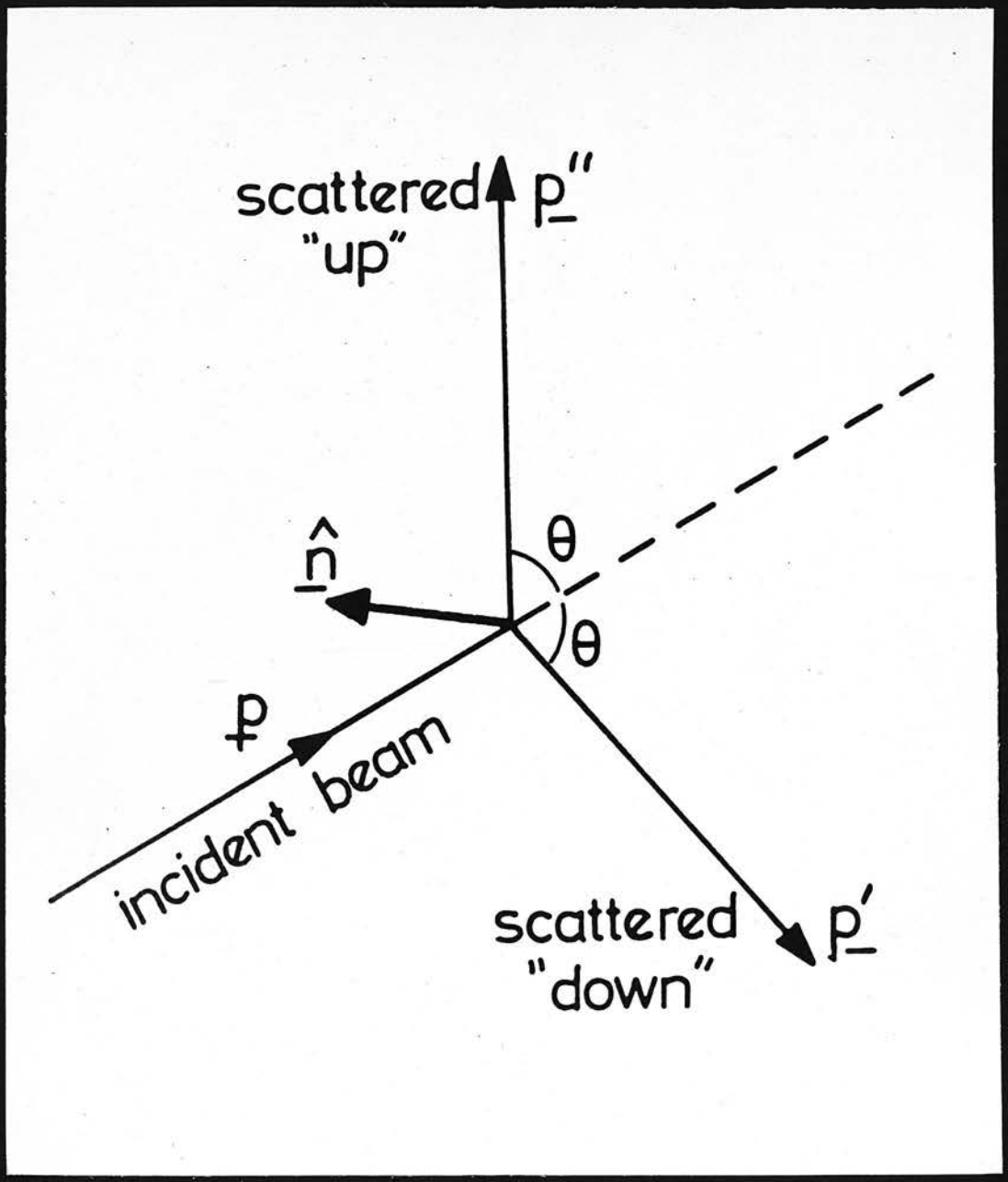

FIG. (II.5.1) Mott Scattering diagram.

This may be pictured classically as arising from the spin-orbit interaction. A relativistic electron moving through the Coulomb field, $\underline{E}$, of the nucleus behaves as though acted upon by a magnetic field $\underline{B} \sim \underline{E} \times \underline{v}$, which, of course, is highly non-uniform and therefore exerts a deflecting force by virtue of its interaction with the electron dipole-moment, $\underline{\mu}$. This spin-orbit force $\underline{F}$ will be given, to order of magnitude, by

$$\underline{F} \sim -\nabla(\underline{\mu}.\underline{B}') \sim -\nabla\, \underline{E}.(\underline{v} \times \underline{\mu}) \quad .$$

In a pure Coulomb field $E \sim -Z\underline{r}/r^3$, and a straightforward calculation leads to

$$\underline{F} \sim -\frac{Zv}{\gamma r^3}\left\{(\underline{s}_o.\hat{\underline{n}})(\hat{\underline{n}}\times\hat{\underline{v}}) - \left[(\underline{s}_o \times \hat{\underline{v}}).\hat{\underline{n}}\right]\hat{\underline{n}}\right\}$$

where $\underline{v}$ is assumed constant for simplicity and Z is the atomic number of the scatterer. Considering that in the typical case of an electron of 100 KeV energy scattered at 90^o the classical impact parameter is only of the order of 1/30 of the de Broglie wavelength, one cannot expect such a result to be other than qualitative. Qualitatively, then, the first term will give rise to an up-down asymmetry of the type discussed above. Three important features of the phenomenon are brought out by this simple formula.

(a) The asymmetry will be greatest for scatterers of high atomic number.

(b) The asymmetry will be greatest for large-angle scattering since the spin-orbit force increases as $1/r^3$ in contrast to the $1/r^2$ dependence of the Coulomb force.

(c) The asymmetry will be a maximum in the energy region where $v/c \sim 0.7$ since this is where v/γ has a maximum. This corresponds to a kinetic energy of the order of 200 KeV.

Only for light elements ($Z/137 \ll 1$) can the amplitudes F and G be given in analytic form (Mott, 1929). Numerical calculations have been carried out for certain elements over a range of values of energy and scattering angle. The most detailed and extensive tabulation is that of Sherman (1956) for aluminium, cadmium and mercury, which was later extended to cover the case of gold (Sherman and Nelson, 1959). The former paper gives values of $S(\theta)$ as well as of $\sigma(\theta)$. The calculations of Doggett and Spencer (1956), for $Z = 6, 13, 29, 50, 82$ and 92, are also useful although they quote only the cross-sections for scattering of an unpolarised beam. These calculations broadly confirm the conclusions reached under the headings (a), (b) and (c) above.

Corrections for screening by atomic electrons have been considered by Bartlett and Watson (1940), Bartlett and Welton (1941) and Mohr and Tassie (1954) and the effects of screening have probably been observed experimentally (Nelson, 1958; Murray, 1960). The magnitude of these effects would be too small to be an important consideration in the present experiment, but in any case would tend to increase rather than diminish the observed polarisation asymmetry.

The work of Pidd and Nelson (1959) and of Bienlien, Felsner, Fleischmann, Guthner, Issendorf and Wegener (1959) constitutes the most satisfactory experimental verification of the predictions of the theory, and in particular of the tables of Sherman. The agreement was sufficiently good for our present purpose in the range of scattering angle from about 80° to 130° for electron energies in the neighbourhood of 120 Kev.

The way in which the characteristics of Mott scattering affect the design of the present experiment will be discussed more appropriately in Section (III.3).

CHAPTER III

THEORY AND DESIGN OF THE EXPERIMENT

(III.1) Outline of the Method

While the experiment of Schupp, Pidd and Crane was in course of preparation a new proposal was put forward by Farago (1958), inspired by the discovery of the non-conservation of parity in weak interactions and the consequent realisation that the beta-particles emitted in radio-active decay processes should be longitudinally polarised (Lee & Yang, 1957; Landau, 1957; Salam, 1957). Farago's method differs from that of the first-named authors in the following two essential respects. First, the polarised beam of free electrons is obtained from a beta-active nuclide directly, thus eliminating the need for an initial Mott scattering. Second, the time spent by the electrons in the homogeneous magnetic field is not measured directly but in terms of the number of cyclotron revolutions performed by the electrons between emission and detection. This number is calculated from the measured strength of an auxiliary electrostatic field, as well as from the magnetic field and electron velocity.

Figure (III.1.1) shows the general scheme of the experiment, as proposed by Farago (loc. cit.)

Beta-particles from a sulphur-35 line-source, S, are injected into a homogeneous magnetic field, B_z, normal to the plane of the diagram and perform nearly circular orbits

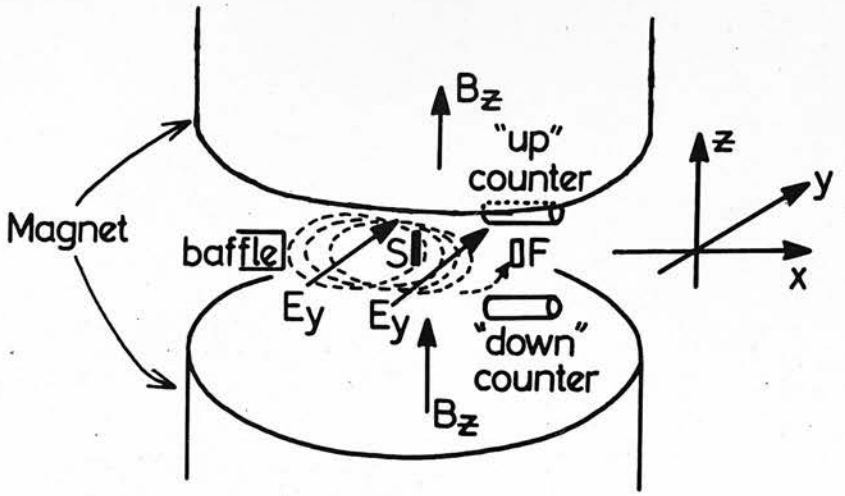

(a)

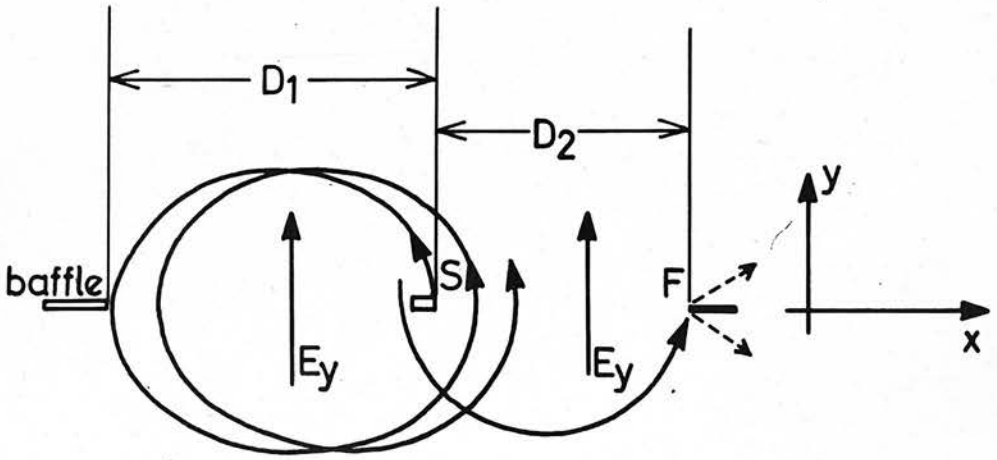

(b)

FIG. (III.1.1) General scheme of the present experiment.

of about 10 cm. diameter. A relatively weak homogeneous electrostatic field, E_y, is applied perpendicular to the magnetic field and to the line joining the source to the "analyser" foil, F. The electric field is too weak seriously to alter the shape of the orbit ($E_y \ll cB_z$) and its effect may be characterised as a "slow drift" of the circular orbit in the direction of the x-axis (the line SF) such that the beam passes the edge of the source holder on completion of the first revolution and strikes the target foil after an integral number, k, of cyclotron orbits given by

$$2\pi k = \omega_c D_2 B_z / E_y \qquad \text{(III.1.1)}$$

where ω_c = cyclotron frequency

$$= e B_z / m_o \gamma , \qquad \gamma = (1 - \beta^2)^{-\frac{1}{2}}$$

D_2 = distance from source to scatterer.

The derivation of this formula is given in Appendix C.

The direction of polarisation of the beam is measured after k orbits by allowing the beam to impinge upon a thin gold foil F and observing the Mott single-scattering asymmetry by means of counters placed above and below the plane of the diagram Fig. (III.1.1)(b). The theory (see Section III.2) shows that the polarisation vector will have performed one complete cycle of its precession relative to the momentum vector after a number of turns,

k_o, given by

$$a.k_o.\Upsilon(v) = \Upsilon(V_o) \simeq 1 \qquad \text{(III.1.2)}$$

where

$a = (g/2) - 1$,

v = electron velocity,

V_o = drift-velocity of orbit for k_o turns

$= E_y/B_z$,

$\Upsilon(x) = (1 - x^2/c^2)^{-\frac{1}{2}}$.

$\Upsilon(V_o)$ differs from unity by a few parts in 10^7 (Section III.2). k_o turns out to be of the order of 750 for the electrons used in this experiment.

The change in polarisation direction relative to the momentum direction per complete orbit is predicted to be independent of the number of orbits, k, and hence the measured asymmetry, written as

$$y(k) = (I_1 - I_2)/(I_1 + I_2),$$

where I_1, I_2 are the rates at which singly-scattered electrons are counted in the two counters, is expected to vary sinusoidally with k, the period being k_o. The procedure proposed by Farago for measuring the g-factor anomaly was, therefore, to vary k (by varying E_y only) and to observe the asymmetry y(k). By fitting a sine curve to the observations one should be able to determine the period k_o, and hence the g-factor anomaly from equation (III.1.2).

An account of the extent to which this programme

has been achieved in practice will form the subject of Chapter V. The remainder of this chapter will be devoted to detailed discussion of the theory and design of the experiment.

(III.2) Calculation of the Orbit and of the Relative Spin Precession Rate.

First we give an elementary calculation of the motion, valid in the non-relativistic approximation.

Let $\underline{v} = \underline{V} + \underline{v}'$,

where $\underline{v}$ is the electron-velocity in the lab-frame, $\underline{V}$ is a constant velocity such that

$$\underline{V} \times \underline{B} = -\underline{E} ,$$

and $\underline{v}'$ is just the difference between $\underline{v}$ and $\underline{V}$.

Since the fields are given by

$$\underline{B} \equiv (0, 0, B_z)$$

$$\underline{E} \equiv (0, E_y, 0)$$

where $E_y \ll cB_z$, we see that

$$\underline{V} = (V_x, 0, 0) = (E_y/B_z, 0, 0)$$

and $V_x \ll c$.

Now the equation of motion is

$$m\dot{\underline{v}} = e(\underline{E} + \underline{v} \times \underline{B})$$

$$\therefore \quad m\dot{\underline{v}}' = e(\underline{E} + \underline{V} \times \underline{B} + \underline{v}' \times \underline{B})$$

$$= e\,\underline{v}' \times \underline{B} .$$

Thus, in a frame of reference moving with velocity V, the motion of the electron is the same as if only the magnetic field were present, namely a circular orbit executed at constant speed $\underline{v}'$. The approximation $V_x \ll c$ is, in fact, well satisfied in the present experiment for even as few as 10 orbits (k = 10). For, using the notation of

Section (III.1) and referring to Figure (III.1.1), we have

$$V_x/|v| \simeq D_2/(\pi D_1 k)$$

$$\simeq 1/(\pi k)$$

Now, for electrons of about 100 KeV,

$$v/c \simeq \tfrac{1}{2} .$$

Therefore $V_x \simeq (1/2\pi k).c$

Hence, for $k = 10$, say,

$$V_x \simeq (1/60).c$$

and $\gamma(V) \simeq 1.00014$.

However, it is well known that, if $E < cB$, one may transform away the electric field by making a Lorentz transformation to the same moving frame of reference as above, the only differences being that the electron now sees a slightly modified magnetic field, $B'_z = B_z/\gamma(V)$, and that its velocity $\underline{v}'$ in the moving frame must be obtained by using the relativistic law for composition of velocities (see Appendices A and B). The picture of the motion which was obtained non-relativistically is therefore confirmed by a relativistic calculation.

Coming now to the calculation of the rate of precession of the polarisation of the electrons relative to their momentum, we only have to apply the results of the general theory discussed in Section (II.4). In order to relate the observed scattering asymmetry to the g-factor anomaly

we need to know the angle $\phi(k)$ which the polarisation vector makes with the momentum vector after k complete orbits, as a function of the g-factor anomaly, a. In terms of the time spent by the electrons in the field we need to know $\phi(kT)$ where T is the period of one complete orbit in the lab-frame. Now in Section (II.4) we saw that

$$d\phi/dt = \Omega = \frac{e}{m_o}\left\{\frac{\underline{E}.\hat{\underline{n}}}{|v|}\left[g/2 - 1 - g/(2\gamma^2)\right] + \hat{\underline{v}}.\underline{B} \times \hat{\underline{n}}(g/2 - 1)\right\} \qquad (II.4.5)$$

where $\hat{\underline{n}}.\hat{\underline{v}} = 0$ and $\hat{\underline{n}}$ lies now in the x-y plane. Therefore we need to calculate

$$\phi(kT) = \int_o^{kT} \Omega \, dt.$$

In the present experiment we have the relations

$$\begin{aligned} \hat{\underline{v}}.\underline{B} \times \hat{\underline{n}} &= B_z \\ \underline{E}.\hat{\underline{n}}/v &= -E_y v_x/v^2 \end{aligned} \qquad (III.2.1)$$

On substitution of these expressions into equation (II.4.5) the integration may be carried out. However, the direct integration is rather heavy and it may be avoided by recognizing that ϕ is actually a Lorentz invariant. For the product $s_\mu(t + T)s_\mu(t)$ of the axial vector s_μ at time t with its value at the later time, $t + T$, where T is defined as before, will be a pseudo-scalar and will therefore be invariant under proper Lorentz transformations.

Evaluating the product in the lab-frame, using

equation (II.4.4) we find

$$s_\mu(t+T)s_\mu(t) = S^2\left[e_{l\mu}\,e_{l\mu}\cos(\phi+\Delta\phi)\cos\phi + e_{t\mu}\,e_{t\mu}\sin(\phi+\Delta\phi)\sin\phi\right]$$
$$= S^2\cos\Delta\phi\ ,$$

where $\Delta\phi$ is the change in ϕ over any one complete orbit. So $\Delta\phi$, and hence $\phi(kT)$, is invariant under proper Lorentz transformations.

We may now write

$$\phi(kT) = \int_o^{kT'} \Omega'\,dt'$$

the primed quantities being evaluated in the moving frame of reference where $\underline{E}' = 0$. In that frame equation (II.4.5) becomes simply

$$\Omega' = \frac{e}{m_o} B_z' \cdot a$$
$$= \Upsilon' a\,\omega_c'$$

where ω_c' is the cyclotron frequency in the field B_z' and $\Upsilon' = \Upsilon(v')$ is constant since the electron sees only a pure magnetic field.

Hence $\phi(kT) = \Upsilon' a\int_o^{kT'} \omega_c'\,dt'$

$$= 2\pi k\Upsilon' a$$

It may be shown by direct Lorentz transformation (Appendix B) that

$$\Upsilon(v) = \Upsilon(v')\cdot\Upsilon(V)\left(1+\frac{\underline{V}\cdot\underline{v}'}{c^2}\right)$$

and since $\Upsilon(v')$ is a constant it may be evaluated at $t = t' = 0$, when the electron is emitted from the source. At that instant, $\underline{V}.\underline{v}' = 0$ and

$$\Upsilon' = \Upsilon(v)/\Upsilon(V) \quad .$$

Hence, finally,

$$\phi(kT) = 2\pi k.\Upsilon(v).a/\Upsilon(V) \quad .$$

There remains the matter of the observed scattering asymmetry. According to equation (II.5.5) this is proportional, for a given scattering angle, θ, to $\underline{s}_o.\hat{\underline{n}}$, the component of polarisation normal to the plane of scattering in the laboratory frame of reference. Since $\hat{\underline{n}}$ is normal to the velocity we have

$$\underline{s}_o.\hat{\underline{n}} = \underline{s}.\hat{\underline{n}} = s_\mu e_{t\mu} = S \sin\phi$$

where $s_\mu = (\underline{s}, s_4)$ in the lab-frame.

Regarded as a function of the number of complete orbits, the asymmetry, $y(k)$ will then be given by

$$y(k) \propto \sin \phi(k) = y_o \sin(2\pi k/k_o) \qquad (III.2.2)$$

where $$k_o = \Upsilon(V)/a.\Upsilon(v) \quad .$$

It is of interest to recall the original argument given by Farago (1958), in obtaining essentially the result just quoted. The reasoning was as follows. Regard the precessing momentum vector of the electron in the moving frame of reference as constituting a clock and let a second clock be defined by the precession of the

polarisation vector relative to the momentum vector in the same frame of reference. Then these clocks are at rest relative to one another and the ratio of their readings should be Lorentz-invariant. In the moving frame the electron experiences a pure magnetic field $B' = B/\Upsilon(V)$ and the ratio of the precession rates, Ω'/ω_c' , had been calculated previously for such a situation by quantum mechanical methods (Mendlowitz and Case, 1955; Carrassi, 1958) giving

$$\Omega'/\omega_c' = \Upsilon(v').a \quad .$$

In fact, as Farago pointed out, this result can also be obtained from a straightforward classical calculation taking account of the Thomas precession (Appendix A). According to Farago's reasoning the same value should be observed in the lab-frame and so the relation

$$\Omega/\omega_c = \Upsilon(v).a/\Upsilon(V)$$

follows as before.

Although the result was correct, the reasoning on which it was based was not completely valid, as was pointed out by Telegdi and Winston (1959). It is quite true that the readings of two clocks which are at rest relative to one another will be in an invariant ratio. The difficulty lies in defining clearly what kind of variable may properly be employed as a clock in special relativity. According to Telegdi and Winston (loc. cit.) any observable that is periodic in time may be admitted as a clock provided that

that the periodicity occurs at the same spece-point in some inertial frame, the proper frame of the clock in question. This is merely an expression of the natural requirement that the interval between two readings of a clock must be time-like. The conditions are satisfied by the momentum vector of the electron in the moving frame of reference (where the orbits are closed circles). If a polarisation clock exists, its proper frame must be the same as that of the momentum clock since this is the only inertial frame in which the polarisation can be observed at the same space point at different times. However, the period T_p' of the polarisation vector must be assumed to be incommensurate with the period T' of the momentum vector, in the absence of any evidence to the contrary. The assumption that the polarisation vector forms a clock is not, therefore, justified. The reason why Farago's final result was correct was, of course, that $\Delta\phi$, the relative precession of the polarisation per complete orbit, is, as we have seen, a Lorentz invariant.

One can see fairly easily what happens when the integration over a complete orbit is carried out. If we evaluate Ω/ω_c from equation (II.4.5) using (III.2.1), we find

$$\Omega/\omega_c = \gamma.a + (V_x/v\gamma)(g/2 - a\gamma^2)\cos\theta$$

where $\cos\theta = \hat{\underline{V}} \cdot \hat{\underline{v}}$.

In the approximation where $Vv \ll c^2$ the first term represents Farago's result and in the same approximation the coefficient of cos θ in the second term can be regarded as a constant. On integrating over a complete period it is clear that the second term gives no contribution.

(III.3) Choice of Experimental Parameters

The choice of values for the experimental parameters was restricted partly by practical considerations such as the size of the available magnet and the availability of suitable radio-active nuclides, and partly by the need to obtain the maximum polarisation asymmetry in the Mott scattering.

Source

We begin quite arbitrarily, by considering the best source-material to use. A suitable nuclide must satisfy the following requirements.

(1) It should be a pure beta-emitter, so that the background count is not unnecessarily increased by gamma radiation.

(2) As large a proportion as possible of the emitted electrons should have energies in region of 100-150 KeV, since this is the energy region in which the Mott asymmetry is greatest at reasonable scattering angles.

(3) The nuclide should be obtainable in carrier-free form so that strong sources may be used without introducing too much source-scattering and depolarisation.

(4) The nuclide should have a reasonably long half-value period (say $t_{\frac{1}{2}} > 30$ days) so that long runs may be carried out without interruption. The only available nuclide satisfying even the majority of these conditions is Sulphur-35 and this was the material chosen for the source.

In respect of condition (2) it falls short of the ideal since the maximum number-density in the beta-spectrum lies at about 45 keV energy, which is too low by a factor of about 3.

Sulphur-35 is a pure beta-emitter with a half-value period of 87.1 days and an end-point energy of 167.4 keV (Connor and Fairweather, 1957). The spectrum is of the allowed shape down to at least 5 keV (Moljk and Curran, 1954). Finally, the beta-particles have been shown to conform to the predictions of the two-component neutrino theory in respect of their polarisation (Murray, 1960). That is, they are longitudinally polarised with

$$S = v/c = \beta$$

(in the notation of Section (II.4)) and with negative helicity.

Figure (III.3.1) shows a plot of $N(\eta)$ against η, where $N(\eta)d\eta$ is the number of electrons per second emitted by a Sulphur-35 source of arbitrary strength (the figures are actually normalised to a source-strength of about 34 μC) with their momenta lying in the range $\eta\, m_o c$ to $(\eta + d\eta)\, m_o c$. The values of $N(\eta)$ were calculated from the formula

$$N(\eta) = f(Z,\eta)(1.3276 - \Upsilon)^2$$

using the Tables for the Analysis of Beta Spectra of the U.S. Department of Commerce (N.B.S. Applied Maths. Series

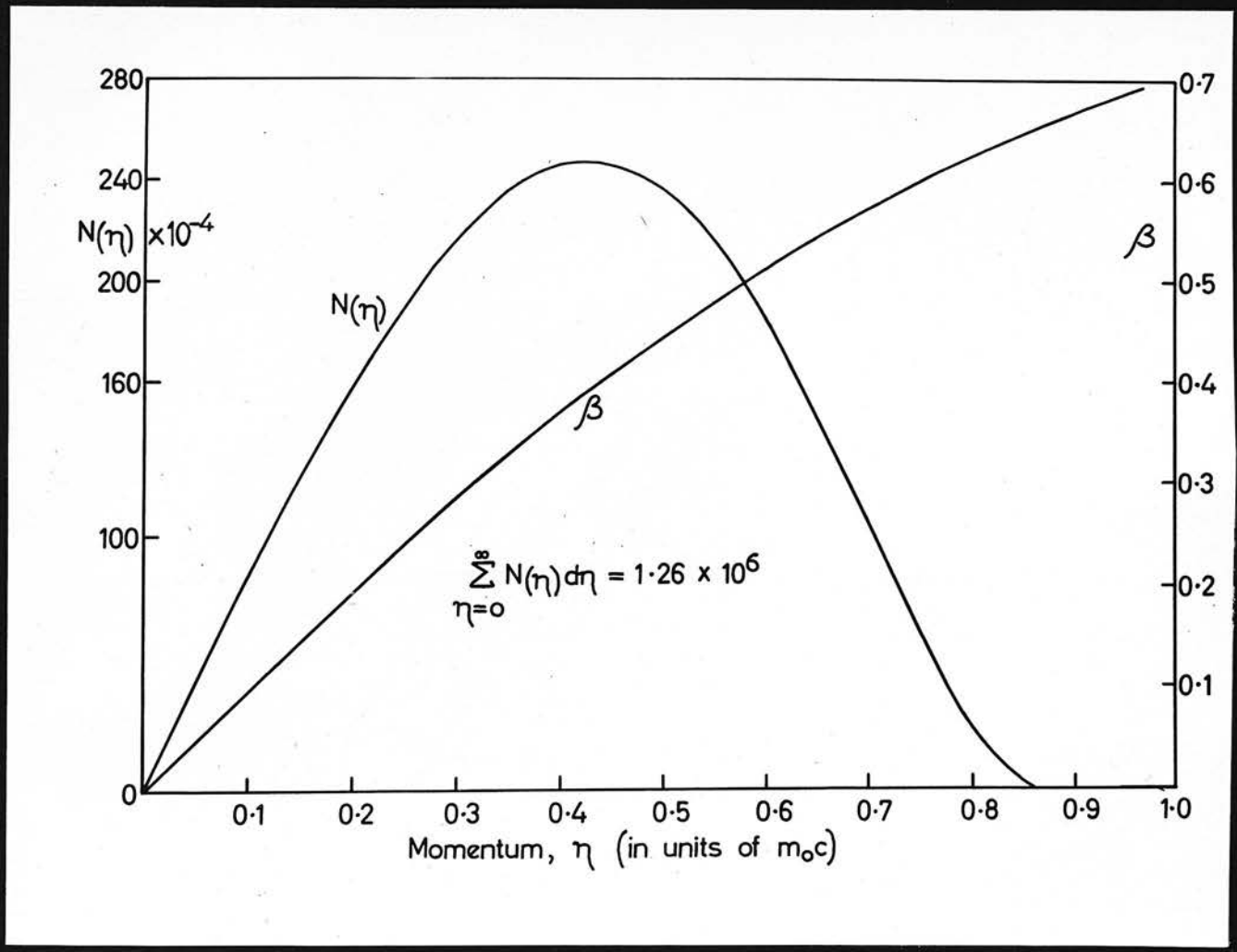

FIG. (III.3.1) Number-density of electrons in the S^{35} spectrum as a function of momentum.

13) to obtain values of the Fermi function $f(Z,\eta)$. The value $\gamma = (1 - \beta^2)^{-\frac{1}{2}} = 1.3276$ at the end-point of the spectrum corresponds to the end-point energy of 167.4 keV given by Connor and Fairweather (1957).

The magnitude, β, of the polarisation has also been plotted on figure (III.3.1) as a function of η .

Electron Energy

The next point which needs consideration is the optimum electron energy for the experiment. This depends on a number of factors, which may conveniently be combined to give a "figure-of-merit", M, a function of electron-energy only. This figure-of-merit will be defined to be proportional to the maximum observed scattering asymmetry as well as to the actual total single-scattering rate and to contain the entire energy-dependence of the asymmetry and the scattering-rate (as far as it is amenable to calculation). The factors contributing to M will now be discussed in turn.

(1) Polarisation

The scattering asymmetry will be proportional to the amplitude, β, of the polarisation of the electron-beam, assumed mono-energetic.

(2) The beta-spectrum

The total single-scattering rate will be proportional to the number-density, $N(\eta)$ of electrons emitted by the source into a beam of the chosen momentum, η . The greater

the beam intensity, the less time will be required to attain a given accuracy in the asymmetry measurement. Hence this factor should be included in the expression for M. In practice, of course, the beam will be characterised by a finite range of momentum about a mean value, $\bar{\eta}$, given by

$$\bar{\eta} = \left(\int_{\eta_1}^{\eta_2} \eta\, N(\eta)\, d\eta \right) \Big/ \left(\int_{\eta_1}^{\eta_2} N(\eta)\, d\eta \right) .$$

If the range of momentum, $\eta_2 - \eta_1$, is not too large we may replace $N(\eta)$ in the formula for the figure-of-merit by $N(\bar{\eta})$.

(3) <u>The asymmetry factor, S(θ)</u>

According to the Mott-scattering theory the asymmetry for a given electron-energy is proportional to a certain function of the angle of scattering, θ. This function, S(θ), (see Section (II.5)), has been tabulated by Sherman (1956) for a series of values of scattering angle and of β. Table (III.3.1) summarises the relevant parts of Sherman's table for $Z = 80$.

Sherman and Nelson (1959) have given values of S(θ) and of the scattering cross-section for a gold target ($Z = 79$) at two energies only (75 keV, $\beta = 0.49$; 121 keV, $\beta = 0.59$). However, the values for $Z = 79$ do not differ significantly from those given in Tables (III.3.1) and (III.3.2), at least for the present purpose.

TABLE (III.3.1)*

Mott-scattering Asymmetry-Factor S(θ) for various β.

(Z = 80)

θ \ β	0.4	0.5	0.6
60°	2.2×10^{-3}	-3.8×10^{-2}	-6.2×10^{-2}
75°	-0.104	-0.143	-0.160
90°	-0.234	-0.260	-0.270
105°	-0.333	-0.356	-0.367
120°	-0.372	-0.400	-0.424

TABLE (III.3.2)*

Differential cross-section, $d\sigma/d\Omega$, for Mott Scattering, in units of 10^{-21} cm.^{2} per steradian

(Z = 80)

θ \ β	0.4	0.5	0.6
60°	74.5	31	14.2
75°	38	16	7.25
90°	23.5	9.6	4.3
105°	16.6	6.56	2.8
120°	13	4.9	2

* From Sherman, (1956).

(4) The scattering cross-section

The more scattered electrons there are for a given beam intensity the less time will be required to attain a given accuracy in the asymmetry measurement. Hence a factor $d\sigma/d\Omega$ should be included in the figure-of-merit; this cross-section is again a function both of energy and of scattering angle. Table (III.3.2) gives the relevant values from Sherman's table for Z = 80.

(5) Counting efficiency

Finally we come to the most difficult factor to calculate, namely the variation of the counting efficiency with electron energy. Both Geiger-Müller counters and scintillation counters were used at different stages of the experiment. Unfortunately the energy region over which there is an appreciable number of electrons in the S^{35} spectrum is also the one in which the efficiencies of both types of counter fall off rapidly with energy. As the efficiency of a Geiger-Müller counter in these circumstances depends mainly on the transmission of its mica window and as observations of this quantity are available in the literature, we consider the latter system for purposes of calculation. We characterise the transmission of a window of given thickness by a function $f(\beta)$, the fraction of the incident beam transmitted. Values of this function may easily be calculated from data given by

Saxon (1951) for a mica window of about 1.3 mg./cm.^{2} thickness. In fact his data are fitted very well over a wide range of energy by the formula

$$1 - f(\beta) = \exp(- E/E_o)$$

where E is the electron kinetic energy and the formula is fitted to Saxon's data at a particular value, E_o, of the energy. The figures given in Table (III.3.3) were calculated from this formula with E_o = 97.4 keV. It is believed that these figures would give a fair indication also of the efficiency of the scintillation counters used in the present experiment, although their efficiency probably falls off much more rapidly at the lowest energies.

TABLE (III.3.3) *

Transmission of 1.3 mgm./cm.^{2} mica window as a function of electron energy

β	E (keV)	f(β)
0.4	46.9	0.56
0.45	61.2	0.66
0.5	79.4	0.75
0.55	100.9	0.83
0.6	128	0.90

* From data given by Saxon, (1951).

TABLE (III.3.4)

Figures-of-Merit for Forward (M_F) and Backward (M_B) Scattering

E(keV)	β	$\eta = \beta\gamma$	$N(\eta)$	$\frac{d\sigma(\theta)}{d\Omega} \times S(\theta)$	$f(\beta)$	M_F	M_B
				75° / 105°			
46.9	0.40	0.435	246	3.95 / 5.50	0.56	218	303
61.2	0.45	0.504	235	2.82 / 3.55	0.66	197	248
79.4	0.50	0.577	200	2.29 / 2.34	0.75	172	176
100.9	0.55	0.660	139	1.62 / 1.55	0.83	103	98
128	0.60	0.750	61	1.16 / 1.03	0.90	38	34

The factors (1) to (5) above can now be combined to give

$$M = \beta . N(\eta) . S(\theta) . (d\sigma/d\Omega) . f(\beta)$$

It will be convenient to calculate two sets of values of M, one characteristic of backward scattering and one of forward scattering. The former, M_B, will be obtained by taking $\theta = 105^\circ$ and the latter, M_F, by taking $\theta = 75^\circ$. Then Table (III.3.4) gives the results of the calculation.

The following conclusions can be drawn from this table.

(1) The extra asymmetry available (in theory) at backward scattering angles compensates for the lower scattering cross-section except at the very lowest energies; so that, in practice, the choice of backward or forward scattering must be made on some other basis, such as signal-to-noise ratio.

(2) Because of the rapid falling off of numbers in the β-spectrum of S^{35} it is hardly worth considering electron energies above about 100 keV, despite the better counting. efficiencies. This emphasises again the unsuitability of S^{35} in this one respect.

(3) Very little advantage can be gained by going to energies below about 80 keV in forward scattering, even using Geiger-Müller counters.

(4) With backward scattering using Geiger-Müller counters one might go as low as 60 keV but with scintillation

counters this energy would certainly be too low. In addition it should be remembered that with both types of counter, when the efficiency falls substantially below 100%, there is likely to be great difficulty in obtaining a pair of counters with nearly equal efficiencies, such as are required for making satisfactory asymmetry measurements.

It is concluded then, that the measurements should be carried out using an electron energy in the range 80-100 keV.

Scattering Foils.

Various thicknesses of gold foil were used as targets during the course of the work but for the purpose of measuring Mott scattering asymmetries it is usually considered necessary to use rather thin foils. In measurements of beta-particle polarisation in connection with parity non-conservation it has become customary to use a series of foils of thicknesses ranging from 0.1 mg./cm.^{2} to 1.0 mg./cm.^{2} and to extrapolate the measured asymmetries to zero foil thickness. An absolute measurement of the Mott asymmetry was not called for in the present experiment and, of course, the total counting rate may be expected to fall off approximately in proportion to any decrease in foil thickness. Therefore the thinnest foils need not be the best for this purpose. A brief discussion of two studies of the effect of foil thickness will now be given,

with a view to estimating the optimum foil thickness. Cavanagh et al. (1957) suggested that the spin-dependent asymmetry in their experiment should depend on foil thickness according to a formula of the type

$$a_{obs.} = a/(1 + C.t) \qquad \text{(III.3.1)}$$

where "a" and "$a_{obs.}$" were, respectively, the true and observed spin-dependent asymmetries, t was the foil thickness and C was a constant. On plotting the reciprocal of $a_{obs.}$ against t, they found that the points lay very nearly on a straight line whose equation was

$$1/a_{obs.} = C_1 + C_2\, t \quad ,$$

where $C_1 = 6.4$

$C_2 = 16.9$ per mg./cm.^{2}.

On the other hand Murray (1960) found that his observations were consistent with a straight line whose equation was

$$a_{obs.} = C_1' - C_2'\, t$$

where $C_1' = 0.22$

$C_2' = 0.078$ per mg./cm.^{2}.

Murray's observations could, in fact, almost equally well have been fitted by a straight line on a plot of reciprocal asymmetry against thickness, Figure (III.3.3). In that case the gradient of the line would be

$$C_2 = 2.4 \text{ mg./cm.}^2.$$

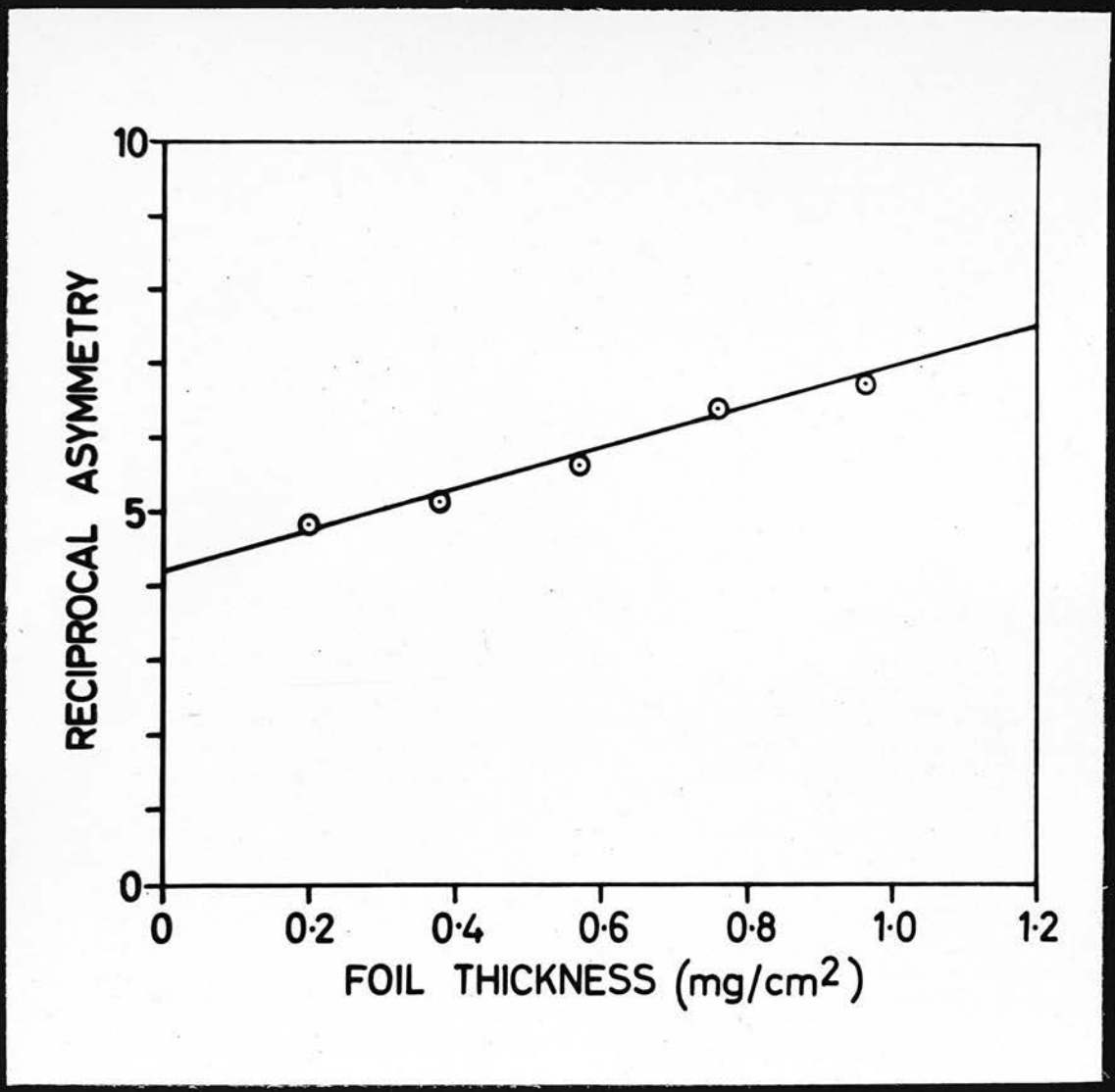

FIG. (III.3.3) Plot of reciprocal asymmetry against foil thickness. (Observations of Murray, 1960).

The considerable discrepancy between this and the result obtained by Cavanagh et al. can probably be explained as being due to the fact that the latter workers observed electrons at a scattering angle of 90° from a foil which was itself set at 60° to the incident beam, while Murray observed electrons at an average scattering angle of 135° from a foil which was set at 90° to the incident beam.

If we assume that the total scattering rate from a foil is proportional to the foil thickness, we may write

$$N_1 + N_2 = kt$$

where N_1, N_2 are the numbers of particles scattered "upwards" and "downwards" respectively and k is a constant.

But $$a_{obs.} = \frac{N_1 - N_2}{N_1 + N_2} \sim 0.1,$$

and to achieve the best statistical accuracy in the asymmetry one should maximise $N_1 - N_2$.

We have, using the formula of Cavanagh et al.,

$$N_1 - N_2 = kt \cdot \frac{a}{1 + C\,t}$$

and this expression increases monotonically with t. However, there will be little to be gained in going beyond that value of t where $Ct \sim 3$, say.

With the values given by Cavanagh et al. this leads to $t \sim 1$ mg./cm.^{2}. On the other hand, using Murray's linear formula, we obtain

$$N_1 - N_2 = kt(C_1' - C_2't)$$

and this is a maximum when

$$t = C_1'/2C_2' = 1.4 \text{ mg./cm.}^2$$

With foil thicknesses greater than 1 mg./cm.^{2}, however, the assumption that the number of scattered particles is proportional to thickness is rather questionable. If a particle penetrates a distance x into the foil before scattering and is then scattered through, say, 110°, it must penetrate a further thickness of about 3x in order to reach the counter. Although this effect is difficult to allow for quantitatively, there is probably no advantage to be gained in going beyond 1 mg./cm.^{2} for the foil thickness. Further discussion of the effects of foil thickness will be given in the context of the observations (Section (V.3)).

Effective Aperture

It has already been remarked that the apparatus behaved in some respects like a 180° beta-ray spectrometer, that is to say there was momentum-selection incorporated. This is illustrated in Figure (III.3.2), in which the drift-rate of the orbits is assumed small.

Electrons of momentum greater than $eBD_1/2$ were intercepted by the baffle after the first half turn and were thus removed from the beam. Electrons of momentum less than $eBL_2/2$ were intercepted by the rear edge of the source-holder after a number of turns depending on their actual momentum. The range of momentum transmitted

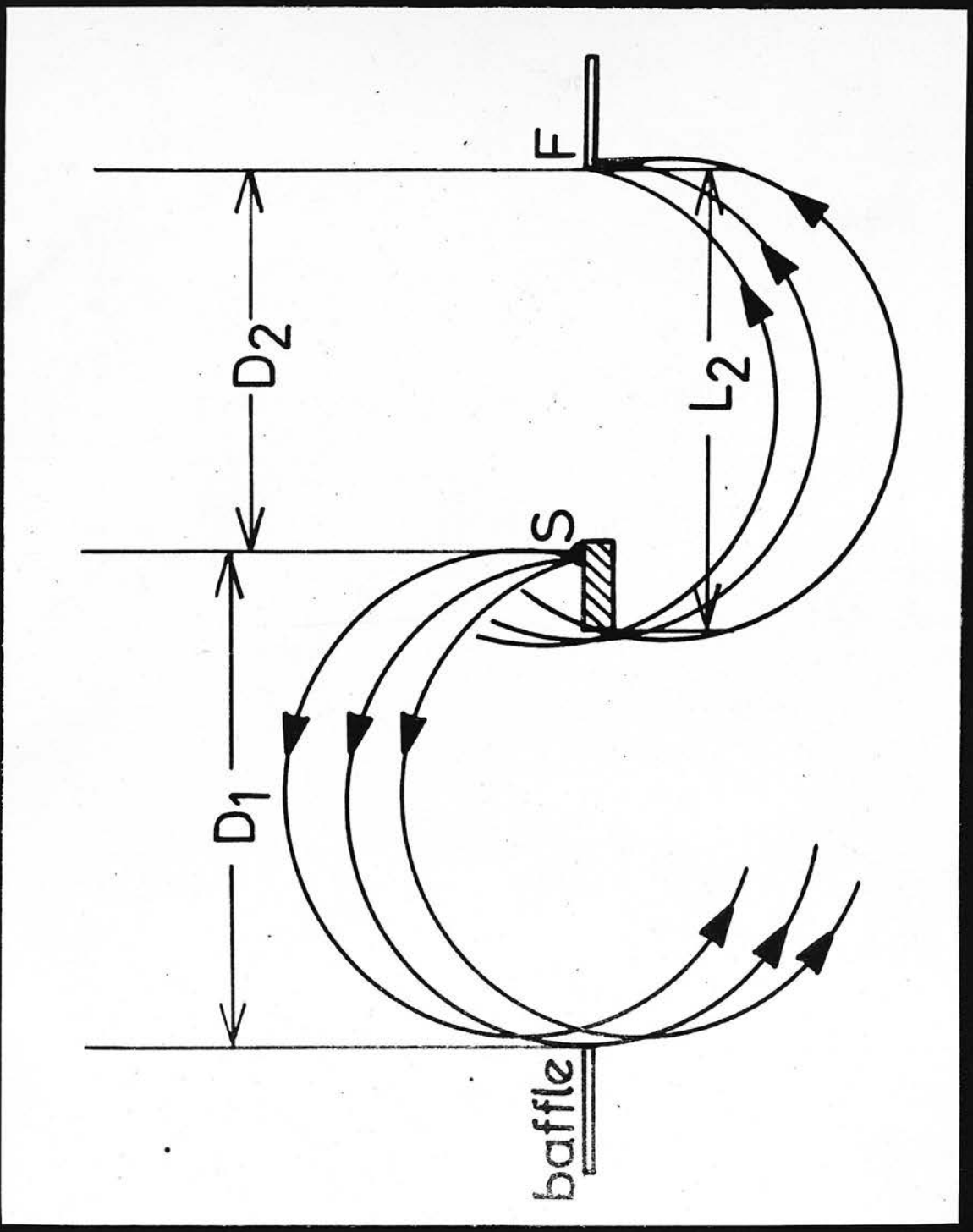

FIG. (III.3.2) The Apparatus as a β-spectrometer.

was therefore proportional to an "effective aperture" given approximately by $D_1 - L_2$. Normally the distance D_1 was fixed and the effective aperture could be adjusted by moving the source-holder and baffle relative to the foil. Now we have already seen (Equation (III.1.1)), that the number of orbits, k, executed by the beam for given fields will be inversely proportional to $\gamma = (1 - \beta^2)^{-\frac{1}{2}}$. Thus corresponding to the finite range of energy transmitted by the effective aperture, there will be a range Δk of k at the target. The question arises how far one may open the effective aperture (to increase the beam intensity) without at the same time causing an excessive spread in k. We have

$$k \propto 1/\gamma$$

and thus $$\frac{\Delta k}{k} = - \frac{\Delta \gamma}{\gamma}$$

where Δk, $\Delta \gamma$ are corresponding ranges of k and γ, assumed small.

Now, writing η for the electron momentum in natural units,

$$\eta = \beta\gamma$$
$$= (\gamma^2 - 1)^{\frac{1}{2}}$$

$$\therefore \quad \Delta\eta \simeq \tfrac{1}{2}(\gamma^2 - 1)^{-\frac{1}{2}} \cdot 2\gamma \cdot \Delta\gamma$$

or $$\Delta\eta/\eta \simeq \frac{1}{\beta^2}(\Delta\gamma/\gamma)$$

Hence $$\Delta\eta/\eta \simeq - \frac{1}{\beta^2}(\Delta k/k)$$

$$\simeq - 4(\Delta k/k)$$

for electrons of about 100 keV energy. If we call the effective aperture A,

then $A/D_1 \simeq \Delta\eta/\eta$

and so $A \simeq \frac{4D_1}{k} \cdot \Delta k$ in magnitude.

Now the measured asymmetry is expected to vary as $\sin(2\pi k/k_o)$ (equation (III.2.2)), so the systematic error arising from the finite value of Δk will be primarily a function of Δk itself and not of the fractional spread, $\Delta k/k$. For any fixed value of A the range Δk will increase without limit as k increases. One must therefore fix the maximum allowable aperture by choosing a maximum allowable range Δk_{max} in conjunction with the greatest value k_{max} of k likely to be encountered in the experiment. The aperture having been fixed at that value, the range Δk will then be less than Δk_{max} for all k less than k_{max}. Let us take $k_{max} \sim 1000$ as a reasonable estimate. Then

$$A_{max} \simeq \frac{4 \times 8}{10^3} \cdot \Delta k_{max} \quad \text{cm.}$$

for an 8 cm. diameter orbit. A safe value for Δk would be $k_o/25 \simeq 30$.

Thus $A_{max} \simeq 9$ mm.

This would make $L_2 \simeq 80 - 9 = 71$ mm.

and $D_2 \simeq 62$ mm.

Choice of values for the Orbit Diameter and Magnetic and Electric Fields

The orbit diameter, D_1, was restricted by the size of the region over which the necessary field homogeneity could be achieved and was normally about 8 cm. Once this and the momentum, η, had been chosen the required magnetic field could be found from

$$B_Z = \frac{m_o c}{e} \cdot (2\eta / D_1)$$

$$= 3.41 \ \eta / D_1 \quad \text{weber/m}^2,$$

where D_1 is measured in mm. Typically D_1 = 80 mm., η = 0.65 and B = 277 gauss.

From equation (III.1.1) we then have

$$k = eD_2 B_Z^2 / 2\pi \, m_o \, \gamma E_y \qquad \text{(III.3.2)}$$

and this determines the values of E_y required for various orbit numbers, k.

Vacuum Requirement

If the electrons perform 1000 orbits each of radius 4 cm. their total path in the vacuum will be 250 m. If an electron suffers even a small deviation because of gas scattering it is likely to be lost from the beam. The pressure must therefore be reduced to a value at which the probability of a scattering occurring in a path length of 250 m. is quite small. An order-of-magnitude calculation can be carried out by making the reasonable assumption

that the cross-section for scattering of a relativistic electron by a gas molecule is πr^2 where r is $\frac{1}{2}\text{Å}$. If we define a "mean free path", λ, by the relation

$$I = I_o \exp(-x/\lambda)$$

where I_o is the initial beam intensity and I is the intensity of that part of the beam which traverses a distance x without being scattered, then an elementary calculation yields the relation

$$p(\lambda) \simeq 1.2 \times 10^{-3}/\lambda \text{ mm. Hg. per metre}$$

for the pressure required to give a mean free path λ. A mean free path of 1500 m. would be ample to ensure negligible attenuation over a path length of 250 m. According to the above formula a pressure of the order of 10^{-6} mm. Hg. would be necessary to achieve this. Conversely, at a pressure of 2×10^{-6} mm. Hg. (Section (IV.4)) the mean free path would be of the order of 750m. If the value chosen for the effective scattering radius of the gas molecule were too small by a factor of 2, then this last estimate would have to be reduced by a factor of 4 to about 200 m.

(III.4) Estimated Genuine Counting Rate

If the magnetic field is homogeneous there will be strong-focussing of the electron beam in the x-y plane (Fig. (III.3.2)), as in a 180° beta-ray spectrometer. Two types of focus occur in such a system. The first is at the 180° point and is a perfect focus for monoenergetic electrons only in the paraxial approximation. The "effective aperture" stops were located at this kind of focus. The second is at the 360° point and is a perfect focus, in principle, for monoenergetic electrons emerging from the source at any angle. The presence of the electrostatic field does not affect this property (Appendix B). The position of this focal point (always on the x-axis) changed with energy only to the extent that the electron mass varied with energy (Appendix C). Figure (III.4.1) shows how the "angular aperture", 2θ, of the beam was limited in principle by the spacing of the two parallel plates which provided the electrostatic field. We find easily

$$\sin\theta = \frac{BC}{BS} = (L_3/r_1) - 1 \quad .$$

Typical values might be $r_1 = 4$ cm., $L_3 = 6.3$ cm., giving $\sin\theta = 0.575$ and $2\theta = 70^{\circ}$. In most cases the beam was restricted in practice to an angular aperture of about 30° by the form of the source-holder and the latter figure will be accepted for the purpose of the following calculation.

An estimate will now be given of the expected beam

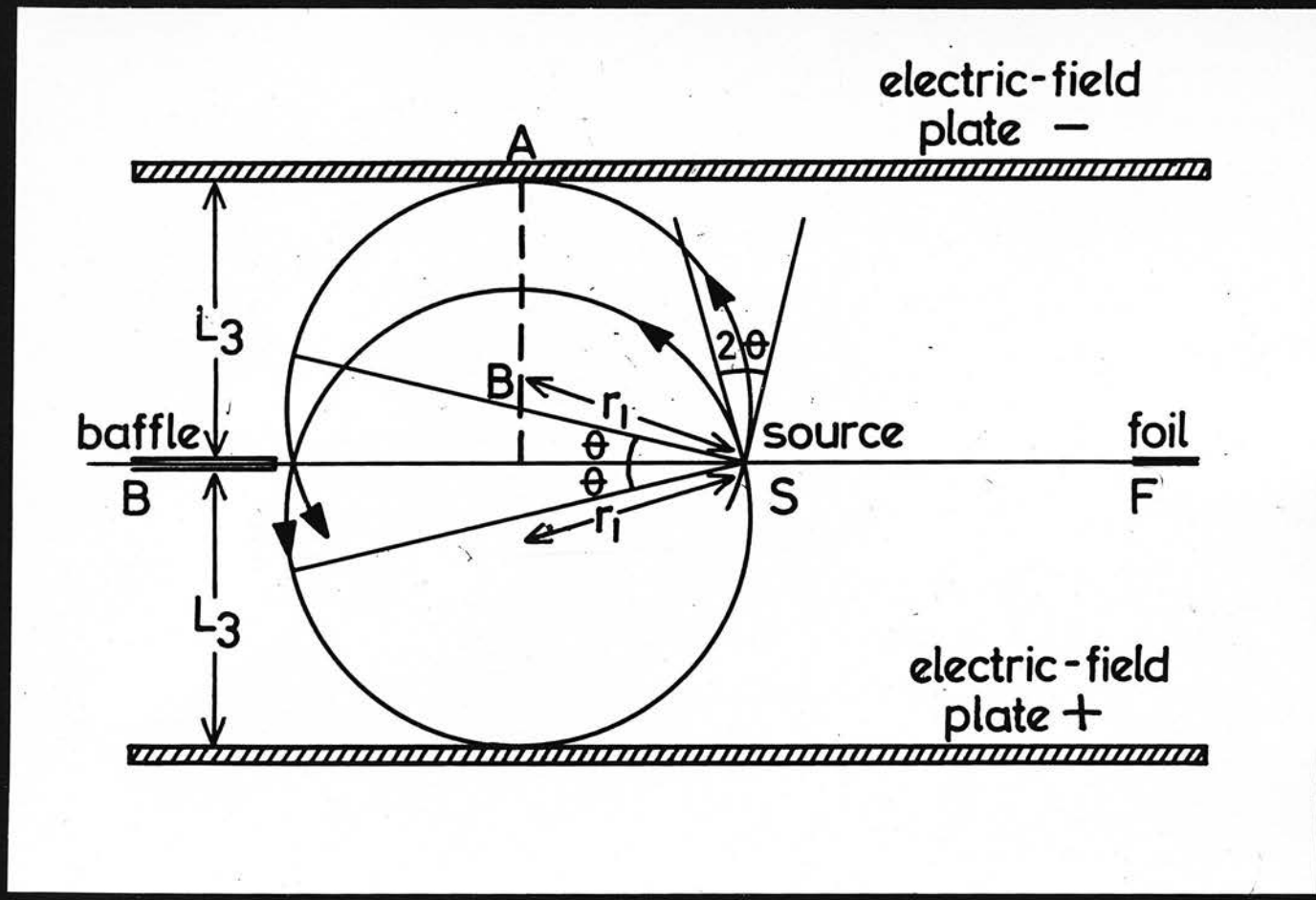

FIG. (III.4.1) Maximum angular aperture of the beam in the x-y plane.

intensity at the target under the assumption of a homogeneous magnetic field; that is to say, there is no other form of focussing than the one just mentioned. Let us assume a source-strength of 10 millicuries of sulphur-35 and an electron energy of 90 keV. Then the momentum, in units of $m_o c$, is $\eta = 0.62$ and, if the effective aperture is set so that $\Delta\eta/\eta \sim 1/10$,

$$\frac{N(\eta)\,\Delta\eta}{\int_o^\infty N(\eta)\,d\eta} = \frac{170 \times 0.062}{126} \qquad \text{(Fig. (III.3.1))}$$

$$= 0.084.$$

The source, assumed for this purpose to be a point source, emits electrons into an effective solid angle, $\Delta\Omega$, defined by the angular aperture of the beam in the x-y plane (because of the 360° focussing) together with the angle subtended by the target foil at the source. Taking an orbit diameter of 8 cm., an angular aperture $2\theta = 30^\circ$ and a foil length of 2 cm. (in the z-direction), one finds that, if the beam executes 200 orbits,

$$\Delta\Omega \simeq 2 \times 10^{-4} \text{ steradian.}$$

A source of 10 mC strength emits about 4×10^8 particles of all energies into all directions per second. Hence the initial beam intensity will be

$$I_o \simeq \frac{4 \times 10^8 \times 0.084 \times 60 \times 2}{4\pi \times 10^4} \text{ electrons per min.}$$

$$= 32{,}000 \text{ electrons per minute.}$$

There are two reasons why fewer particles than this should actually reach the target. One is that electrons from some parts of the source may not be able to pass the edge of the source-holder on completion of their first orbit. For 200 orbits, the drift-distance per orbit would be about $^1/_3$ mm. and it would be impractical to have more than about a tenth of the source-material lying within this distance from the edge (Section (IV.1).

The second reason is that gas scattering will deflect some particles out of the beam. This is difficult to allow for quantitatively, but it is believed (Section (III.3)) that the effective mean-free-path at the pressures normally achieved would be of the order of 200 metres at worst. Since the actual path length assumed above is 50 metres, this effect leads to a decrease in the beam intensity by a factor of only about 0.8.

Finally, then, we arrive at a figure of about 2500 electrons per minute striking the target.

To see what this means in terms of the observed single-scattering rate, N, we write

$$dN = I \cdot \frac{d\sigma}{d\Omega}(\theta) \cdot \frac{l\, dy \sin\theta}{r^2} w.t.dz$$

where I = incident beam intensity = 2500 per min.

l = width of counter "window"

w = width of foil in x-direction

t = number of scattering centres

and dz, dy refer to typical small regions of foil and counter window traversed by electrons (see Figure (III.4.2)).

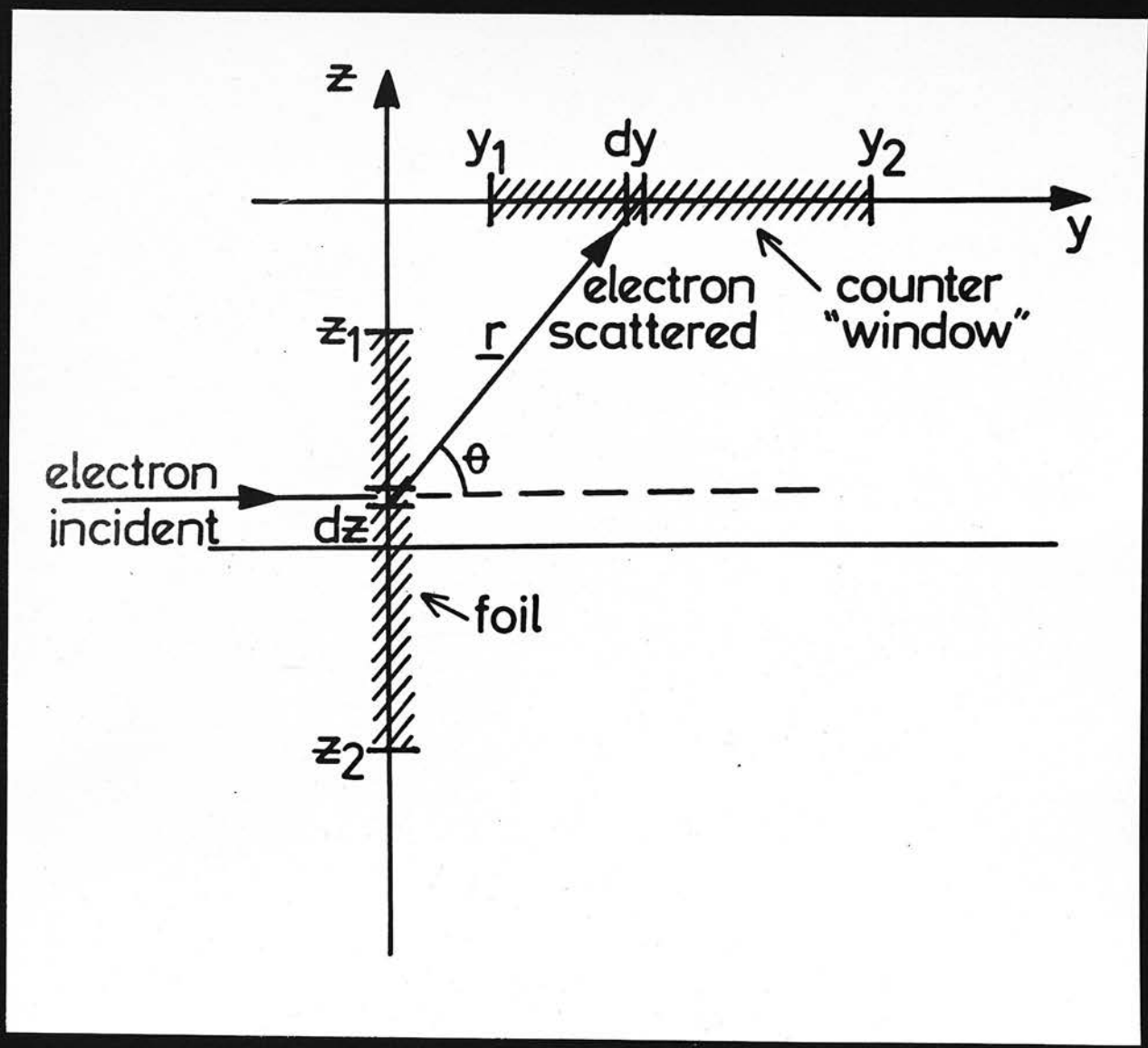

FIG. (III.4.2) Geometry of scattering foil and counter window.

Now $\sin\theta = z/r$

$$r^2 = y^2 + z^2$$

Hence $$N = I\,l\,wt \int_{y_1}^{y_2}\int_{z_1}^{z_2} \frac{d\sigma}{d\Omega}(\theta)\ \frac{z\,dz\,dy}{(z^2+y^2)^{3/2}}$$

This integral may be computed analytically if we assume

$$\frac{d\sigma}{d\Omega}(\theta) = \text{constant} = \overline{\frac{d\sigma}{d\Omega}}\ , \text{ say,}$$

over the range of scattering angle in which we are interested. Reference to Table (III.3.2) shows that this is fairly well justified for backward scattering in the range $90^\circ < \theta < 120^\circ$.

If we choose the values

$$z_1 = 0.5 \text{ cm.} \ ; \ z_2 = 2.5 \text{ cm.}$$

$$y_1 = 0.2 \text{ cm.} \ ; \ y_2 = 1.0 \text{ cm.}$$

we find

$$N = 0.7\ I\,l\,w\,t\ \overline{\frac{d\sigma}{d\Omega}}$$

Taking $\overline{\frac{d\sigma}{d\Omega}} = 6 \times 10^{-21}$ cm.^{2}/stdn., we find, for scattering from a gold foil of thickness 0.35 mg./cm.^{2} and width $w = 2$ mm. into a counter window of width 5 mm.,

$$N = 0.7 \times 2500 \times 0.5 \times 0.2 \times \frac{0.35 \times 10^{-3}}{200} \times 6 \times 10^{23} \times 6 \times 10^{-21} \text{ electrons per min.}$$

$$= 1 \text{ electron per minute.}$$

Experimentally (see Section (V.2)), it was usually found that the background counting rate was of the order of 100 per minute. Clearly, therefore, some means was

required of increasing the genuine counting rate relative to the background in order that the experiment should be feasible.

Two possibilities present themselves. One may seek to increase the beam strength by introducing focussing in the z-direction as well as in the x-y plane or one may try to improve the signal-to-noise ratio by introducing energy selection of the scattered electrons. Let us consider the latter possibility first.

Energy Selection after Scattering

In the work of Nelson and Pidd (1959) on Mott double scattering, the use of an electrostatic energy analyser to select elastically scattered electrons resulted in a substantial improvement in the observed scattering asymmetry, as well as a reduction in background. Again, it has sometimes been the practice in measuring beta-particle polarisation to employ some form of energy selection after the Mott scattering, (Cavanagh et al., 1957). The best energy resolution would be obtained by using a magnetic or an electrostatic analyser. The former was ruled out for the purposes of the present experiment because of the inevitable disturbing effect on the main magnetic field (which cannot itself be used for energy selection after scattering because the scattered particles move nearly parallel to the field.) The latter was ruled out, not only because of its disturbing effect on the fields, but also because of the lack of space to

accommodate such a device between scatterer and counter.

Energy selection in the counters themselves remains a more practical possibility. Proportional counting was not feasible because of the incompatible combination of thin window and high gas pressure required - the former to transmit low-energy electrons without degrading their energy spectrum, the latter to stop them in the confined space available. With a scintillation counter, on the other hand, neither of these problems arises and, within limits, the output is proportional to the electron energy. Unfortunately, because of the need for fairly long light-guides and the rather poor geometry for light collection it was not possible in practice to achieve sufficient resolution to be able to discriminate efficiently between elastically scattered electrons and lower energy background electrons (see Sections (IV.5) and (V.2)).

In any case, no matter how good the energy selection, the problem remains of noise in the counters themselves and of natural background.

A much more fruitful approach to the problem of beam intensity was found to be the alternative one of introducing weak focussing in the z direction.

(III.5) Focussing

Magnetic focussing of the beam in the z direction might be expected to improve the beam intensity very substantially. Because the orbits drift in the x-direction, the focussing field should have the corresponding translation symmetry while in the y-z plane it should have the typical "betatron shape" (Figure III.5.1)). An approximation to such a field could most conveniently be set up in the present experiment by passing current through a pair of rectangular coils, one set against each pole-face, in such a sense as to augment the main field of the magnet. With such an arrangement the increase in the main field would be greater at the pole-faces than in the plane lying mid-way between them (referred to below as the "median plane"), giving the desired field shape apart from some inevitable, but not necessarily detrimental, end-effect due to the finite length of the coils. However, it should be remembered that the same disadvantages will attach to this technique as to the similar technique used by Schupp, Pidd and Crane (1961) (Section (I.4)). Therefore it will be desirable that the degree of field inhomogeneity introduced by the shimming coils should not amount to more than about one or two parts per thousand of the main field. Thus weak-focussing in the z-direction will be the most that one can hope for.

The results obtained experimentally with such a system will be discussed in Section (V.1), and we conclude this section by remarking that a theoretical investigation

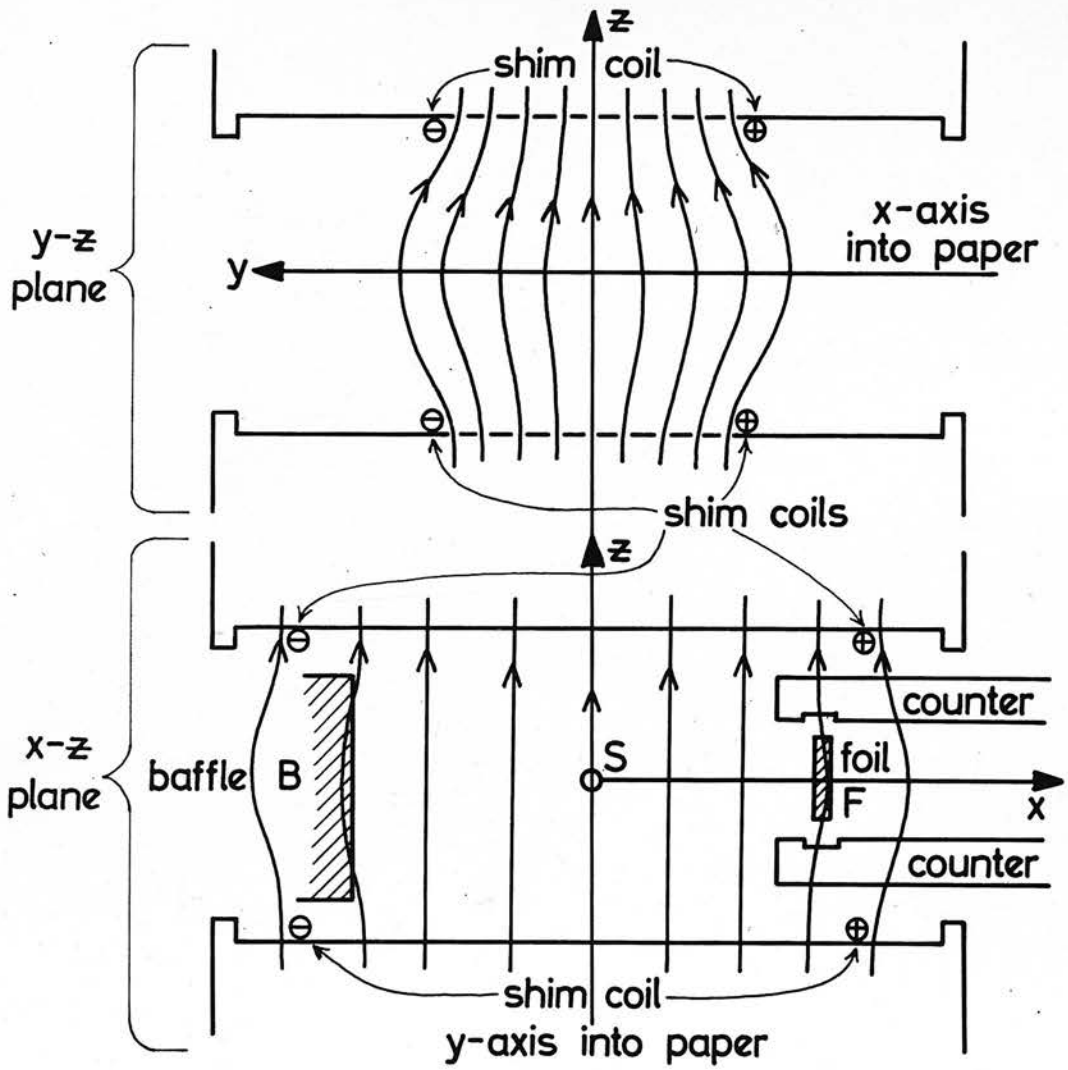

FIG. (III.5.1) Magnetic Field Configuration for focussing in the z-direction.

has recently been made into the weak focussing of electrons in fields of the type described above (Farago, 1961), in particular for the case of the trochoidal motion in crossed fields. In that paper it is shown that the essential features of the trochoidal orbit can be preserved if the orthogonality between the two fields is preserved. However, the focussing properties depend on the shape of the magnetic field only, and if this does not deviate too much from homogeneity it is possible to have focussing in the z-direction as well as in the x-y plane.

Of course the respective periods of small amplitude oscillations about the equilibrium orbit (which must lie in the median plane) are not, in general, commensurate. A particular configuration of crossed fields, which can be described in terms of circular and hyperbolic functions, is fully analysed in the paper just quoted. The properties of the equilibrium orbit are worked out in detail, and the conditions for stable oscillations about the equilibrium orbit are given. It is shown that neither the foci produced by oscillations in the median plane nor those produced by oscillations normal to this plane are spaced at distances which are integral multiples of the circumference of the equilibrium orbit. Although the field configuration chosen for analysis would be difficult to produce experimentally it is not unreasonable to conclude that a similar type of focussing would result with any field of the same general shape provided it did not depart

too much from homogeneity. One would not expect to be able to observe sharp focal lines in practice, of course, but, as Farago pointed out (loc. cit.) the value of using this type of field is that it enables one to confine a considerable part of the initial beam in the z-direction over distances large compared with an orbit diameter.

Finally, we note that, although it is easy to produce a suitable magnetic field configuration with the aid of shimming coils, it is quite another matter to produce a corresponding electrostatic field satisfying the orthogonality relation. Fortunately, the electrostatic field in the present experiment is in any case small compared with the magnetic field; so, if a uniform electric field is set up, any deviation from orthogonality will be a small quantity of second order and should not spoil the focussing effect.

(III.6) Field Asymmetries

Electric Field

Owing to unavoidable departures from perfect mechanical symmetry in the construction of the parallel-plate assembly used to produce the electrostatic field it is possible to have a small z-component of electric field as well as the main y-component. The effect of such a component, E_z, of magnitude independent of position, would be to deviate the beam upwards or downwards from the median plane. The amount of this deviation may be calculated as a function of the orbit-number, k, if the magnetic field is assumed to be homogeneous.

The magnitude of the vertical component of acceleration is given by

$$\ddot{z} = eE_z/m_o\gamma$$

Therefore $$\dot{z} = eE_z t/m_o\gamma$$

and $$z = eE_z t^2/2m_o\gamma \ ,$$

where z is the distance from the median plane at time t of an electron which is ejected from the source on the median plane at t = 0. Consider the displacement z_k at completion of the k-th orbit. It is

$$z_k = (eE_z/2m_o\gamma) \times (k\,T)^2$$

where T is the cyclotron period.

Using Equation (III.1.1), this gives

$$z_k = eE_z(D_2B_z)^2/2m_o\gamma E_y^2$$

$$= (eD_2^2B_z^2/2m_o\gamma E_y)(E_z/E_y)$$

$$= \pi D_2 \tan\theta . k$$

where θ is the angle by which the electric field deviates from the horizontal (Figure III.6.1)).

Taking $D_2 \simeq 7$ cm. and $k = 200$, we see that, in the absence of any compensating effect, the beam would be markedly distorted ($z_k \gtrsim 5$ cm.)

if $\theta \sim \tan\theta \gtrsim 1/840 \simeq 0.07^\circ$.

Fortunately the effects would be considerably mitigated by the magnetic focussing described above. Nevertheless it was thought desirable that careful alignment of the parallel-plate assembly should be attempted.

Two kinds of distortion may be present (Figure (III.6.1)). First, there may be a lack of parallelism between the plates. This should lead to no net deviation of the beam since any effects will cancel out over a complete orbit. Second, there may be a mean deviation of the system as a whole from the vertical. This is the type of error which would lead to an uncompensated z-component of electric field. A simple device was incorporated in the system, by means of which the last-named error could be controlled in a continuous manner (Section (IV.2)).

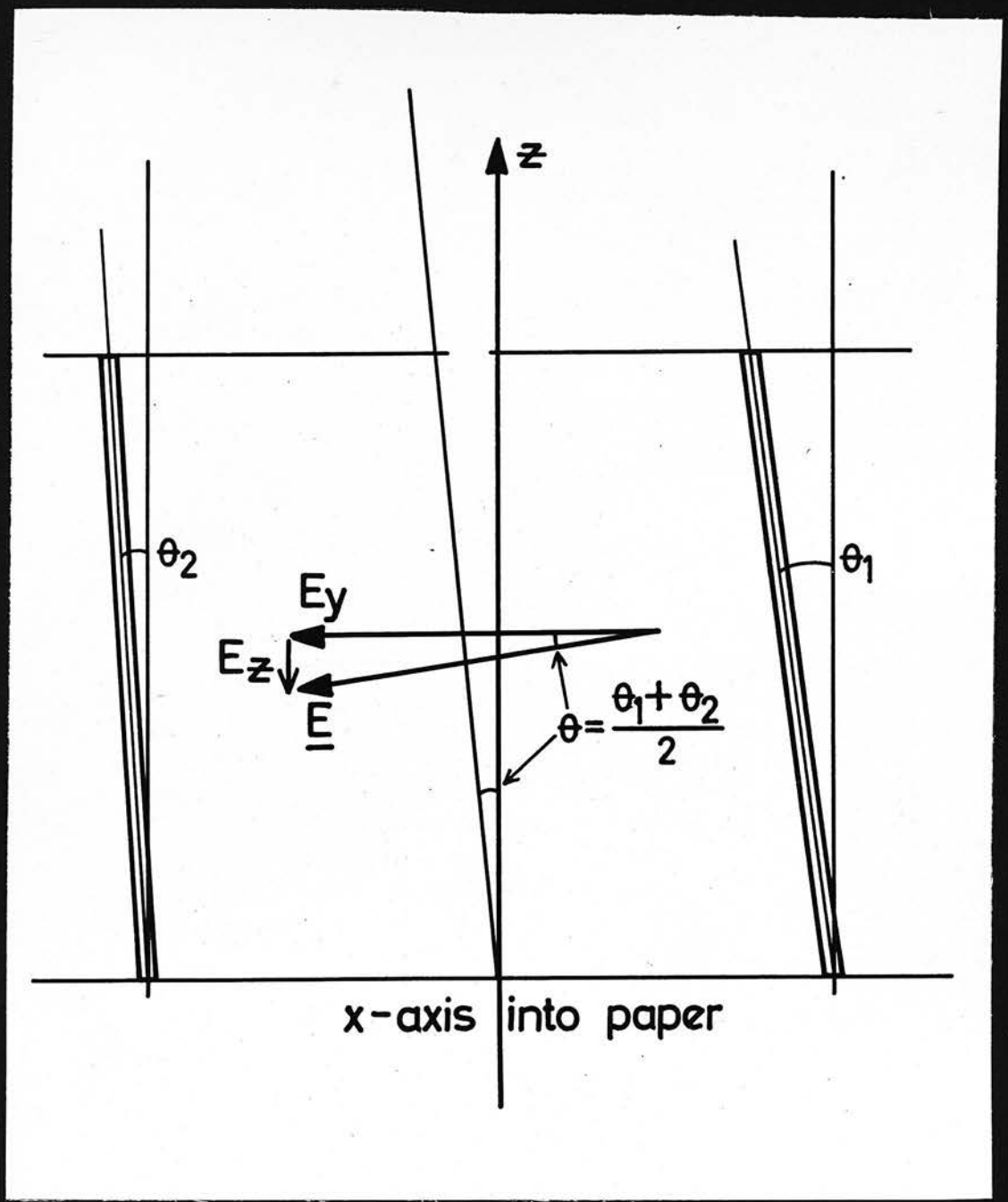

FIG. (III.6.1) Electrostatic Field Asymmetries.

Magnetic Field

If the horizontal symmetry-plane of the magnetic field is displaced upwards or downwards from the geometrical median plane, the effect will be similar to that caused by an uncompensated z-component of electric field. The term "symmetry-plane" as used here, though convenient, is not strictly accurate. What is meant is that plane (assuming one exists) which is everywhere intersected normally by the magnetic flux-lines. If, for instance, this plane is displaced upwards from the median-plane then an electron emitted horizontally from a point on the median plane will experience a small force tending to deflect it upwards. If the displacement of the magnetic symmetry-plane is not too great, the electron will eventually cross the latter and will then begin to oscillate about it. Thus, although the result would be a mean deviation of the beam from the median plane, the effect would not be identical with that due to an electric field asymmetry except in the more extreme cases where the magnetic symmetry plane actually lies outside the vertical limit of the region available to the electron. The possibility arises of making the electric and magnetic asymmetry effects cancel one another. Such an arrangement cannot, however, be as satisfactory as one in which both effects are eliminated independently. Unfortunately, one could only hope to do this by means of direct

observations on the beam itself and as it is very difficult, if not impossible, to distinguish between the effects of the two asymmetries by this means one cannot in practice do more than achieve mutual cancellation.

The magnetic asymmetry just described can easily be controlled in a continuous manner by passing current through a shimming coil of large diameter on one pole-face only (Section IV.3).

An asymmetry of a more intractable nature would be one where the average magnetic flux-density is greater on one side of the x-z symmetry plane than on the other. The effect of this would be to introduce a spurious drift of the orbits indistinguishable in nature from the genuine drift due to the electric field, E_y. Indeed, in the experiment of Charpak, Lederman, Sens and Zichichi (1960) (see also Charpak et al., 1961) to measure the magnetic moment anomaly of the free mu-meson, such an asymmetry was used expressly for the purpose of causing the mu-meson orbits to drift, no electric field being applied at all.

In the present experiment this asymmetry would show up as a phase-shift in the curve of counting-rate asymmetry against orbit-number. Unfortunately the phase shift would not be constant, as the following order-of-magnitude calculation shows.

Let us assume that the mean value, B_+, of the magnetic field on the positive-y side of the x-z plane differs by ΔB from the mean value, B_-, on the side of negative

y. Then, correspondingly, the mean radius, ρ_+, of the orbits on the positive side will differ by $\Delta\rho = \rho_+ - \rho_-$ from the mean radius, ρ_-, on the negative side. We have

$$\Delta\rho = \rho_+ - \rho_- = \frac{C}{B_+} - \frac{C}{B_-} = C\,\Delta\left(\frac{1}{B}\right), \quad \text{say,}$$

where $C \simeq \overline{B\rho}$, the overall mean value of $B\rho$.

Thus $\Delta\rho \simeq -\frac{C}{\overline{B}} \cdot \frac{\Delta B}{\overline{B}} = \overline{\rho} \cdot \Delta B/\overline{B}$.

Now the nominal value of the drift-distance per orbit would be

$$\partial_{nom.} = C'V,$$

where C' is a constant, while the actual value would be

$$\partial_{act.} \simeq C'V - 2\Delta\rho$$

Similarly, with an obvious notation,

$$k_{nom.} = \frac{D_2}{\partial_{nom.}} = \frac{D_2}{C'V} \quad \text{(see Fig. (III.3.2))},$$

while

$$k_{act.} = \frac{D_2}{\partial_{act.}} \simeq \frac{D_2}{C'V - 2\Delta\rho}$$

$$\simeq k_{nom.}\left(1 + \frac{2}{C'V}\rho\right)$$

if $2\Delta\rho \ll C'V$.

$$\therefore \Delta k = k_{act.} - k_{nom.} = \frac{2\Delta\rho}{C'V} \cdot k_{nom.}$$

$$= \frac{2\Delta\rho}{D_2} \cdot k_{nom}^2 \quad \text{(III.6.1)}$$

or, writing $k_{nom.} = k$ from now on,

$$\Delta k \simeq - \frac{2\bar{\rho}}{D_2} \frac{\Delta B}{\bar{B}} k^2$$

$$= - \frac{D_1}{D_2} \frac{\Delta B}{\bar{B}} k^2 \qquad \text{(see Fig. (III.3.2))}$$

A typical value for the ratio D_1/D_2 would be 1.2.

Thus $|\Delta k| \sim 1.2 \frac{\Delta B}{\bar{B}} k^2$

If we now lay down the criterion that $\Delta k \sim 1/25\ k_o \sim 30$ (compare Section (III.3), p. 15), then we require

$$\Delta B/\bar{B} \sim 25/k^2_{max.},$$

where $k_{max.}$, as in Section (III.3), is the greatest number of orbits which we are likely to use in the experiment. Let us choose $k_{max} \sim 10^3$, as before, so that

$$\Delta B/\bar{B} \sim 2.5 \times 10^{-5} .$$

It is believed (Section (IV.3)) that this degree of field homogeneity was actually achieved and, in any case, that $\Delta B/\bar{B}$ was not greater than 4×10^{-5}, in which case $k_{max} \sim 800 \sim 1.1\ k_o$.

There are two ways in which this type of error might be eliminated.

One would be to observe the asymmetry over several complete periods and to plot $1/\ k(N+1) - k(N)$ against $k(N+1) + k(N)$, where $k(N)$ is number of orbits required to reach the N-th complete period. The intercept on the ordinate axis would then be $\Upsilon(v).a$, in the notation

of Section (III.1). For, from equation (III.1.2), assuming $\Upsilon(V) \simeq 1$,

$$1/\Upsilon\, a) = k_{act.}(N+1) - k_{act.}(N) ,$$

$$= k(N+1) - k(N) + \frac{2\Delta\rho}{D_2}\left\{k^2(N+1) - k^2(N)\right\}$$

from equation (III.6.1)

$$= \left[k(N+1) - k(N)\right]\left[1 + \frac{2\Delta\rho}{D_2}\left\{k(N+1) + k(N)\right\}\right]$$

Therefore $$\frac{1}{k(N+1) - k(N)} = \frac{2\Delta\rho\,\Upsilon a}{D_2}\left\{k(N+1) + k(N)\right\} + \Upsilon a$$

Alternatively one might carry out the experiment at different electron energies and assume $\Delta B/\bar{B}$ to be constant. Writing

$$a_{obs.} = 1/\Upsilon\,(k_{nom})_o ,$$

and using equation (III.6.1) again, we find

$$a_{obs.} = a_{true} - \frac{D_1}{D_2} \cdot \frac{\Delta B}{\bar{B}} \cdot \frac{1}{\Upsilon} .$$

Thus a plot of $a_{obs.}$ against $1/\Upsilon$ would give a straight line with intercept equal to a_{true}.

However, neither of these methods would be easy to apply in practice, the former because of the difficulty of obtaining observations over more than one complete period and the latter because of the small range of Υ available.

CHAPTER IV

APPARATUS

(IV.1) Sources and Source-holders

Sulphur-35 was obtained in carrier-free form as a solution of sodium sulphate in water, and the source was formed by evaporating small droplets of the liquid on the source-holder.

In the earlier stages of the work, when depolarisation and back-scattering were not important considerations, the source-holder consisted simply of a suitably shaped piece of aluminium or brass rod near the edge of which a line-source was deposited. Difficulty was experienced in practice in confining the source material strictly to the forward side of the source holder. Electrons which have performed only one semi-circular orbit must not be allowed to strike the target. Therefore, in the later versions of the line-source, the material was deposited on a thin wire and shielded on all but the forward side by a thin aluminium shield or baffle. A line-source of this type is illustrated in Figure (IV.1.1)(a).

The great disadvantage of any such arrangement was that the electrons, on completion of their first orbit, had to pass by the outer edge of the shield and therefore it was not possible to extend the experiment beyond that number of orbits at which the drift-distance per orbit was

equal to the thickness of the shield. Indeed, because of the finite width of the source itself, the beam intensity began to be severely reduced when as few as 50 orbits had been reached (Section (V.1)).

The introduction of the weak-focussing field, however, opened up new possibilities in source-holder design. Referring to Figure (IV.1)(b), we note that, with the type of "point-source" there illustrated, electrons which succeed in passing above or below the source-holder on their first few orbits may ultimately be focussed on to the target. Thus, although there will be some attenuation of the beam over the first few orbits there is the possibility that this will be much less serious than in the case of the line source. Several designs of source-holder were tried out, including a double source-holder in which the source was split into two halves symmetrically disposed with respect to the median plane. The vertical spacing between the two halves could be varied by means of a screwed rod. The aim in this case was that the electrons should pass between the two halves of the source-holder on their first few orbits. Again, a "point-source" of the type illustrated was tried at various distances off the median plane. The best results were obtained with the design shown, however.

When the polarisation of the beam was an important consideration, precautions had to be taken to minimise

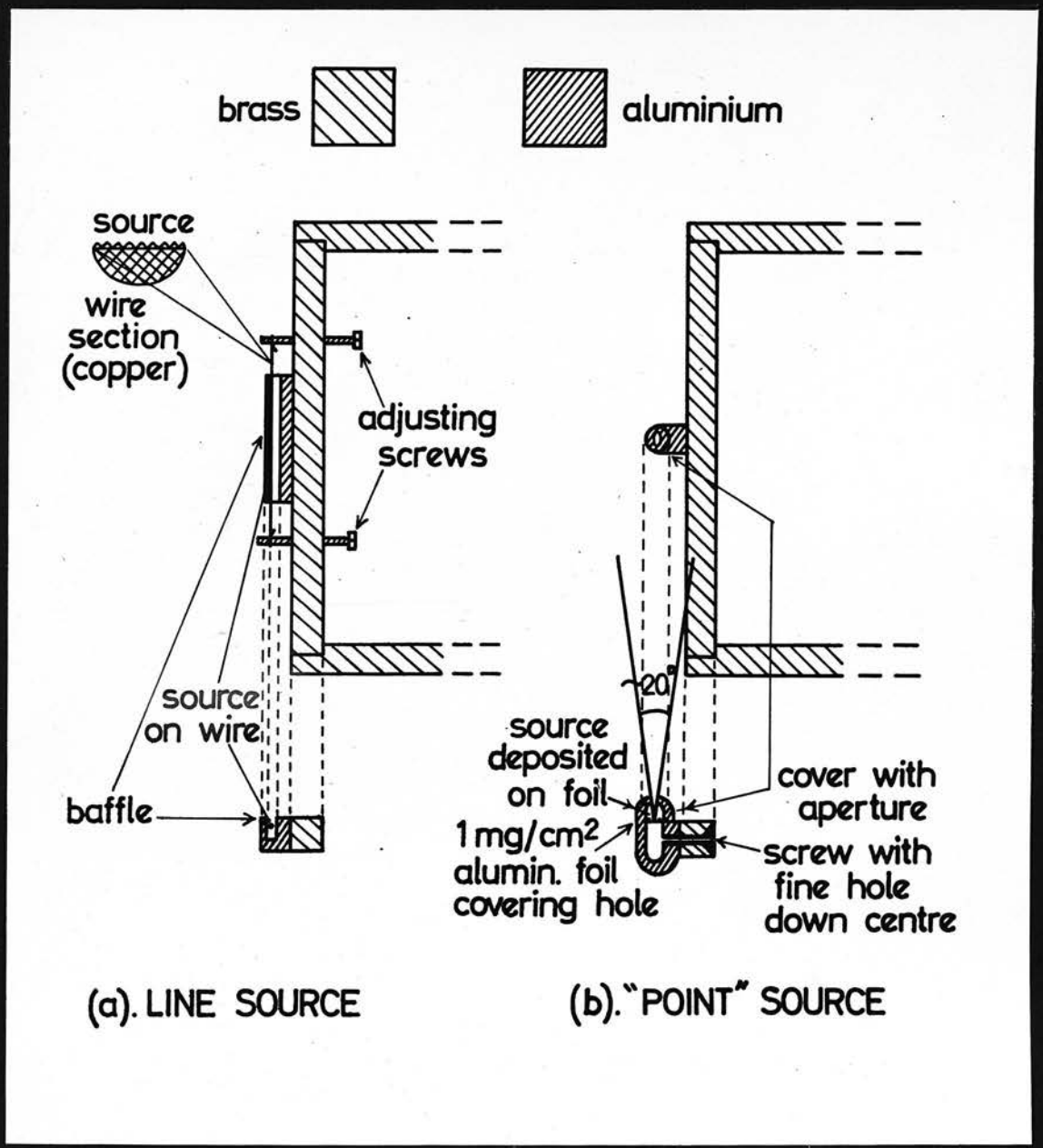

FIG. (IV.1.1) Source-holders.

backscattering from the material upon which the source was deposited, since this was the most important cause of depolarisation of the beam. That appreciable depolarisation of the beam can result from backscattering can be seen from the following semi-quantitative argument. Let us assume an electron-energy of 100 keV, giving an initial beam polarisation of 55 % for an infinitely thin source and no backscattering. According to a remark at the end of Section (II.4) we may picture the beam as consisting to the extent of $77\frac{1}{2}$% of electrons with their spins directed backward (opposite to their momentum) and $22\frac{1}{2}$% of electrons with their spins directed forwards. For every 100 forward-emitted electrons there will be 100 emitted backwards with the same polarisation, that is with $77\frac{1}{2}$% of their spins pointing in the direction of the beam. Let us suppose that the source has been deposited on a thick (> 100 mg./cm.^{2}) aluminium backing. Then a reasonable estimate of the backscattering would be 20% (Paul and Steinwedel, 1955). The polarisation of these backscattered electrons would be little reduced in magnitude by the scattering (Bernardini et al., 1958) so that the result would be a forward beam in which, out of every 120 electrons, $77\frac{1}{2} + 4\frac{1}{2} = 82$ would have their spins directed backward and $22\frac{1}{2} + 15\frac{1}{2} = 38$ would have their spins directed forward. The net polarisation of the beam would therefore be reduced from 55% to 37% . Fortunately the

great majority of the backscattered electrons will have their energy so substantially reduced (Bothe, 1949) that they will not be transmitted to the target. By the same token, however, there will be a contribution to the depolarisation from backscattered electrons whose original energy was greater than 100 keV.

In the present apparatus one must arrange that all backward-emitted electrons are stopped somewhere in the source-holder and it was concluded that the best compromise would be to deposit the source on a thin aluminium foil — about 1 mg./cm.^{2} aluminium gives negligible backscattering depolarisation at 100 keV (Cavanagh et al., 1957; Heintze, 1958) - backed by a hollow space as shown in Figure (IV.1.1)(b). Over the source was placed an aluminium cover having a slot which subtended an angle of about 20° at the centre of the source. Back-scattered electrons, however, besides having to penetrate the aluminium foil in order to get out, would on average "see" a substantially smaller exit aperture than the 20° available to the genuine beam. In this way it was hoped that backscattering would be reduced by a factor of at least three.

A rough calculation shows that the thickness of the source material itself for a 50 mC source deposited on an area of about 4mm.^{2} would be expected to be 120 μgm./cm.^{2}, insufficient to cause noticeable depolarisation.

The use of aluminium instead of organic materials for the supporting foil prevented charging up of the source, a

phenomenon which can seriously affect the electron energy (Slätis, 1955).

The exit slot was about 1 mm. wide. There will therefore be a corresponding range of orbit-number at the target, given by $\Delta k/k \sim \Delta x/D_2$, where Δx is the slit-width. Δk would amount to about 14 orbits at k = 1000 and over this range the asymmetry could be assumed to vary linearly with k. Hence it was customary to measure D_2 from the middle of the slit.

(IV.2) Electric Field

The values of the potential difference which had to be applied between the parallel plates (Figure (IV.2.2)) to give the various orbit numbers, k, satisfied the relation

$$kV = \text{constant.}$$

In a typical case the constant amounted to 160 kilovolts. Thus in order that a range of orbit-number of, say, k = 10 to k = 1000 might be covered, voltages ranging from 16 kV to 160 v. were required. It was desirable that these should be stabilised to better than 1% over long periods.

A radio-frequency voltage generator* was employed to give a continuously variable output from about 300 volts to about 17 kV in three ranges (for voltages below 300 v., batteries were used.) The output was symmetrical with respect to ground (so that the source-holder and target holder would be in a region near ground potential and so that the field would be as symmetrical as possible) and was stabilised by negative feedback taken directly from the negative D.C. output.

The circuit of the E.H.T. generator is given in Figure (IV.2.1). The beam tetrodes, V_8 and V_9, acted in parallel as a Class C power oscillator at a frequency of about 60 kc./s. Their output was transformed up to 3 kV. by the R.F. transformer coils Tr 2, which were housed in an oil-bath to prevent discharges between sections of the transformer, and also for cooling purposes. The

* This was constructed by Mr. R.B. Gardiner (see Gardiner, 1961).

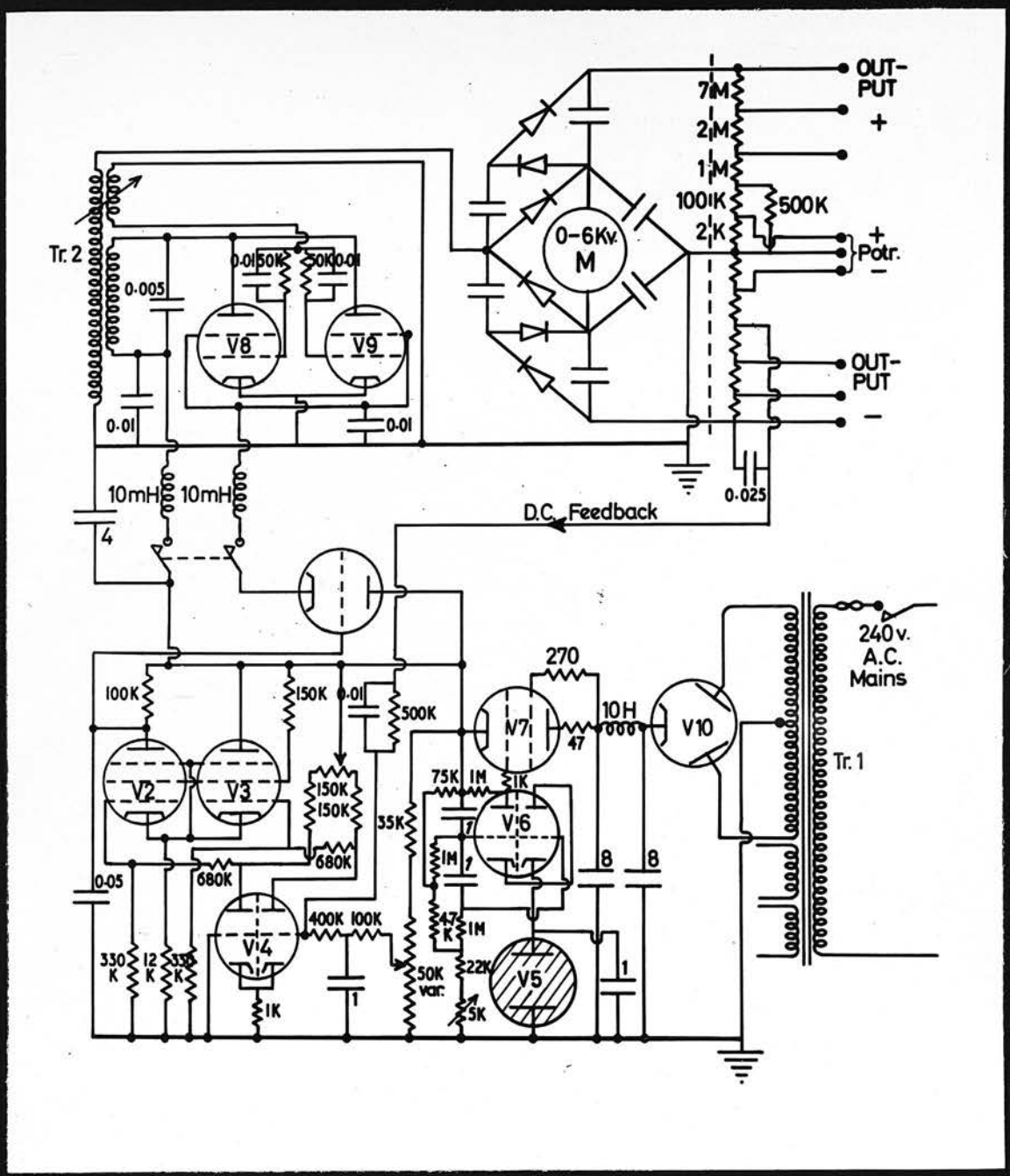

FIG. (IV.2.1) Electrostatic Generator.

positive feedback to the oscillator could be varied by moving the feedback coil relative to the main coils. The R.F. output from the transformer was applied to a double-ended Cockcroft-Walton voltage-trebler using metal rectifiers. The capacitors employed in the voltage-trebler were chosen so as to reduce the ripple voltage at the output to about 0.1 % of the total voltage. A chain of high-precision (0.1 %) wirewound resistors, immersed in an oil bath, was connected between the positive and negative outputs, and the centre of the chain was earthed. Three ranges of output voltage could be obtained by tapping the chain at the points indicated in the diagram. Approximately 1 % of the total negative output was fed back through the D.C. amplifier formed by V_2, V_3 and V_4 to stabilise the oscillator. The necessary control was exercised through the screen-grids of the oscillator tubes, their voltage being regulated by the output of the D.C. amplifier through the cathode-follower, V_1. A 50 kΩ helical potentiometer, providing a reference voltage for the D.C. amplifier, constituted a convenient means of adjusting the output voltage continuously over a range of 4:1.

Absolute measurements of both the positive and negative outputs could be made with a precision potentiometer, by measuring the voltage developed across precision (0.1 %) wirewound 2000 Ω resistors forming part of the

resistor chain.

Figure (IV.2.2) shows, schematically, the construction of the electrodes inside the vacuum box. The orientation of the parallel plates with respect to the vertical could be varied slightly under vacuum by means of the simple screw device illustrated, the control rod for which passed through a vacuum seal in the wall of the chamber.

The electric field was, of course, required to be uniform, as far as possible, in the space between the plates. To this end a series of equally-spaced grids was provided whose relative potentials were fixed by means of a resistor chain. High-stability carbon resistors were used at first, until it was found that the end-caps on this type of resistor were slightly ferromagnetic and were seriously affecting the magnetic field distribution. Ordinary carbon resistors were used thereafter, equal values being obtained by selection from a large group. The total resistance of the chain was 80 MΩ; heating effects and consequent drift of the resistance value were therefore minimised even at the highest voltages.

A sufficient density of grids had to be provided to keep the electric field homogeneous to about 1% at the highest voltages. On the other hand, from the constructional point of view, it was desirable to keep the number of grids to a minimum. Although some information on this type of problem did exist in the literature (for example,

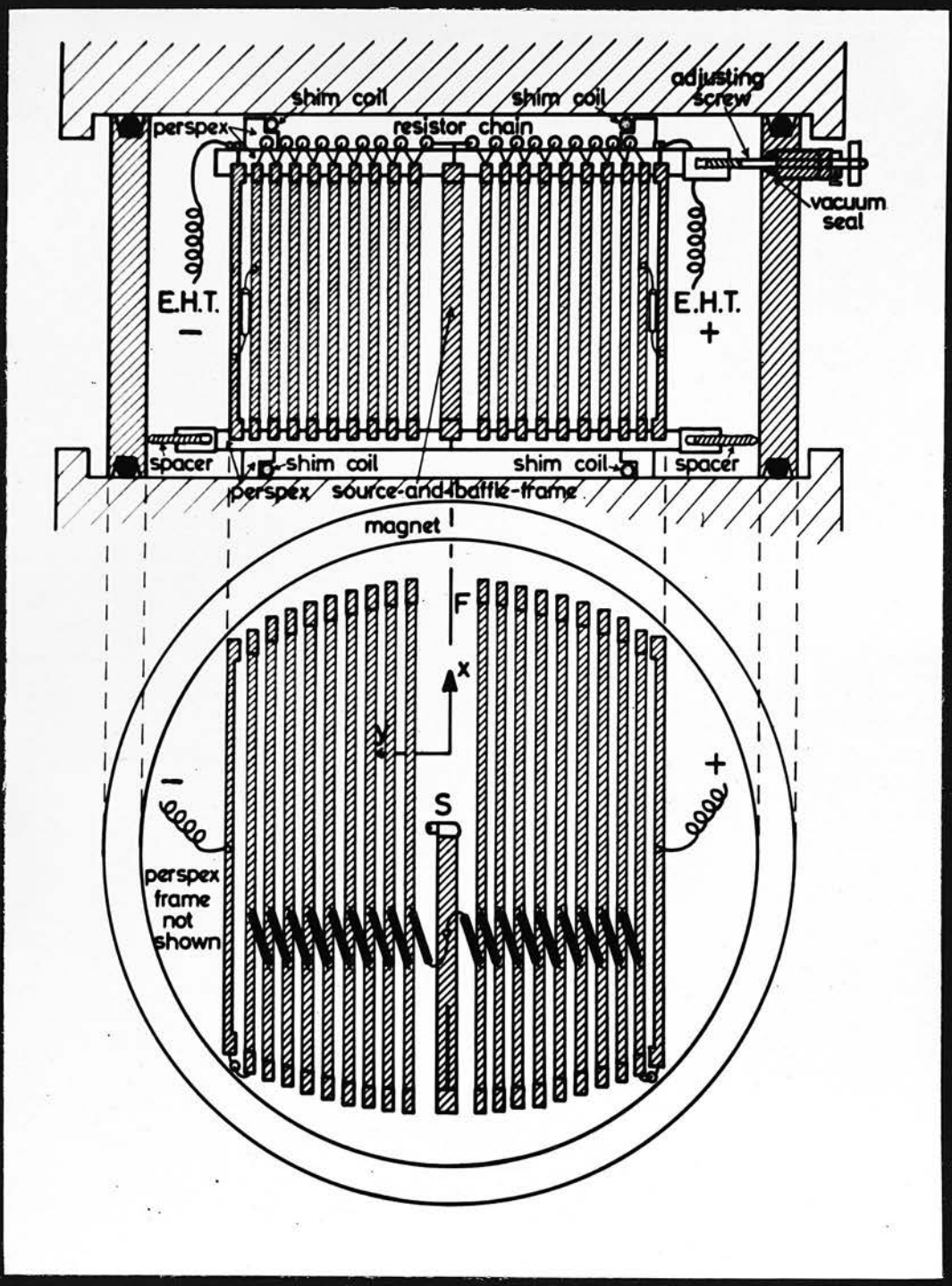

FIG. (IV.2.2) Electrostatic Field Assembly (not to scale).

Kemp and Barber, 1957), there was nothing which could be applied directly to the present case. It was therefore decided to set up an electrolytic tank and to try various configurations.

As some features of this tank were unconventional a brief account may be of interest. The circuit is shown in Figure (IV.2.3), and was quite conventional. The function of the variable capacitors was to annull the effects of the stray capacitances between the probe and the electrodes. It is usual when the highest accuracy is desired (Kennedy and Kent, 1956) to employ a Wagner earthing device, but this was found not to be necessary in the present application. The detector could be a sensitive oscilloscope or, for maximum sensitivity, a specially designed grid-leak detector (Figure (IV.2.3)). The latter combined high sensitivity for small inputs with the useful property of saturating at high inputs so that the meter could not be accidentally subjected to excessive deflections.

The probe assembly, illustrated in Figure (IV.2.4), was so constructed that its position could be transferred directly to a piece of tracing paper without the use of the conventional pantograph which introduces all the uncertainties associated with imperfect mechanical construction. A beam of light was directed upwards in a line with the probe and the image of a fine cross-wire was focussed on the tracing paper supported above the tank on a horizontal sheet of plate-glass. The only mechanical parts of this system which needed care in construction were the two rails

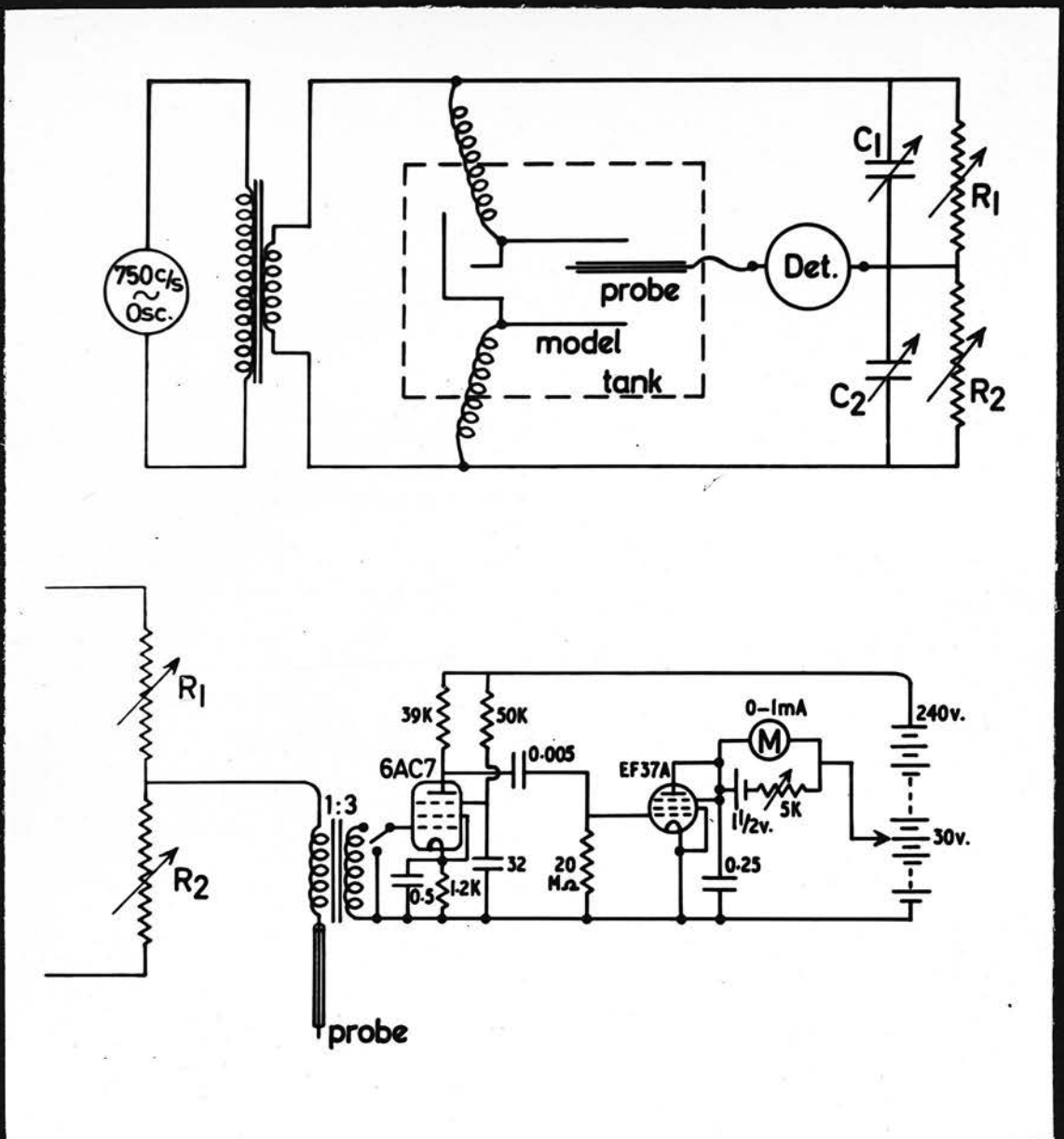

FIG. (IV.2.3) Electrolytic-tank circuit and detector.

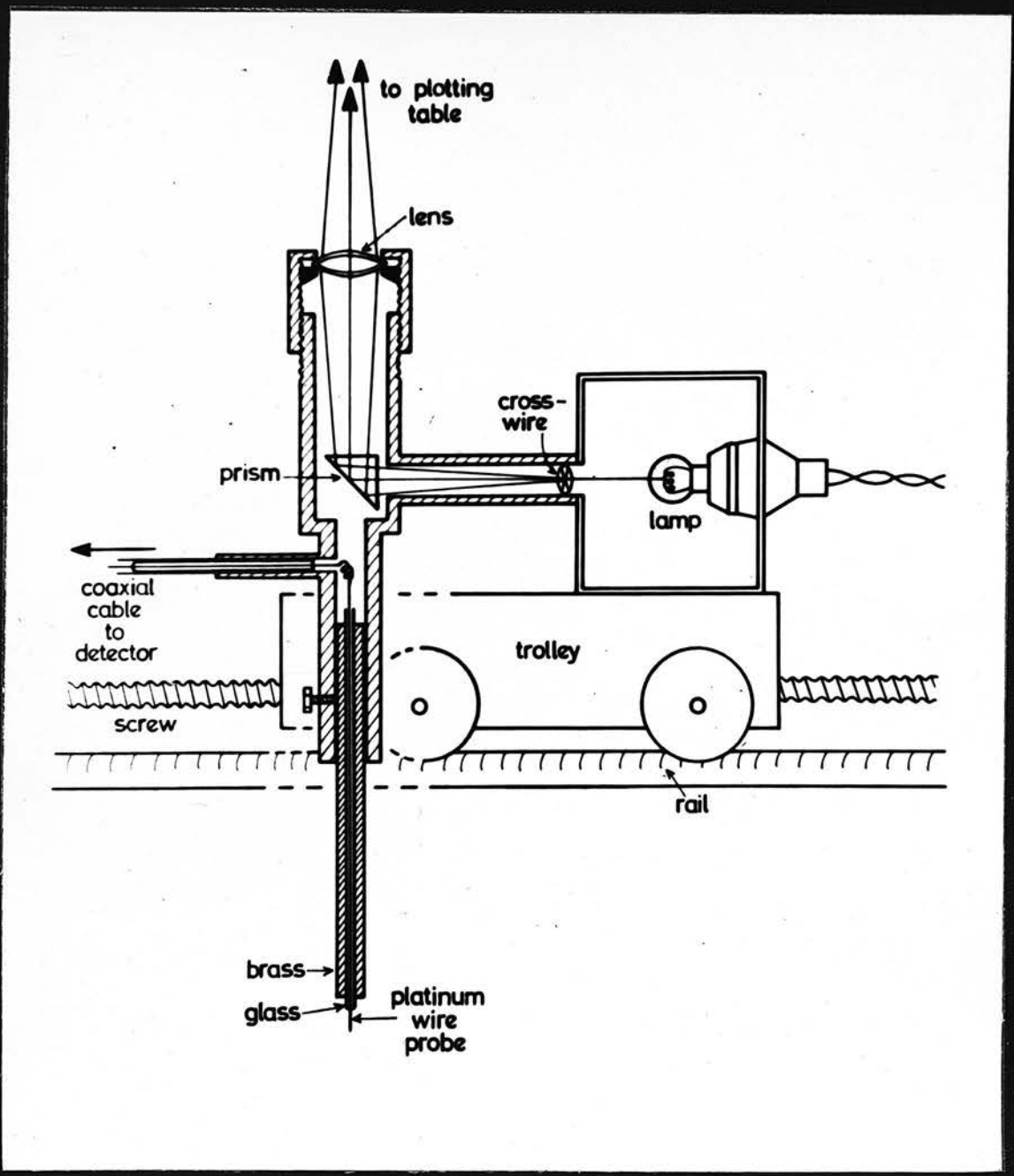

FIG. (IV.2.4) The Probe Assembly.

upon which the probe-trolley ran. These had to be parallel to one another, though in fact even the effects of this error could be eliminated by orienting the model in the tank so that the equipotentials lay as nearly as possible at right angles to the rails in question. These rails were themselves supported on trolleys, one at each end, so that the probe could be traversed in two directions mutually at right angles.

A test of the accuracy of the whole device was made by plotting the equipotentials for a simple electrode system and comparing with theory. A model was constructed to represent a normal section of a cylindrical condenser (Figure (IV.2.5). Ordinary tap water was used as the electrolyte and the electrodes were of untreated brass. The probe supporting assembly was carefully levelled so that the probe, a fine platinum wire, just touched the surface of the water over the whole area of interest.

The potential at a distance r from the centre of a cylindrical condenser is given by

$$V(r) = C_1 \log r + C_2,$$

where C_1 and C_2 are constants. If $\log r$ is plotted against x where

$$x = (V(r) - V(a))/(V(b) - V(a)),$$

a, b being the radii of the inner and outer cylinders respectively, then the points should lie on a straight line of gradient $\log(a/b)$. When the observations were treated

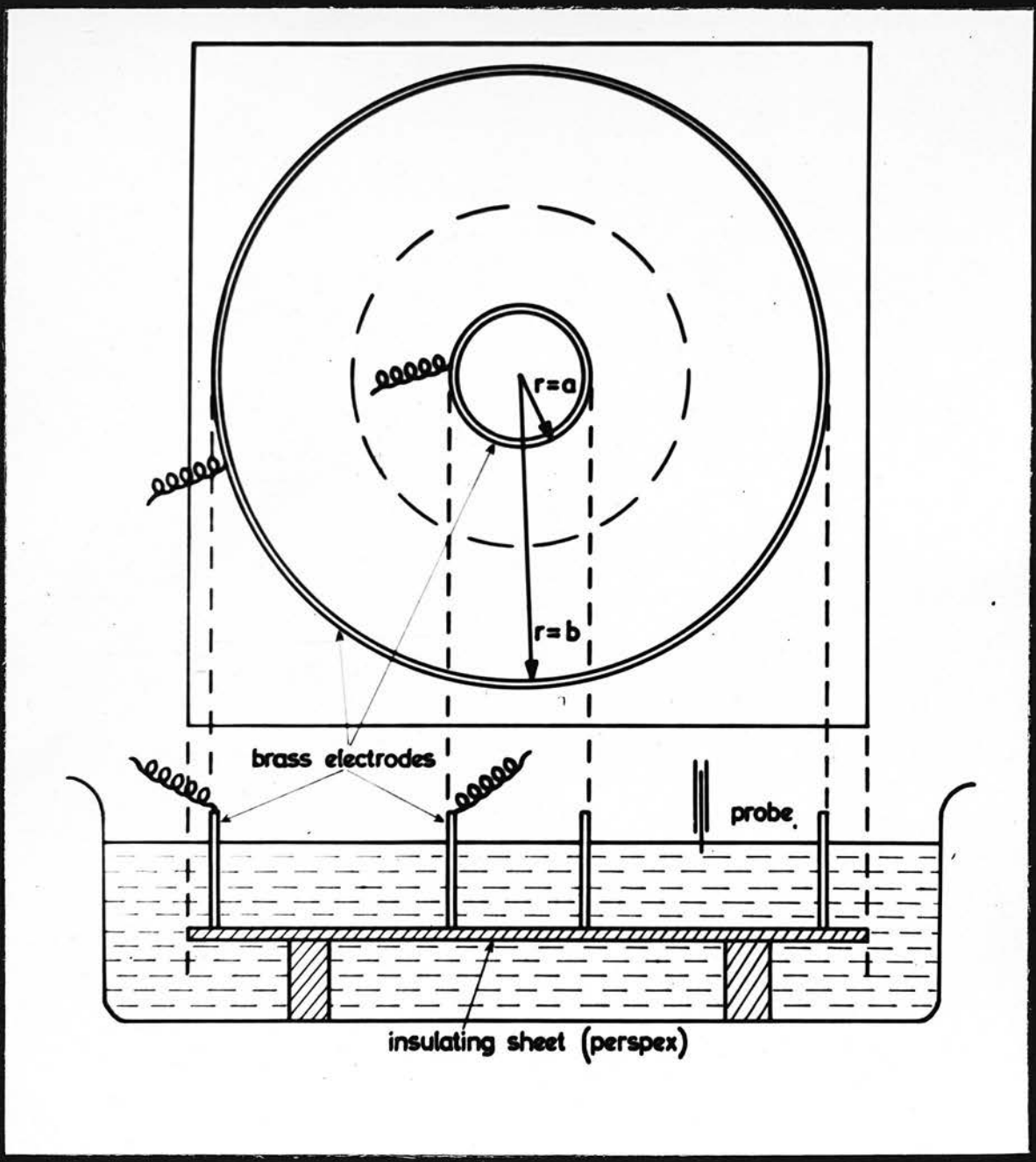

FIG. (IV.2.5) Test Model for Electrolytic Tank.

in this way they were found to lie on a straight line to an accuracy of 0.5% . Furthermore, this line, when extrapolated to x = 1, gave a value

$$b = 27.93 \pm 0.07 \text{ cm.},$$

while the actual radius of the outer cylinder was 28.0 cm. This showed that any surface effects at the brass electrode were negligible (Einstein, 1951; Kennedy and Kent, 1956). In any case the accuracy of simulation of any given electrode configuration by a tank model was not more precise than this.

One of the models used in tests relevant to the design of the grid system is shown in Figure (IV.2.6). In order to obtain the most reliable results it is necessary to make a model on the largest possible scale, and this can often be done by taking advantage of any symmetry which may be present in the original system. The model shown in the figure represents a section normal to the grids, including one complete inter-grid gap and half each of the two neighbouring grids. In this way the effect of varying the grid-width to gap ratio could be studied. This also gives an answer, as we shall see, to the problem of the minimum density of grids required. The equipotentials for various grid-to-gap ratios were plotted successively on the same sheet of paper. It was found that, at all distances from the grids greater than $1\frac{1}{2}$ times the grid spacing (centre-to-centre distance), the equipotentials corresponding to grid-to-gap ratios from 1:1 to 4:1 could not be distinguished

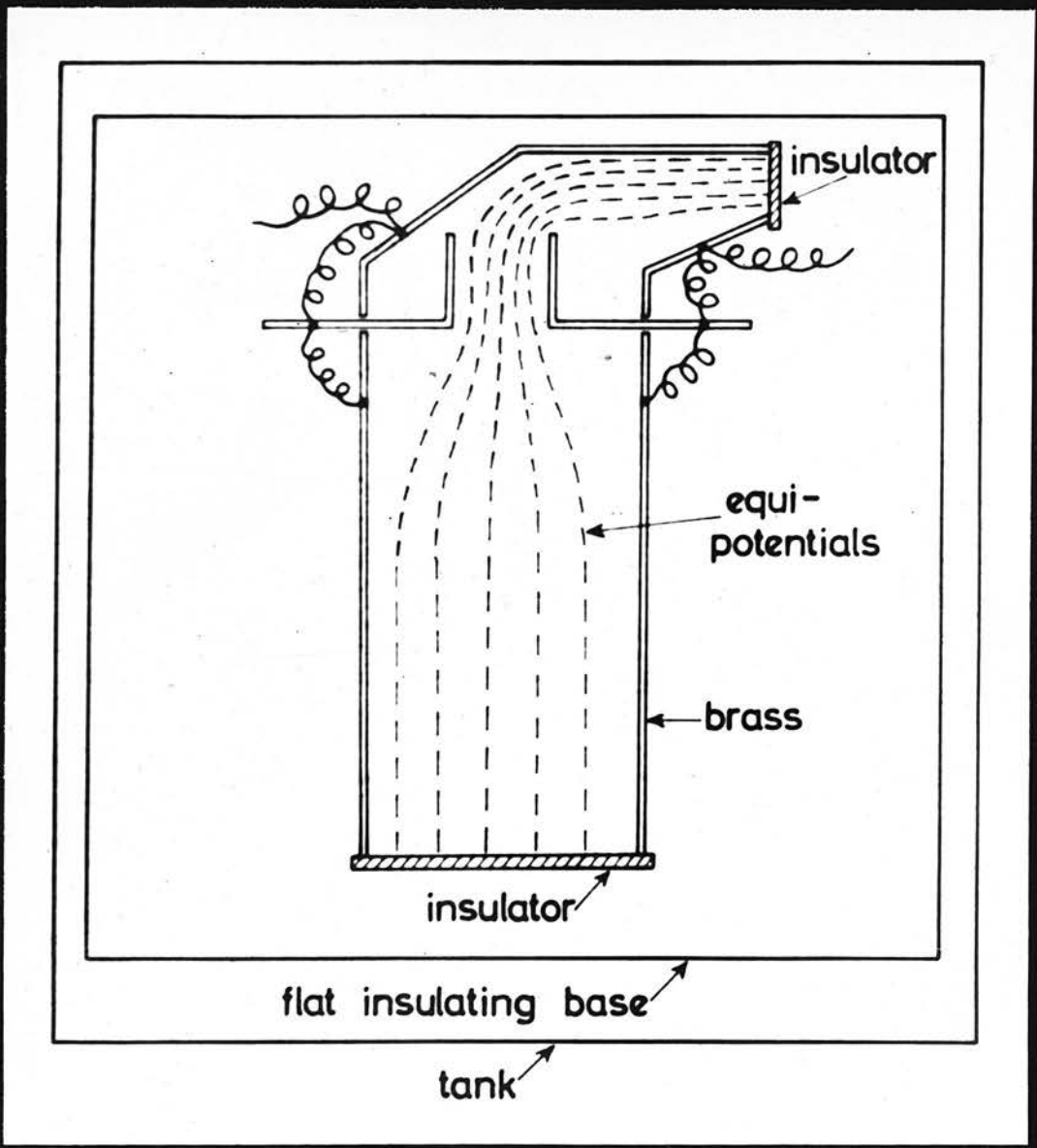

FIG. (IV.2.6) Model of section of grid system used in electrolytic tank tests.

from one another. In addition, beyond the same limit, the equipotentials themselves showed no detectable deviations from straight lines. To allow a sufficient margin of safety a distance of three times the grid-spacing was chosen as the criterion for field homogeneity. Now the electron orbits occupy a region between planes spaced about $\pm$ 2 cm. above and below the median plane (the effective vertical length of the scattering-foil was usually about 2 cm.), while the total vertical space between the magnet pole-faces available for a grid-system was 9 cm. Deducting 4 cm. for the orbits and making a reasonable allowance for the vertical thickness of the grids themselves leaves a vertical "dead-space" of 18 mm. top and bottom. The grid-spacing, on the above criterion, should then be 6 mm. In the practical design (Figure (IV.2.2)) the centre-to-centre grid spacing was $\frac{1}{4}$ inch, and the grids were $\frac{1}{8}$ inch thick and $\frac{1}{4}$ inch deep. With these dimensions 18 grids could be fitted in, the spacing between each of the innermost pair and the source-holder grid being 70% greater than the average to allow of detectors being inserted above and below the scattering-foil. The centre of the system being in any case at earth potential, the greater spacing of the innermost grids should not cause undue inhomogeneity.

In conclusion, the following points must be emphasized. Provided any small deviation from homogeneity is (a) rapidly fluctuating as seen by the electron or (b) symmetrical

with respect to the x-z plane, no deleterious effect on the orbits need be expected. Finally, it is not necessary to rely solely on the kind of criterion given above. Observations on the electron beam itself (Section (V.1)) showed that the electric field was performing its function correctly, at least up to 50 orbits.

(IV.3) The Magnetic Field

Figure (IV.3.1) shows the electromagnet with the arrangement of the coils. The magnet was machined from commercial soft iron of a type relatively free from structural inhomogeneities such as gas bubbles ("rolled bar") and was designed so that the pole faces could act as the closing sides of the vacuum vessel. The upper yoke and pole-piece could be raised by means of a block and tackle to allow access to the vacuum vessel. The pole-faces were machined flat but were not optically polished. Rose shims were machined round the perimeter of each pole-face to improve the field homogeneity.

Power for the magnet was provided by a rectifier set whose output was smoothed and to some extent stabilised by a system of floating batteries, (Figure (IV.3.2). For greater short-term stability a transistorised stabiliser was designed and built. The complete circuit is shown in Figure (IV.3.2). The stabiliser was of the conventional series type, the series transistors being mounted on cooling fins. A potential difference proportional to the magnet current was developed across a 1 ohm standard oil-immersed resistor and was compared with a constant voltage obtained from a Zener Diode. The error voltage was amplified by a D.C. difference amplifier consisting of two silicon transistors in the "long-tailed pair" configuration. The output of this stage was fed to the series controlling

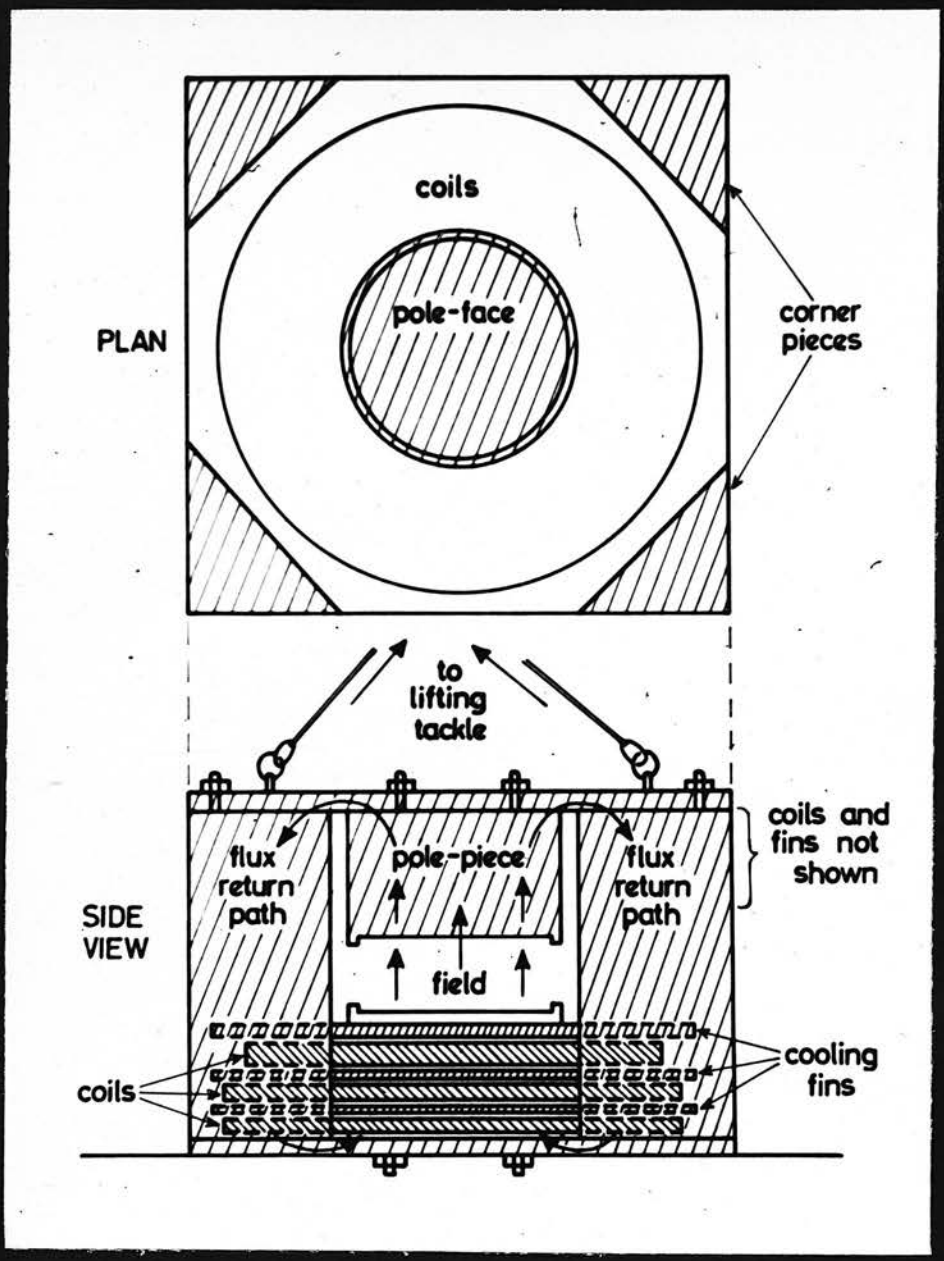

FIG. (IV.3.1) Magnet (not to scale).

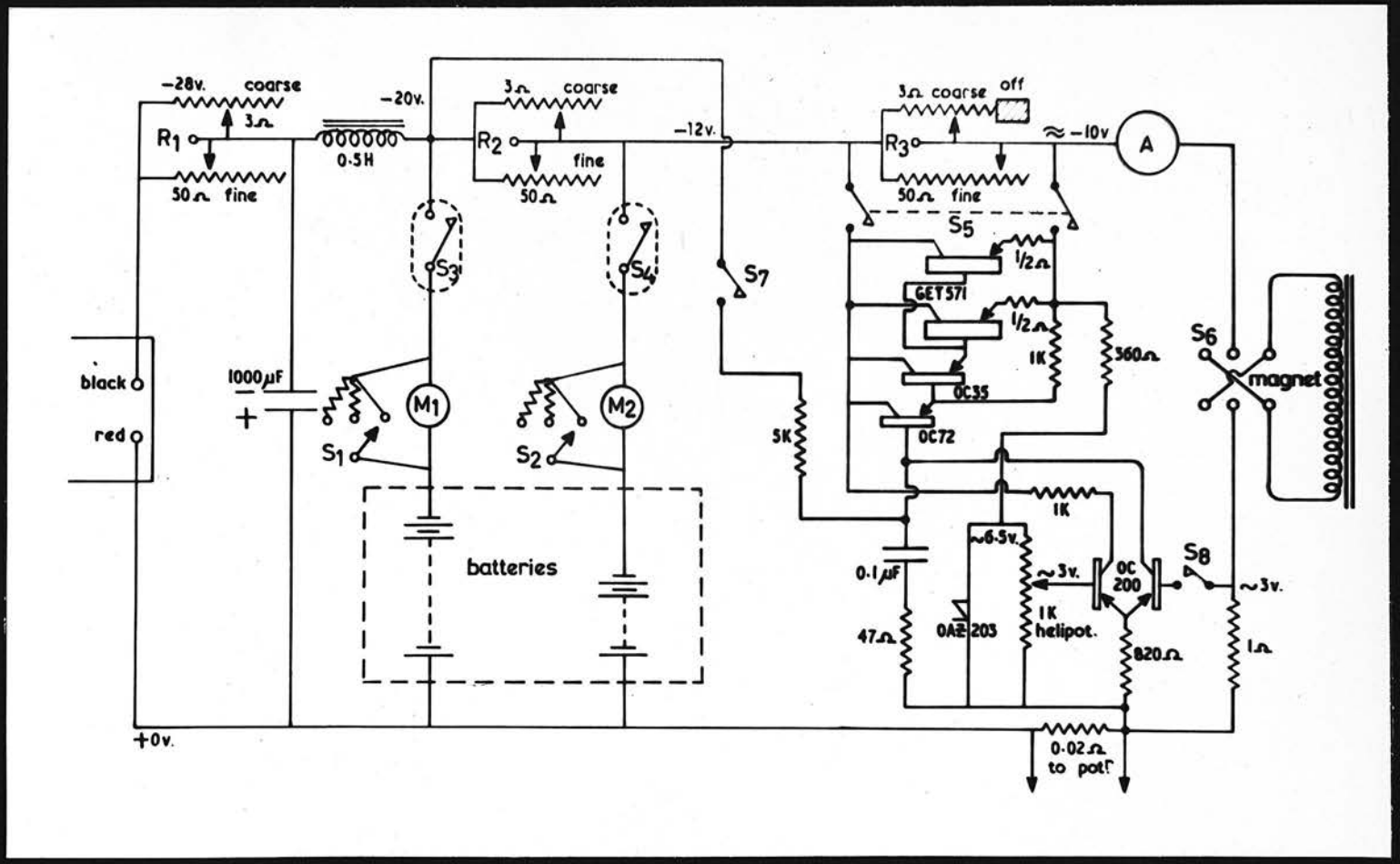

FIG. (IV.3.2) Magnet Current Stabiliser.

transistors in the correct phase to give overall negative feedback. Two series transistors were employed in parallel, so that currents of up to 4 amps could be stabilised without excessive heat dissipation.

The primary purpose of the transistor stabiliser was to suppress rapid fluctuations of the magnet current (due to mains fluctuations) which made proton resonance magnetometry almost impracticable. The fact that the stabiliser was uncompensated for temperature fluctuations was therefore of no importance. The short-term stability achieved was better than one part in 10^4. The main cause of long-term drift would be expected to be the variation with ambient temperature of the Zener diode reference voltage. The diode was chosen so as to give a stabilised voltage of 5.6 v., the value near which the temperature coefficient of voltage for this type of diode is zero. Certainly, in practice, long-term fluctuations were less than $\frac{1}{2}\%$.

Since the magnetic field was required to be homogeneous to a few parts in 10^4 over the area swept out by the electron orbits, it was necessary to have some means of making relative field measurements to this degree of precision. Absolute measurements of the field were required to about 1% only. These requirements are conveniently met by the method of proton magnetic resonance for fields as low as 100 gauss. A proton resonance magnetometer, based on the circuit of Watkins and Pound (1951) (see also

Pound, 1952), was built* and was subsequently modified for the direct measurement of field inhomogeneity.

Figure (IV.3.3) is a block diagram of the magnetometer and Figures (IV.3.4) and (IV.3.5) show the complete circuit. The operation of the basic magnetometer circuit will be described very briefly and the modifications made to it will then be discussed in more detail. The tank coil of the oscillator was wound on a small piece of glass tubing which contained the proton sample (Figure (IV.3.6)).

The frequency of oscillation was controlled manually by the variable air capacitors C_1 and C_2 and was normally about 1 Mc/s. The cathode-coupled oscillator was conveniently stabilised in amplitude by means of the D.C. bias on the grid of V_{1b}. The proton absorption signal was passed to the two-stage R.F. amplifier and rectified by V_{4a} and V_{4b}. The rectified output from V_{4a} was returned to the grid of V_{1b} to stabilise the level of oscillation at the low value necessary to avoid saturation of the proton absorption. The output of V_{4b} was further amplified by a two-stage audio-frequency amplifier and could then be displayed on an oscilloscope.

In the first version of the circuit the oscillator was incorporated with the probe head in a separate metal box and a cathode follower was included to feed the R.F. signal through a length of coaxial cable to the R.F. amplifier input. It was later found, however, that removal

* The first version of the magnetometer was built by Mr. R.B. Gardiner (see Gardiner, 1961).

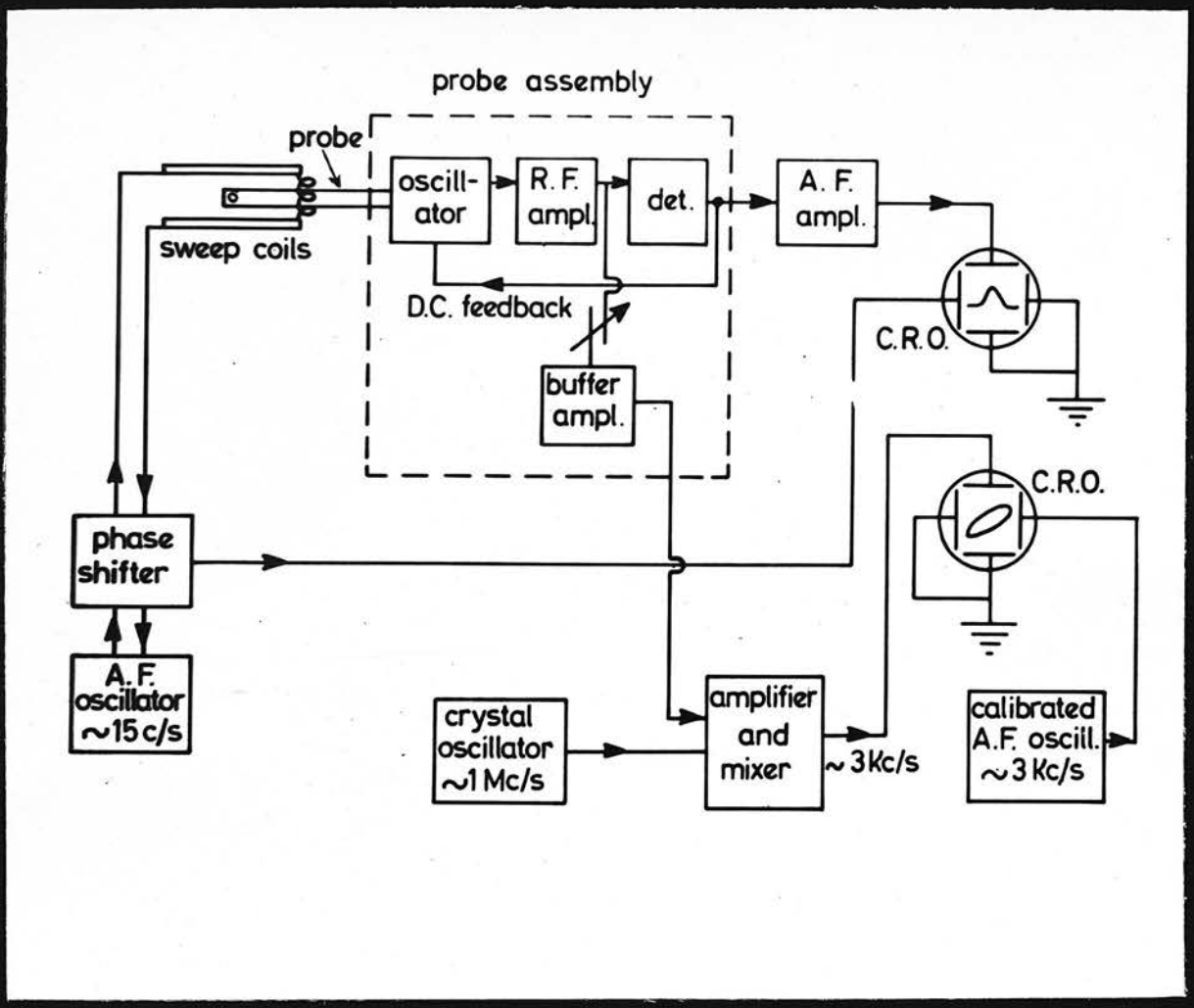

FIG. (IV.3.3) Block diagram of Proton Magnetometer.

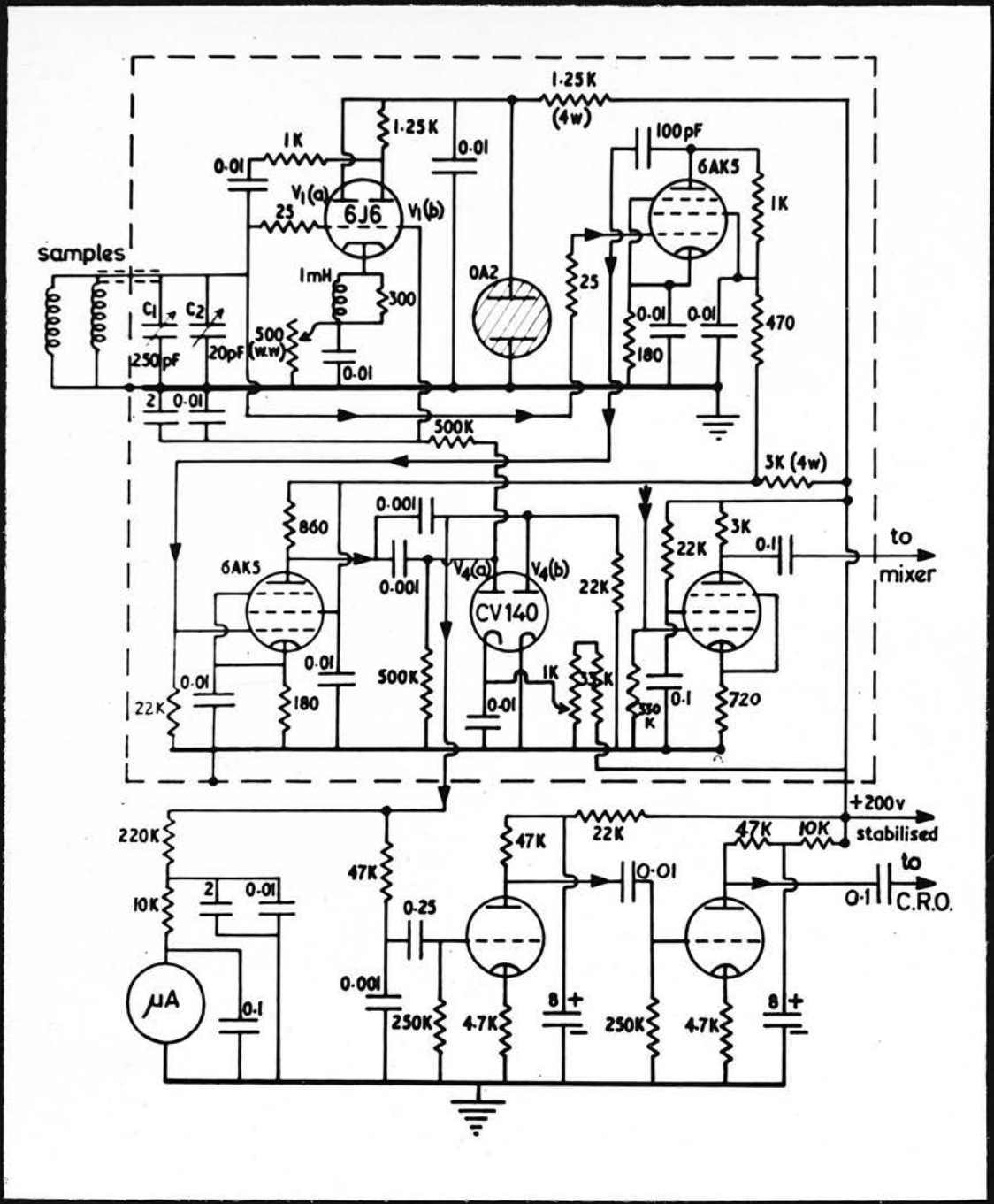

FIG. (IV.3.4) Circuit for Proton Resonance Magnetometer.

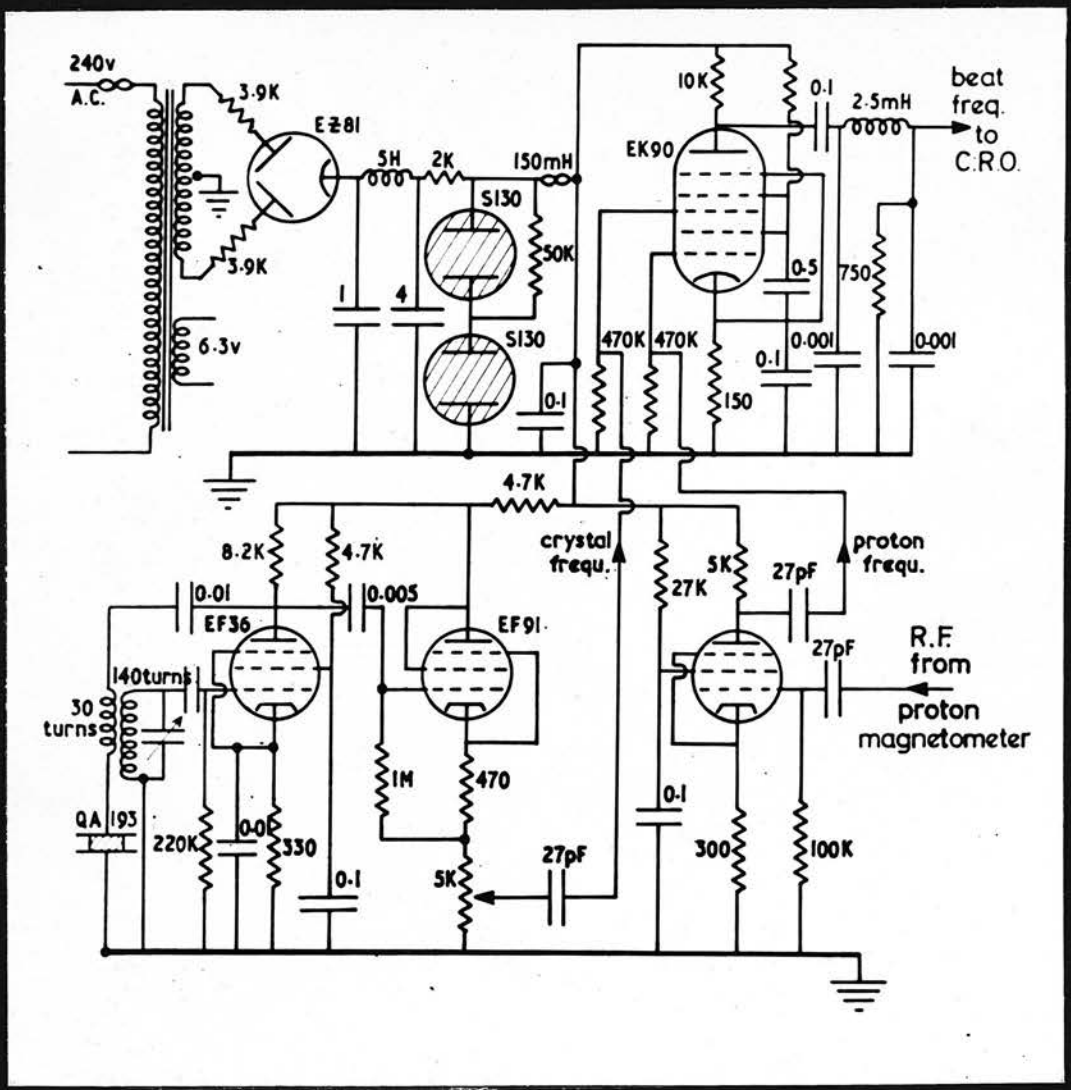

FIG. (IV.3.5) Frequency measuring circuit.

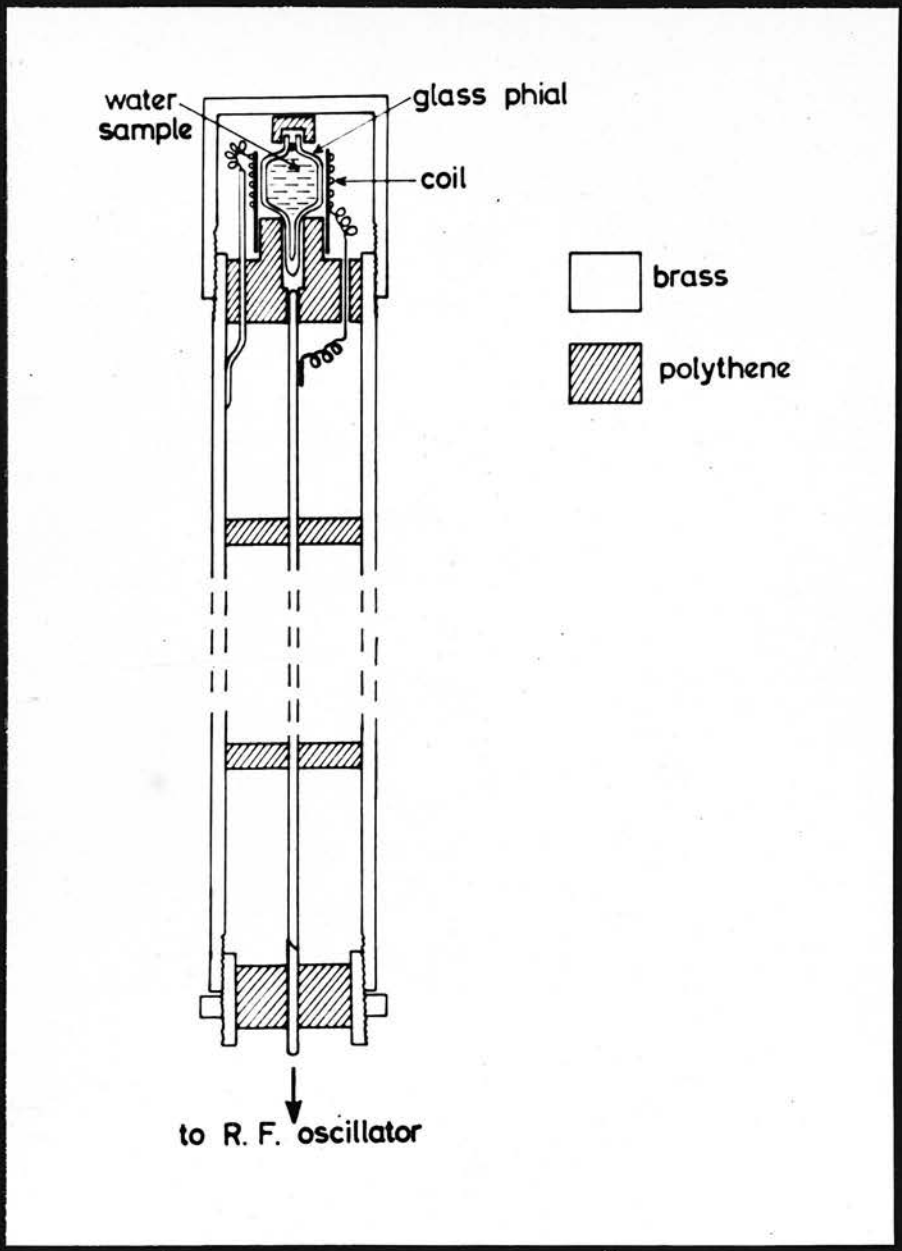

FIG. (IV.3.6) Proton magnetometer-probe head.

of the cathode follower circuit improved the signal-to-noise ratio by a factor of about 3, and in the final model all stages except the A.F. amplifier were incorporated in the probe-head box.

Figure (IV.3.6) shows the design of the probe-head. The volume of the sample was about 0.5 ml. and it normally consisted of tap-water with the addition of ferric nitrate at about 10 gm. per litre or manganese sulphate at a similar concentration.

The purpose of adding these paramagnetic ions was, of course, to decrease the spin-lattice relaxation time and so make it possible to obtain a larger signal. The natural line-width was increased at the same time but in the present application where most of the line-width was accounted for by the field inhomogeneities, a suitable compromise was easily reached empirically.

A pair of auxiliary coils on the pole-pieces of the magnet enabled the main field to be modulated sinusoidally at about 15 c/s about its mean value, the necessary current being provided by an A.F. power oscillator whose output, suitably shifted in phase, was also applied to the X-plates of the oscilloscope. The absorption peak was thus displayed directly against magnetic field.

Several systems, of varying degrees of elegance and complexity, suitable for the direct estimation of magnetic field inhomogeneities have been described in the literature

(for example, Baker and Burd, 1957). The most obvious method is to have two independent oscillators, each with its own probe, and to measure directly the frequency difference when both are on resonance. As well as being uneconomic, this system is unsatisfactory in practice because it is a matter of considerable difficulty to avoid coupling between the two oscillators, especially when the two frequencies are nearly equal. Before constructing one of the more complex circuits it was decided to try an easy modification of the original system whereby one simply introduces a second probe head with its R.F. coil connected in parallel with the first one. This arrangement is indicated in Figure (IV.3.4). The second probe-head was connected to the oscillator chassis by about 3 feet of coaxial cable and could be traversed horizontally and vertically in the magnetic field while the first probe-head was kept fixed. This system was found to work very well, although, of course, the signal-to-noise ratio was reduced by half. Two absorption peaks were observed whose separation on the oscilloscope display was directly proportional to the difference in field strength between the fixed and the movable probes. The necessary calibration of the oscilloscope scale could be carried out directly in terms of frequency.

The frequency-measuring circuit was designed for the present application and is shown in block form and in

detail in Figures (IV.3.3) and (IV.3.5). The R.F. signal was taken through two buffer amplifier stages to the first grid of a mixer tube. A fixed-frequency signal generated by a quartz-crystal oscillator was applied to the second grid. The output of the mixer tube was taken through a low-pass filter whose cut-off frequency was of the order of 100 Kc/s and the beat-frequency, normally in the range 2-5 Kc/s, was displayed on an oscilloscope against the signal from a good-quality commercial A.F. oscillator. Troublesome feed-through of the quartz-crystal signal to the proton resonance circuit was reduced to an insignificant amount by picking up the proton R.F. signal in a short length of wire suitably placed near the R.F. amplifier, thus avoiding any direct connection between the two circuits.

Contour maps were plotted of the total magnetic flux density over various horizontal planes in the magnet gap, and some of these are reproduced in Figures (IV.3.7 - 9).

Initial exploration of the field in the mid-plane showed (Figure (IV.3.7)) that it was not quite axially symmetric. A simple and convenient method of correcting this was found to be to wrap a few turns of wire round each of the four corner-posts (return-paths for the flux) and to adjust a D.C. current through each coil independently until a symmetrical field distribution had been attained. The coils were then replaced by the appropriate numbers of turns of a single wire carrying the stabilised magnet

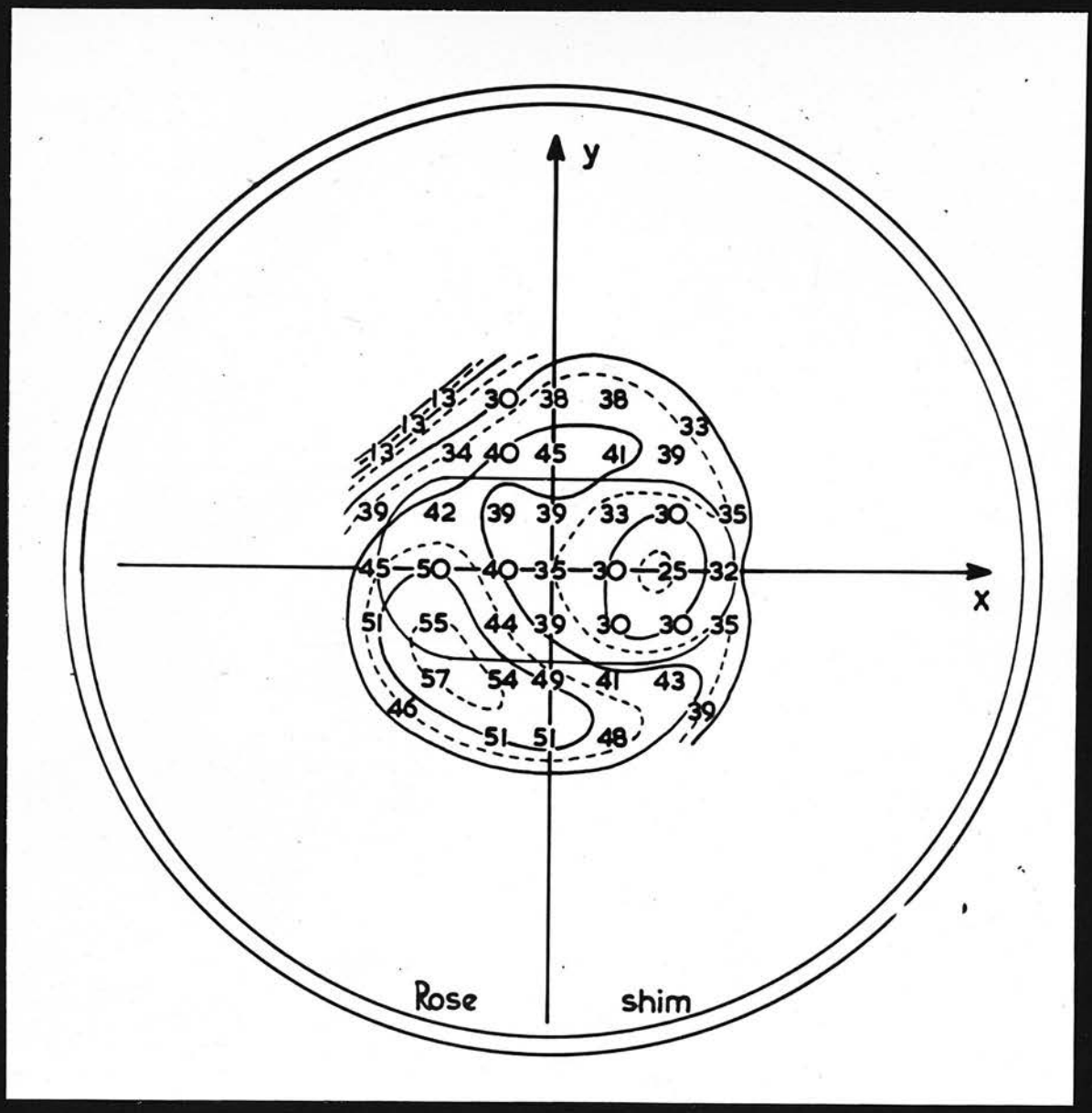

FIG. (IV.3.7) Contour map of magnetic field in median plane before adjustment;
1 unit ≡ 1 part in 10^5 (arbitrary zero);
region of electron orbits indicated.

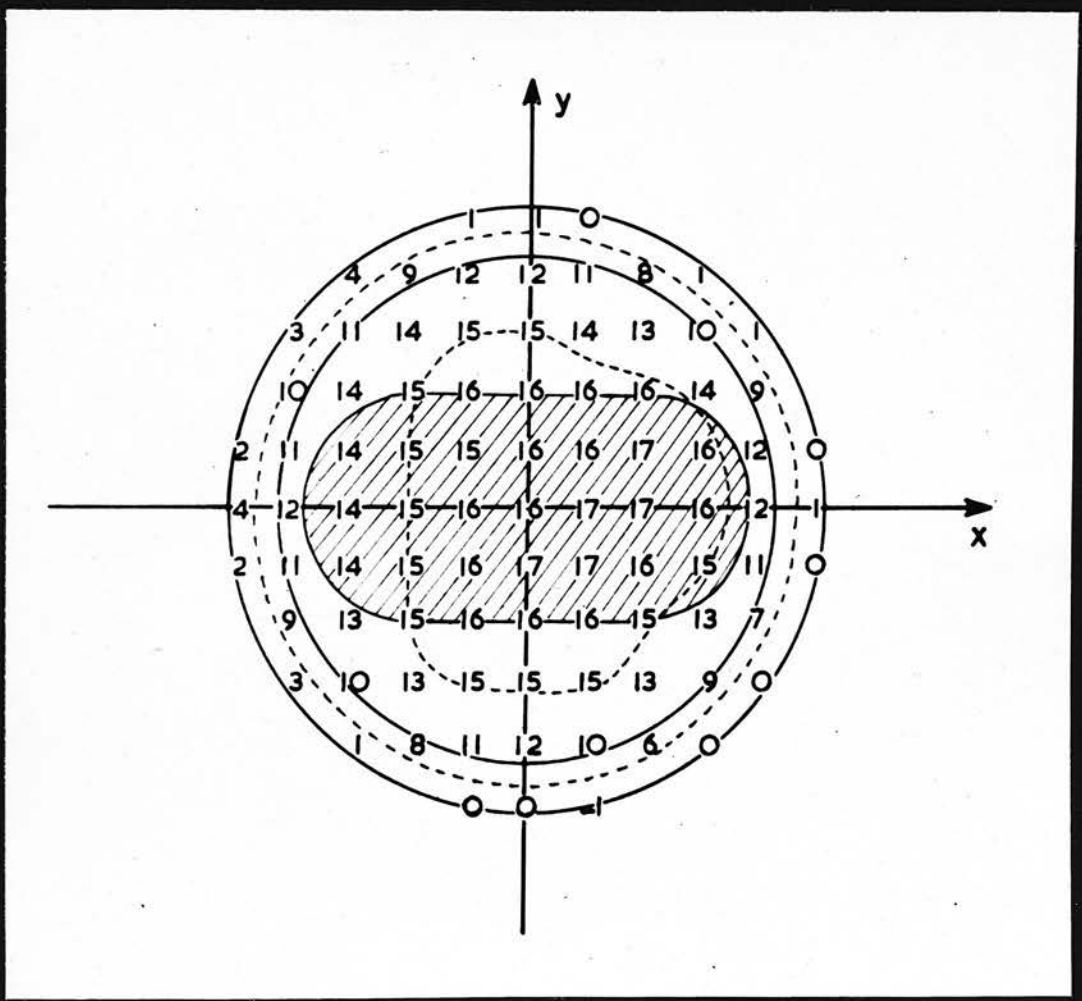

FIG. (IV.3.8) Contour map of magnetic field in a horizontal plane 1 cm. below median plane; 1 unit ≡ 1 part in 10^4 (zero arbitrary).

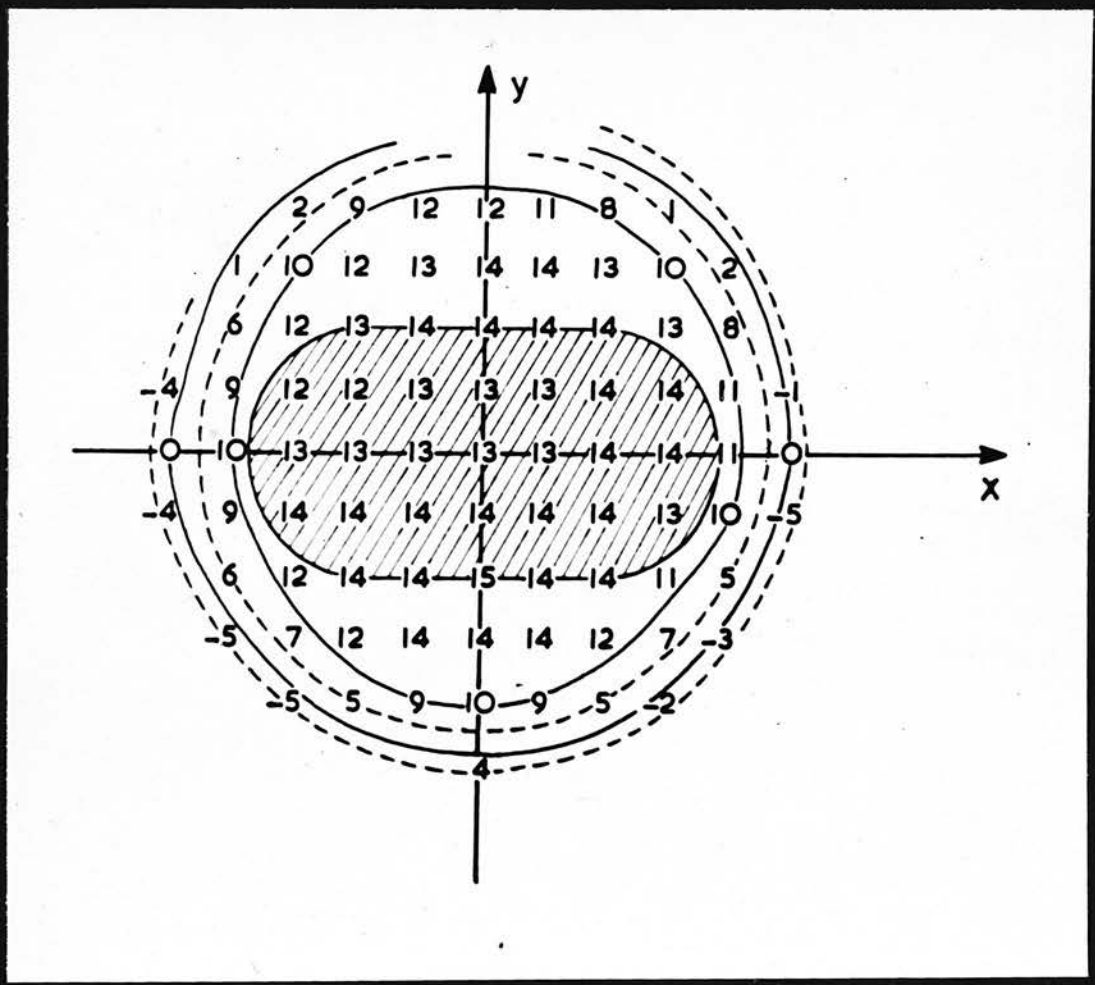

FIG. (IV.3.9) Contour-map of magnetic field in a horizontal plane 1 cm. above median plane; 1 unit ≡ 1 part in 10^4 (arbitrary zero).

current to the main coils, so that the same number of ampère-turns as before (to a sufficiently good approximation) were provided at each corner-post. The number of turns needed ranged from +4 to -4, representing a total range of 1% of the number of ampere-turns in the main coils.

There still remained a substantial variation of field strength in the vertical direction, which appeared to originate in some small asymmetry between the two sets of main windings. To compensate this asymmetry a coil of 30 turns was placed against one pole-face just inside the Rose-shim and outside the vacuum chamber. A current of the order of 0.5 Amp was needed in this coil, representing approximately 1% of the total ampere-turns. In what follows this coil will be referred to as the "correcting coil" and the current in it as the "correcting current, i_c". To illustrate the final field profile two contour-maps are reproduced. These give the field profiles over horizontal planes respectively 1 cm. above (Figure (IV.3.8)) and 1 cm. below (Figure (IV.3.9)) the median plane. The region swept out by electron orbits of 8 cm. diameter has been indicated to show the scale.

With regard to the type of magnetic field asymmetry referred to at the end of Section (III.6), scrutiny of these and their companion charts for planes at from +2 cm. to -2 cm. from the median plane, suggests that $\Delta B/\overline{B}$ was not greater than 2.5 parts in 10^5 on average.

The magnet was cycled when switched on to ensure reproducibility of the field. The main current could be measured by means of a standard 0.01Ω resistor and a potentiometer, but was normally reset to 0.3% using a good quality ammeter whose calibration was checked against the potentiometer. A magnetisation curve, Figure (IV.3.10), was taken with a Grassot Fluxmeter, and showed satisfactory linearity. Two spot values measured with the proton resonance magnetometer in the neighbourhood of the working field gave an absolute calibration and thereafter all magnetic field values were derived from the straight line passing through the origin and through the proton points. It was of course necessary to make a correction for the contribution due to the correcting current, i_c, and the appropriate calibration curve is given in Figure (IV.3.11). It will be noted that the contribution in question amounts to 3.04 gauss/amp.

For the purpose of effecting weak focussing (Section (III.5)) a pair of so-called shimming coils of rectangular shape and of 15 turns each were placed one above and one below the parallel-plate assembly inside the vacuum chamber. The width of the coils was equal to their separation, about 11.5 cm. The calibration curve for these coils is included in Figure (IV.3.11). Under normal working conditions the shimming current, i_s, did not exceed 0.4 Amps; thus the contribution to the main field from this source at the centre of the working region was normally not greater than

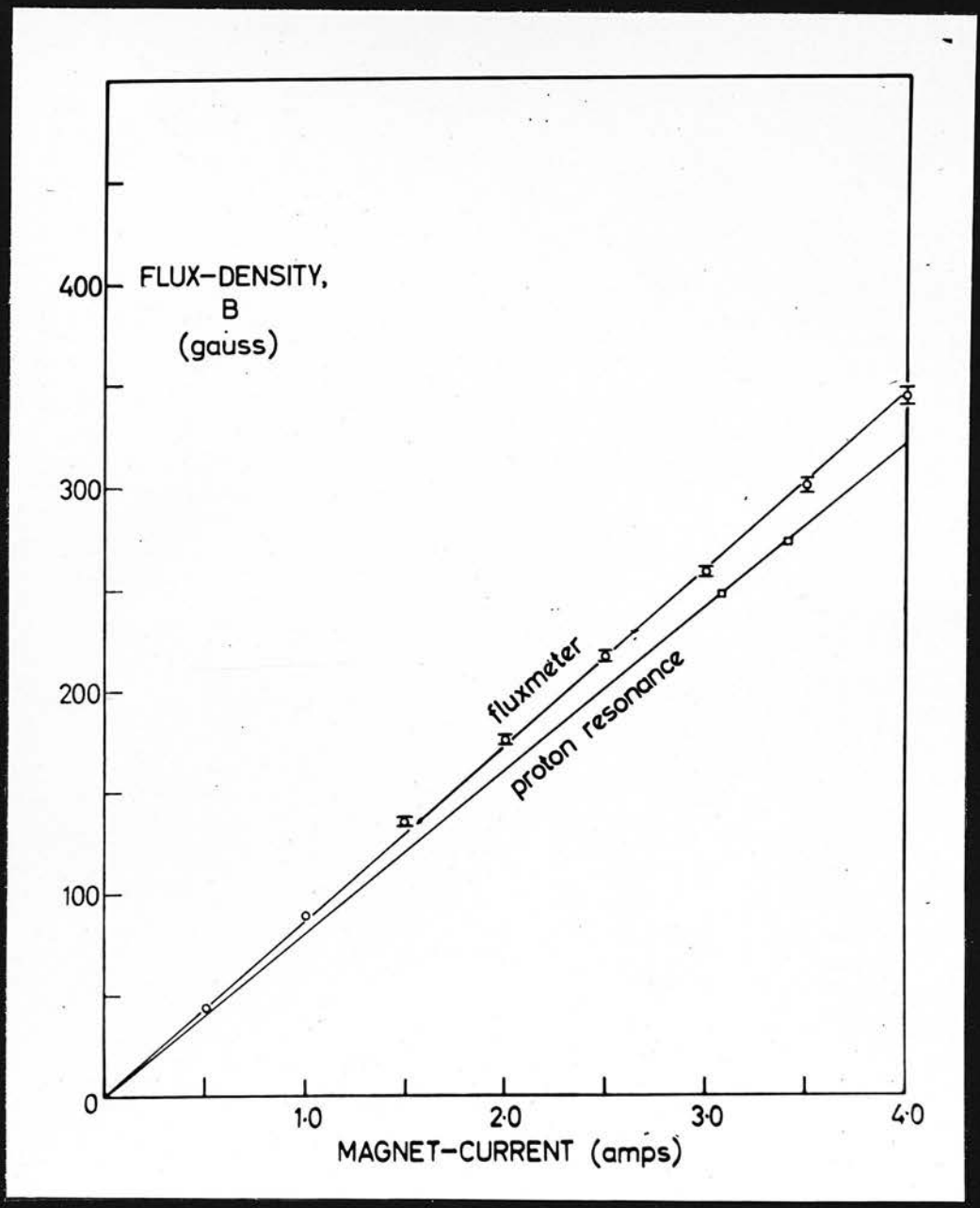

FIG. (IV.3.10) Magnet calibration.

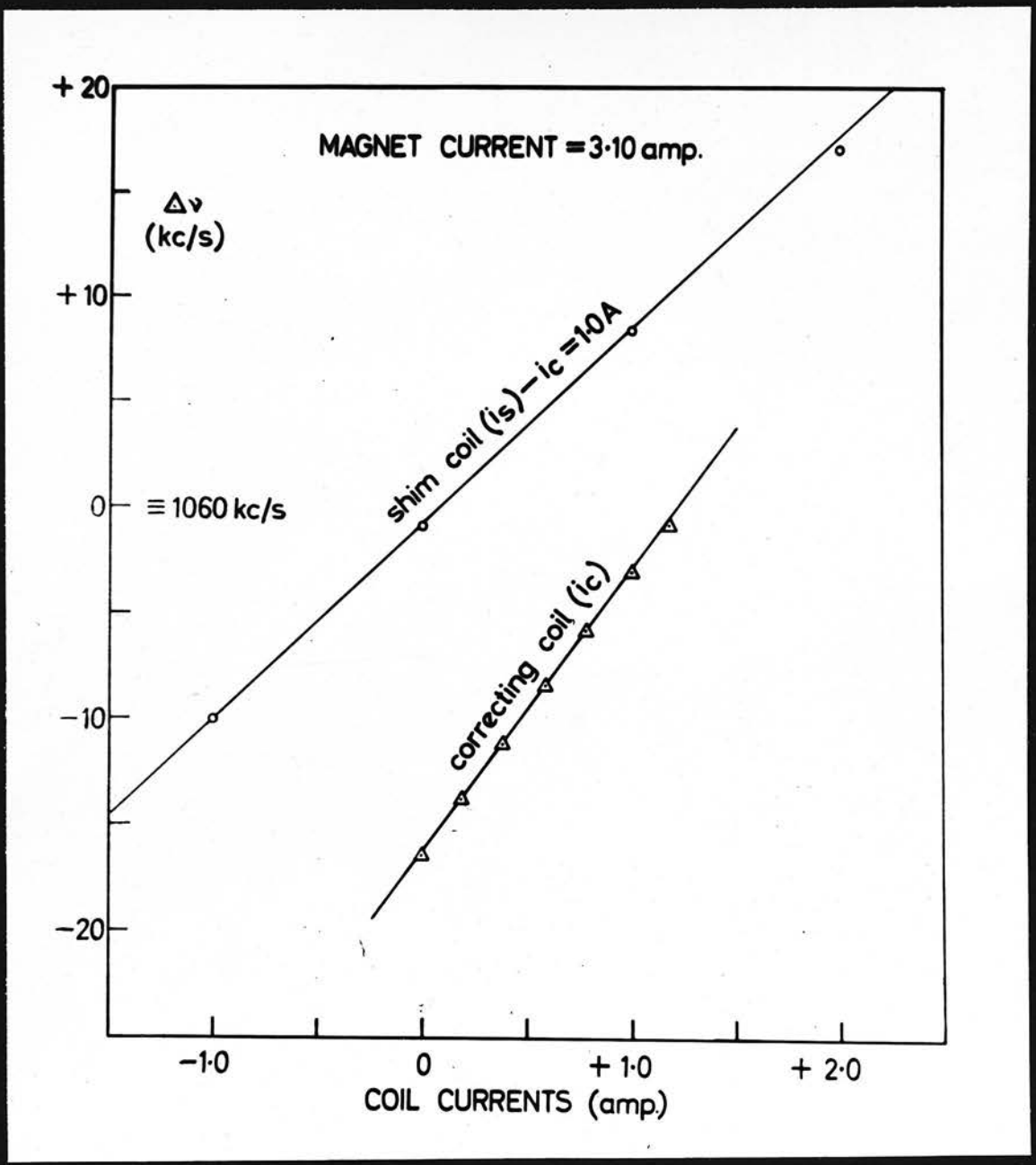

FIG. (IV.3.11) Correcting current and shimming current contributions to the magnetic field.

0.3 % , and the inhomogeneity associated with this contribution was clearly within the limits mentioned in Section (III.5).

(IV.4) The Vacuum

We have seen that a pressure of the order of 10^{-6} mm. Hg. would be desirable in the present experiment. Such a pressure can be reached and even surpassed in an unbaked metal apparatus provided certain conditions are met.

(a) All exposed surfaces should be clean and substances having an appreciable vapour pressure (such as perspex) should be excluded.

(b) A fast pump should be used, followed by a high-conductance pumping line.

(c) An efficient trap should be provided for oil and other vapours.

(d) All detectable leaks must be rigorously suppressed.

The vacuum system was designed with these requirements in mind, although it was not possible to satisfy the first condition completely. The vacuum vessel itself was of brass, the magnet pole-faces forming the closing sides. Silicone rubber O-rings were used to make the seals, since this material retains its resilience for long periods under stress. A six-inch fractionating oil-diffusion pump, provided with a water-cooled baffle, was backed by a single-stage rotary pump. Pressures were measured with a calibrated ion-gauge.

The steady vacuum attainable after prolonged pumping was, in practice, critically dependent on the rate of

leakage from the outside air and, after all detectable leaks had been sealed up, a pressure of less than 2×10^{-6} mm. Hg. was reached with several square inches of perspex surface in the system. A useful method of leak detection at low pressures was to direct a jet of helium gas at the suspected part and to observe the ion-gauge reading. When helium entered the system a marked decrease in the reading could be observed.

It was necessary to pass perspex light-guides through the wall of the vacuum vessel. Fortunately a simple type of compression seal proved adequate for this purpose (Figure (IV.5.2)).

(IV.5) The Counters

Certain advantages attach to the use of Geiger-Muller counters for detecting the scattered electrons. First, the counting efficiency depends almost entirely on the area and thickness of the window, and, with care, a pair of counters can be made nearly identical in these respects. Second, the counting rate due to natural background can be reduced to quite a low level (10-15 counts per minute) and will be closely equal in the two counters. Third, the counting rate is largely independent of small fluctuations or drift in the high voltage supply and, if a quenching circuit is used, electronic amplifiers may be dispensed with. Thus long counts may be taken without fear of drifts in counting rate.

In the earlier investigations of the scattering commercial thin-window counters were used. However, these suffered from three disadvantages. The window thicknesses varied from one tube to the next, though they were all specified to lie within the range 1-2 mg./cm.^{2}. Unfortunately, at electron energies as low as 100 keV, quite small differences in thickness become important. In addition the window area was very small, about 3 mm. x 9 mm., and as the counter could not be brought very close to the scattering foil the effective solid angle was small.

Finally, the metal parts of the glass-to-metal seals were of a magnetic alloy so that there was a risk of distorting the magnetic field.

At one stage in the investigation a pair of non-magnetic Geiger-Muller tubes was constructed. As some of the constructional features were not completely conventional, a brief description may be of interest. The tungsten anode-wire, of 6 mil. thickness, was sealed directly into Pyrex glass (Figure (IV.5.1)), an operation needing considerable care. The body of the counter was of smooth drawn aluminium tube and the ends were sealed with "Araldite", close-fitting "Teflon" ("P.T.F.E.") plugs having previously been inserted to prevent any possibility of the filling gases being contaminated by the "Araldite". Both windows were cut from the same piece of 1.5 mg./cm.^{2} mica sheet and were about 12 mm. long by 5 mm. wide. They were sealed on with a little "Araldite". The counters were filled to a pressure of 10 cm. Hg. with a mixture of dry argon and ethyl acetate vapour in the ratio of 9:1. For Co^{60} γ-radiation the plateaux of the two tubes, used as self-quenching counters, were 250 volts long and had slopes of 3% and 3½% per 100 volts respectively. For soft β-rays (S^{35}) the plateaux were 300 volts long and of negligible slope. The starting voltage in both cases was somewhat less than 1100 v.

It was found convenient, for the reason mentioned above, to use quenching circuits with these and with the commercial counters. The two anode leads had then to be shielded rather carefully to avoid triggering of one quenching circuit by the 240 v. quenching pulse of the other.

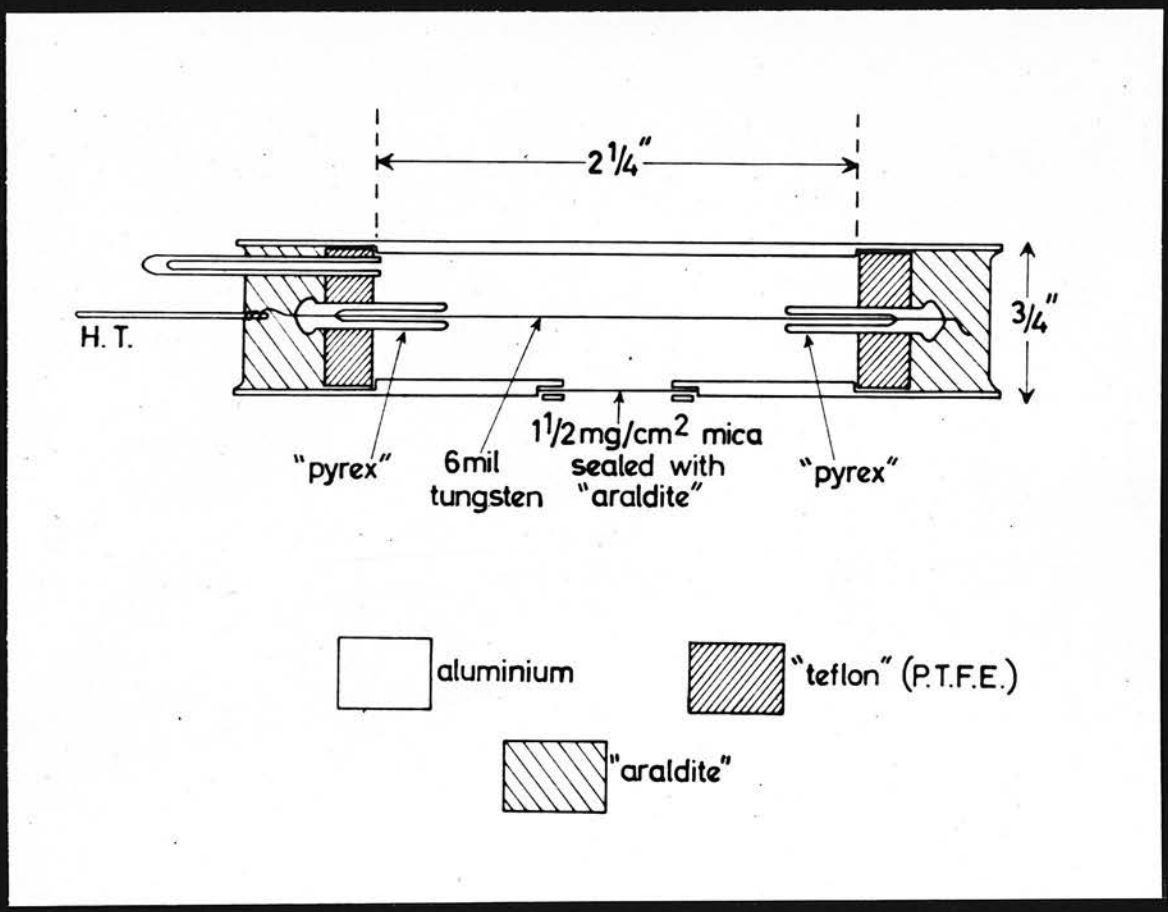

FIG. (IV.5.1) Geiger counter.

Although the tubes just described avoid some of the disadvantages of the commercial types, the use of Geiger-Muller tubes turned out in practice to be unfruitful and was discontinued in favour of scintillation counting. As sometimes happens, not all the reasons for abandoning the method still appear valid in the light of later work. Two, however, can be mentioned which still weigh heavily.

These may be summed up loosely in the term "signal-to-noise ratio". The first, and perhaps the most important, reason was the almost complete absence of energy resolution in the counter, while the second was related to the geometry of the system and in particular to the difficulty of making a sufficiently large window in a counter whose form was restricted to that shown in Figure (IV.5.1) by the cramped space available inside the vacuum vessel.

In studying the electron optics of the system it had in any case been found convenient to employ a scintillation counter to count electrons at the position of the target foil. A small piece of plastic scintillator (NE102) was attached to the end of a Perspex light-guide 12 ins. long and of 1 in. diameter. An E.M.I. 6097B photomultiplier picked up the scintillations and its output was passed to a pulse-amplifier, a single-channel pulse height analyser and a scaler. The necessity for such a long light-guide arose, of course, from the need to keep the photomultiplier well away from the influence of the magnetic field (the

use of a mu-metal shield would have caused gross distortion of the magnetic field itself). It was found that the efficiency of light collection could be increased very considerably by coating the scintillator and the end of the light-guide with a thin layer of magnesium oxide and by keeping the remainder of its surface polished and, in particular, grease-free. A special siliconeoil (Nuclear Enterprises (G.B.) Ltd.) was used to make good optical contact between the end of the light-guide and the photocathode.

This system was modified for the purpose of making scattering measurements, as follows. The single 1"-diameter light guide was replaced by two ½"-diameter light guides, as shown in Figure (IV.5.2). The E.M.I. 6097B tube was replaced by a pair of Twentieth Century Electronics RBMS10/14B miniature 10-stage photomultipliers with 14 mm. photo-cathodes, mounted one above the other (Figure (IV.5.2)). By using these tubes and the thinner light-guides not only could the double system be fitted into the space formerly occupied by the single scintillation counter, but also the scintillators could be brought close up to the scattering foil, thus greatly improving the solid angle for acceptance of scattered electrons. The greater length of the light guides relative to their diameter entailed some loss of energy resolution, unfortunately, but this was not serious.

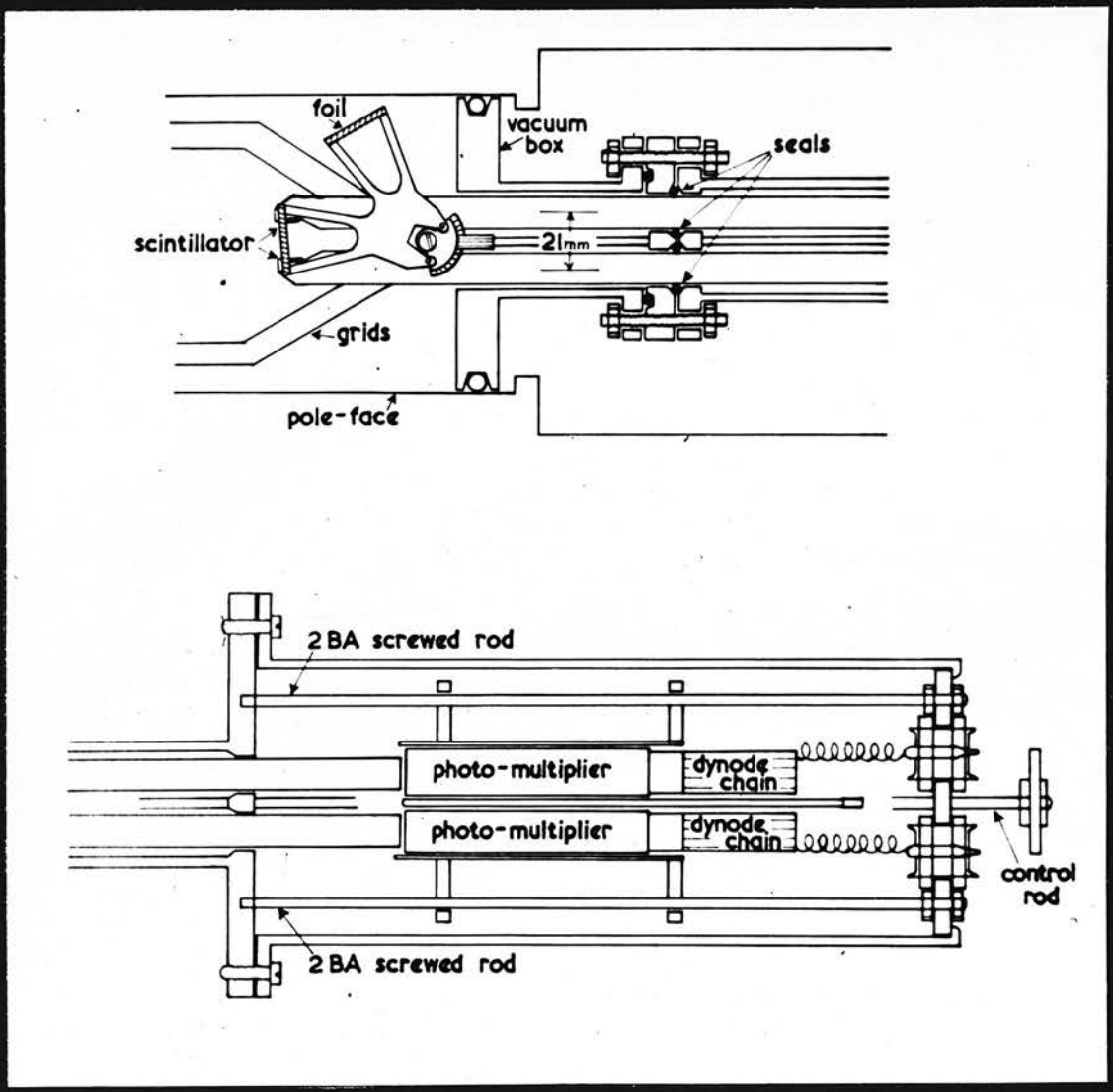

FIG. (IV.5.2) Double scintillation counter.

Once this system had been set up it was possible, by using suitably shaped scintillator-light-guide combinations to make observations on the direct beam also. Examples are given in Figure (IV.5.3) of pulse-height spectra obtained with such an arrangement for the nearly-monoenergetic electrons falling upon the scintillators when the magnetic field was reversed so that a semi-circular electron-beam was formed with the scintillator at the 180° point. Clearly, even at 100 keV energy, one cannot expect to be able to work at a very high overall counting efficiency especially when it is remembered that in practice the bias had to be turned up to about 20 v. when counting scattered electrons so as to reduce the relative number of photomultiplier noise pulses.

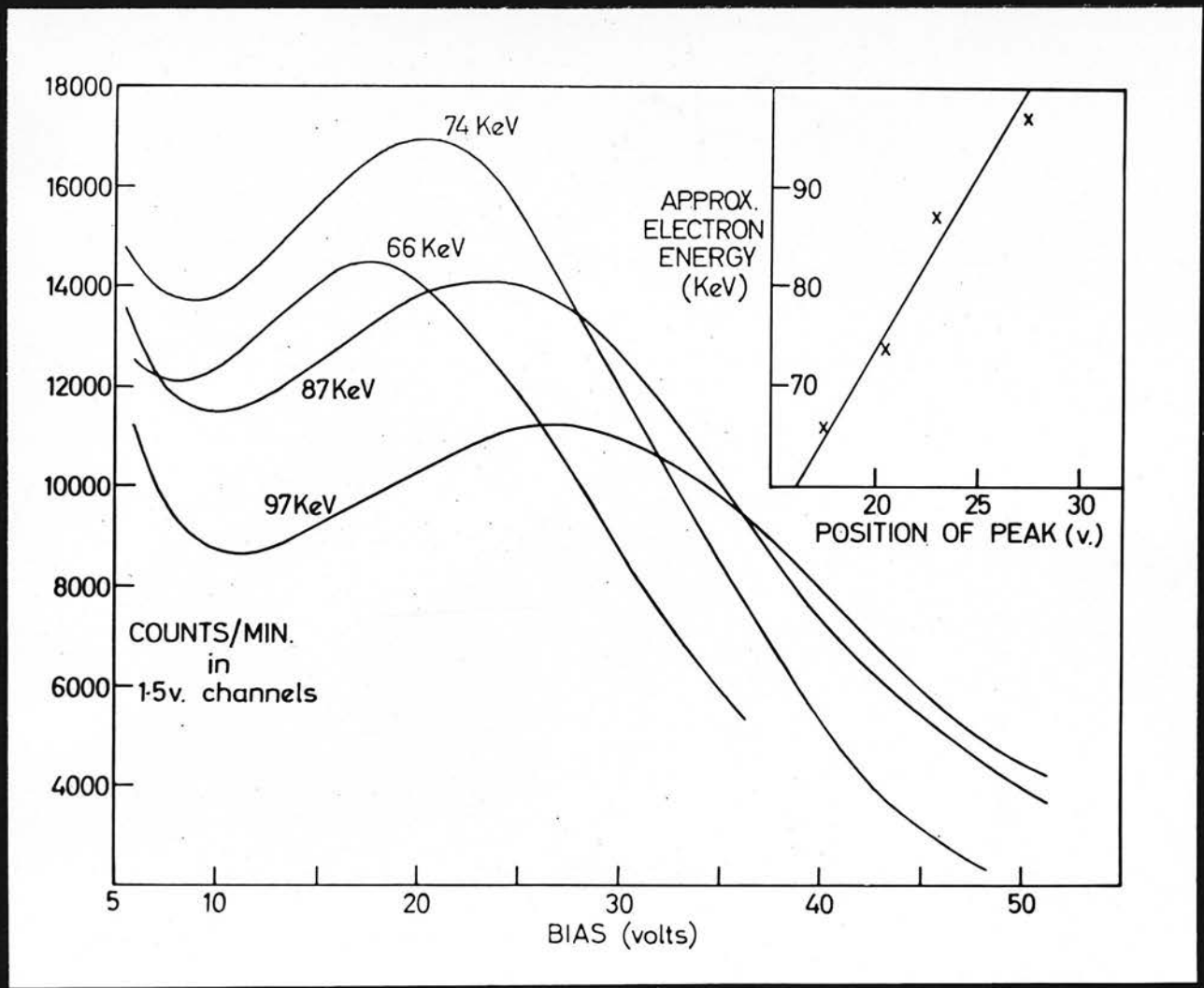

FIG. (IV.5.3) Pulse-height spectra for various electron-energies.

CHAPTER V

OBSERVATIONS AND CONCLUSIONS

(V.1) The Electron Beam

In an experiment involving the observation of electron-nuclear scattering it is clearly of vital importance to have an adequate beam intensity incident upon the scatterer. When the beam is derived from a β-active substance this may raise some problems. In the present experiment there have been two central experimental problems, that of beam intensity and that of eliminating instrumental asymmetries. The first will be discussed in this section.

For a long time line-sources were used exclusively but, even with the introduction of the z-focussing (Section (III.5)), it proved impossible to maintain a reasonable beam strength over much more than about 50 orbits. The reason for this, as has already been indicated (Section (IV.1)), was the necessity for the beam to pass the edge of the source-holder on completion of the first orbit. Because of this a progressively smaller segment of the source was effectively contributing to the final beam as the drift-distance per orbit was decreased.

The effect of this is illustrated by the lower curve in Figure (V.1.1). Each point on this curve represents (on a logarithmic scale) the best beam intensity obtainable with a particular line-source (Fig. (IV.1.1) at a given orbit-number after adjustment of the correcting current, i_c.

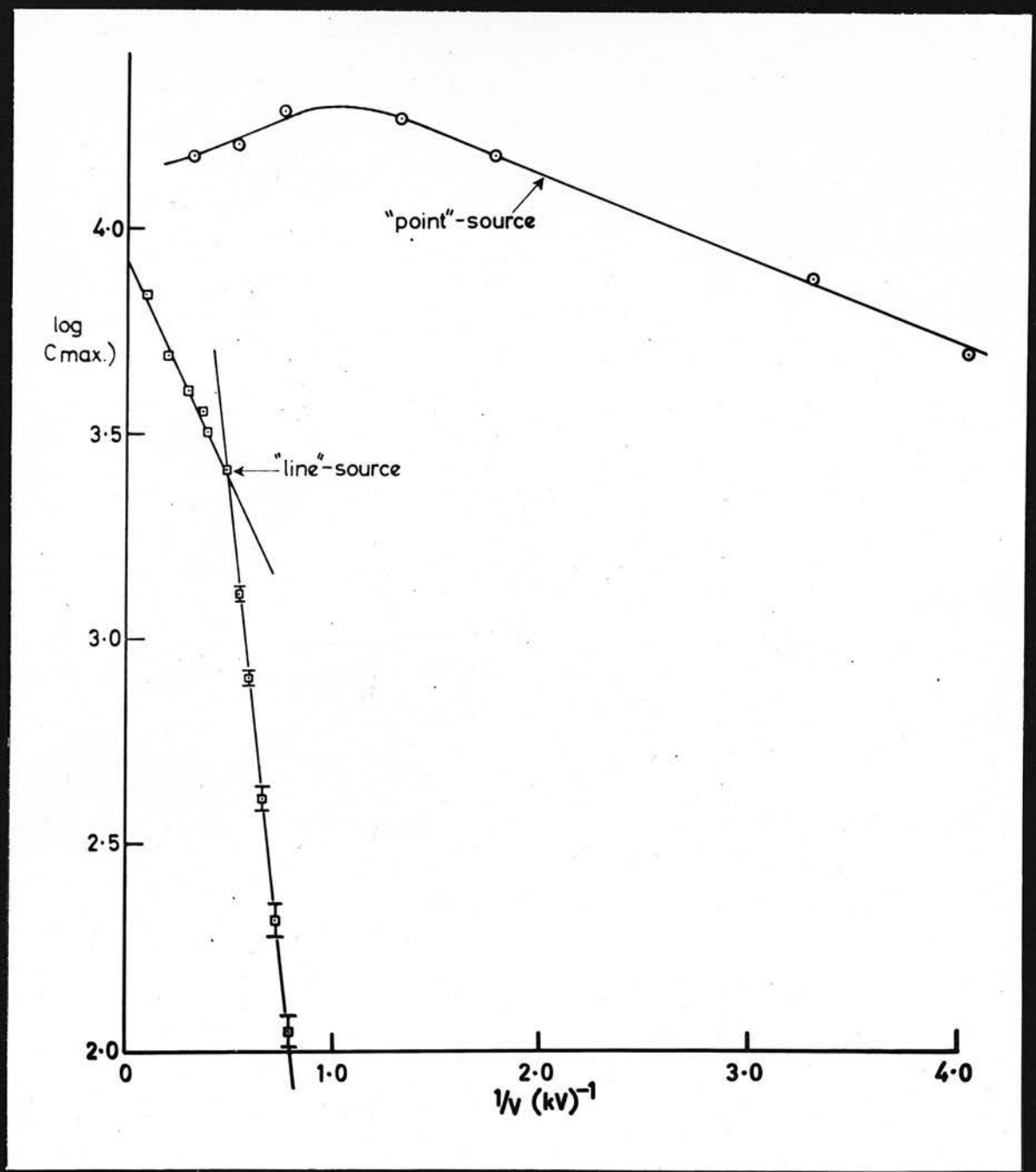

FIG. (V.1.1) Beam intensity with Point and Line Sources.

The magnetic field and shimming current, i_s, were fixed and the beam was observed by means of the scintillation counter with 1"-diameter light-guide mentioned in Section (IV.5).

The curve falls into two parts, the first section corresponding to those values of orbit-number, k, for which the whole beam was able to pass the source-holder. Even on this part of the curve, which extends up to about k = 60, there is an exponential fall-off in beam intensity with k. The slope is such that the intensity falls by a factor of "e" in the first 55 orbits. This is now believed to have been due largely to a distortion of the magnetic field in the region between source and baffle, caused by the presence of ferromagnetic end-caps on the cracked-carbon resistors used with the grid-assembly. The second section of the curve, which shows a much more rapid exponential fall-off of intensity, corresponds with orbit-numbers for which an ever-increasing fraction of the initial beam was cut off by the source holder as the drift-distance per orbit was decreased. Two quantitative considerations support this interpretation. First, the drift-distance per orbit, δ, is given by

$$\delta = 2\pi m_o \gamma E_y / dB_z^2 \qquad \text{(Appendix C)}$$

and, in the present case, this gives for the drift-distance, δ_c, at which the cut-off effect began to occur

$$\delta_c \simeq 1.5 \text{ mm.},$$

corresponding approximately with the distance of about 1.2 mm. from the outer edge of the source-holder to the inner edge of the source. Secondly, it was found that the beam intensity was reduced practically to the background level by the time a drift-distance of 0.8 mm. had been attained, corresponding to the distance from the outer edge of the source-holder to the outer edge of the source.

The improvement which was brought about with the introduction of the "point"-source (Fig. (IV.1.1))(b) was most striking, as can be seen from the upper curve in Figure (V.1.1), the more so inasmuch as the weak-focussing field was less by a factor of 7 in the second case than in the first. The upper curve was taken with the double scintillation counter described in Section (IV.5) using the Type A scintillator design shown in Figure (V.1.2). By the time these observations were taken the field homogeneity had been improved and the orbit diameter had been reduced from 10 cm. to 8 cm., but these factors could have made no more than a relatively minor contribution to the overall improvement. There was still an exponential decrease of intensity with orbit-number at orbit-numbers greater than about 150. Most of this must have been due to the removal of a definite fraction of the beam at each extra orbit by reason of its striking the back of the source-holder. The slope of the log plot can be accounted for quantitatively by assuming that the vertical width of the beam was about 8.5 times that of the source-holder, the latter being 3.5 mm. wide. A total beam width of 3 cm.

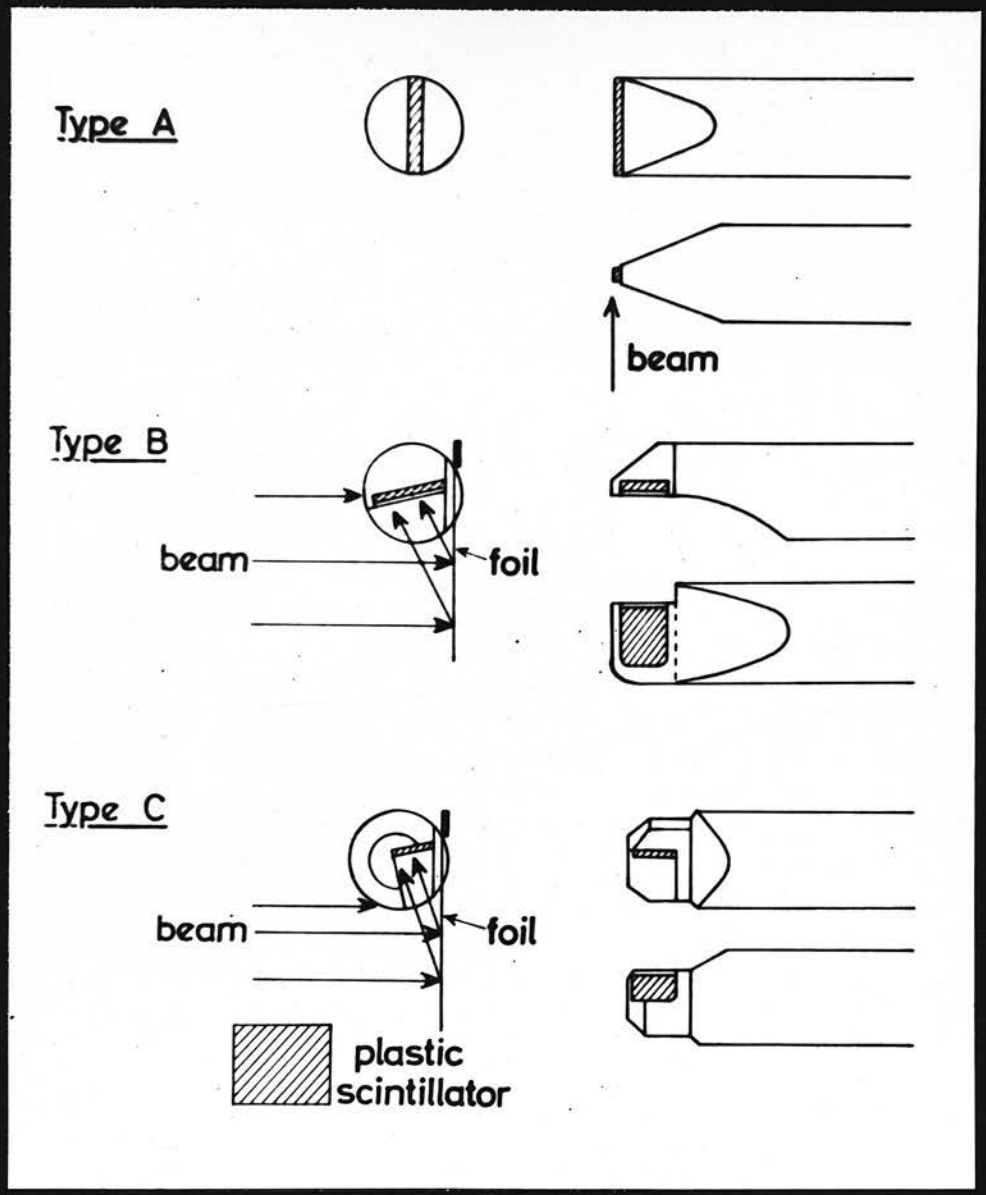

FIG. (V.1.2) Light-guide designs.

seems a very reasonable value. The apparent anomaly in beam intensity at the smallest orbit-numbers was probably not a genuine effect but simply a result of the fact that the drift-distance per orbit was greater than the width of the scintillator (0.6 mm.) as also was the width of the source ($\sim$ 2 mm.). Thus part of the beam may have missed the scintillator altogether.

A satisfactory beam intensity having been obtained, it was essential to examine how its distribution in the z-direction depended on such parameters as the correcting current, i_c, the shimming current, i_s, and the orientation of the parallel-plate assembly. This could be investigated rather conveniently using the double counting system referred to above, with the Type A scintillation heads.

Figure (V.1.3) illustrates the effect of altering the mean angle made by the parallel-plate system with the vertical at a relatively low orbit number ($k \simeq 35$), and with no weak-focussing ($i_s = 0$). Without weak-focussing, of course, one could not observe the beam at high orbit-numbers, whereas with weak-focussing present the orientation of the parallel-plate system had no effect on the respective counting-rates in the two counters. The latter observation indicated that the beam was being efficiently trapped by the weak-focussing field. Returning now to Figure (V.1.3) we see that, for each of the three values of correcting current, i_c, there appears to have been a well-defined electron beam which could be swept across each

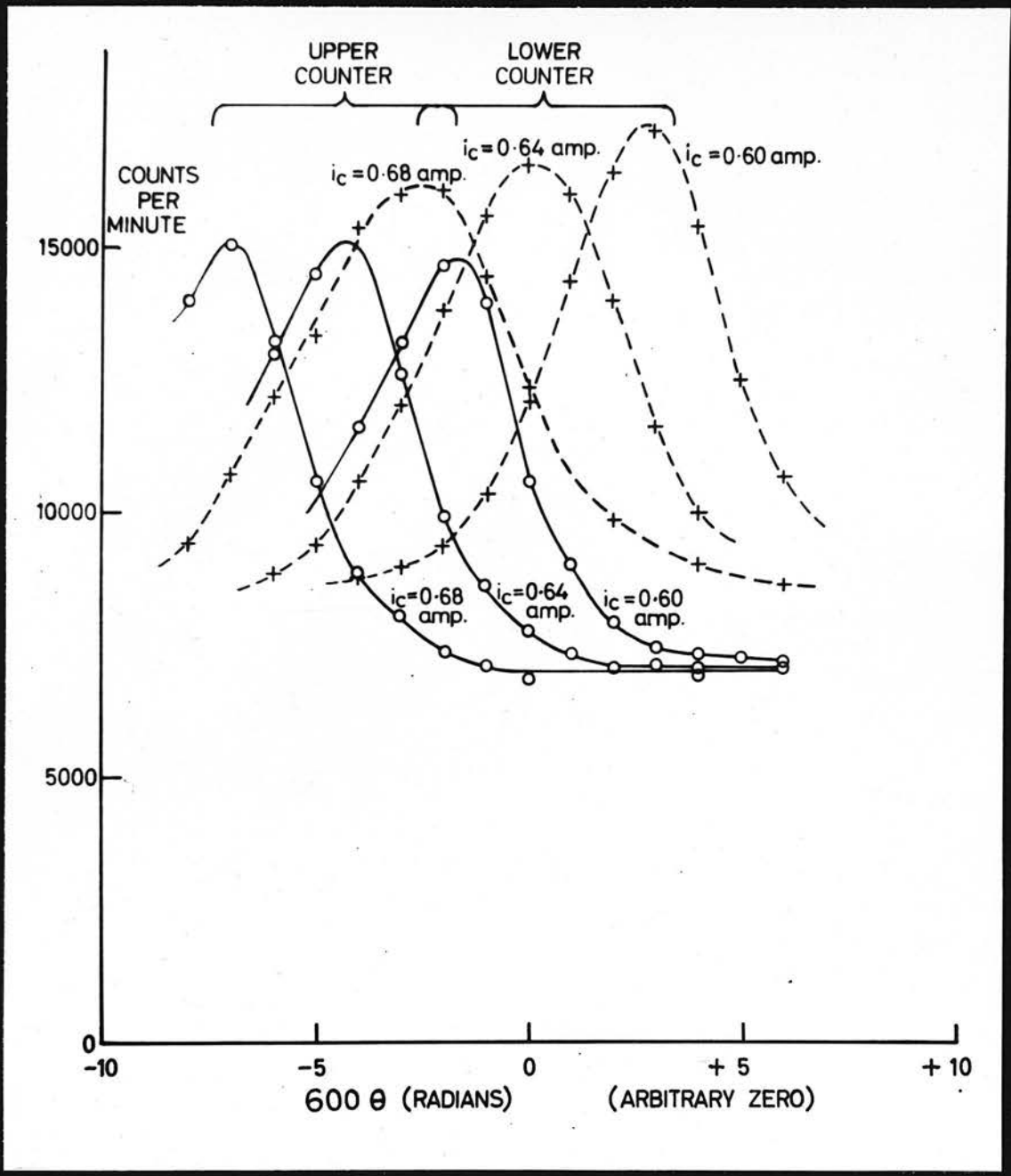

FIG. (V.1.3) Effect of Parallel-plate Orientation.

counter in turn. Positive deviations on Figure (V.1.3) corresponded to an increasing positive z-component of electric field and therefore to a downward displacement of the beam, in accordance with the observations. The separation of the peaks in terms of parallel-plate angle was nearly independent of i_c and was about 0.007 radians in magnitude. Using the formula

$$z = \pi D_2 \sin \theta k$$

derived in Section (III.6), we find, for the conditions of the experiment (D_2 = 79 mm.),

$$z \simeq 6 \text{ cm.}$$

The most plausible explanation for the discrepancy between this and the actual distance of 2.1 cm. separating the centres of the scintillators is that a small degree of weak-focussing existed even in the absence of a shimming current. Had this not been so, in fact, it is difficult to see how such an apparently well-defined beam could have been formed at all. The presence of this residual focussing effect was not unexpected, since positive values of i_c were such as to make a positive contribution to the total magnetic field while at the same time improving its symmetry with respect to the median plane, and these effects in combination imply the introduction of a weak-focussing configuration. It will be observed that the effect on the beam of increasing i_c was such that a negative orientation change was required to counteract it, indicating that increasing

values of i_c tended to depress the beam. This is in accord with the view already expressed (Section (III.6)) that the effect of increasing i_c should be to lower the horizontal symmetry-plane of the magnetic field and, with it, the beam. We note that there is no means of deciding, from this type of observation alone, what settings of i_c and of the plates give the ideal field configurations. The only way one can see of achieving this would be to observe the beam over a wide range of orbit-number and to adjust the two parameters in turn until the beam could be maintained in the median plane at all orbit-numbers. It has not been thought worthwhile to attempt this very lengthy operation at the present stage of development of the experiment, especially as the presence of even a small shimming current makes the beam distribution quite insensitive to the plate orientation.

As might be anticipated, however, the beam configuration was still moderately sensitive to i_c even with the weak-focussing field present. This is illustrated in Figure (V.1.4) for a particular value of electric field ($V = 760$ v.; $k = 185$ orbits) and for three values of shimming current, i_s. Only the curves for the lower counter have been shown, for greater clarity. It seems reasonable that, the greater is the shimming current, the greater will be the variation of i_c required to shift the horizontal magnetic symmetry-plane through a given vertical distance. This would explain the greater "half-widths" of the curves corresponding to higher values of i_s.

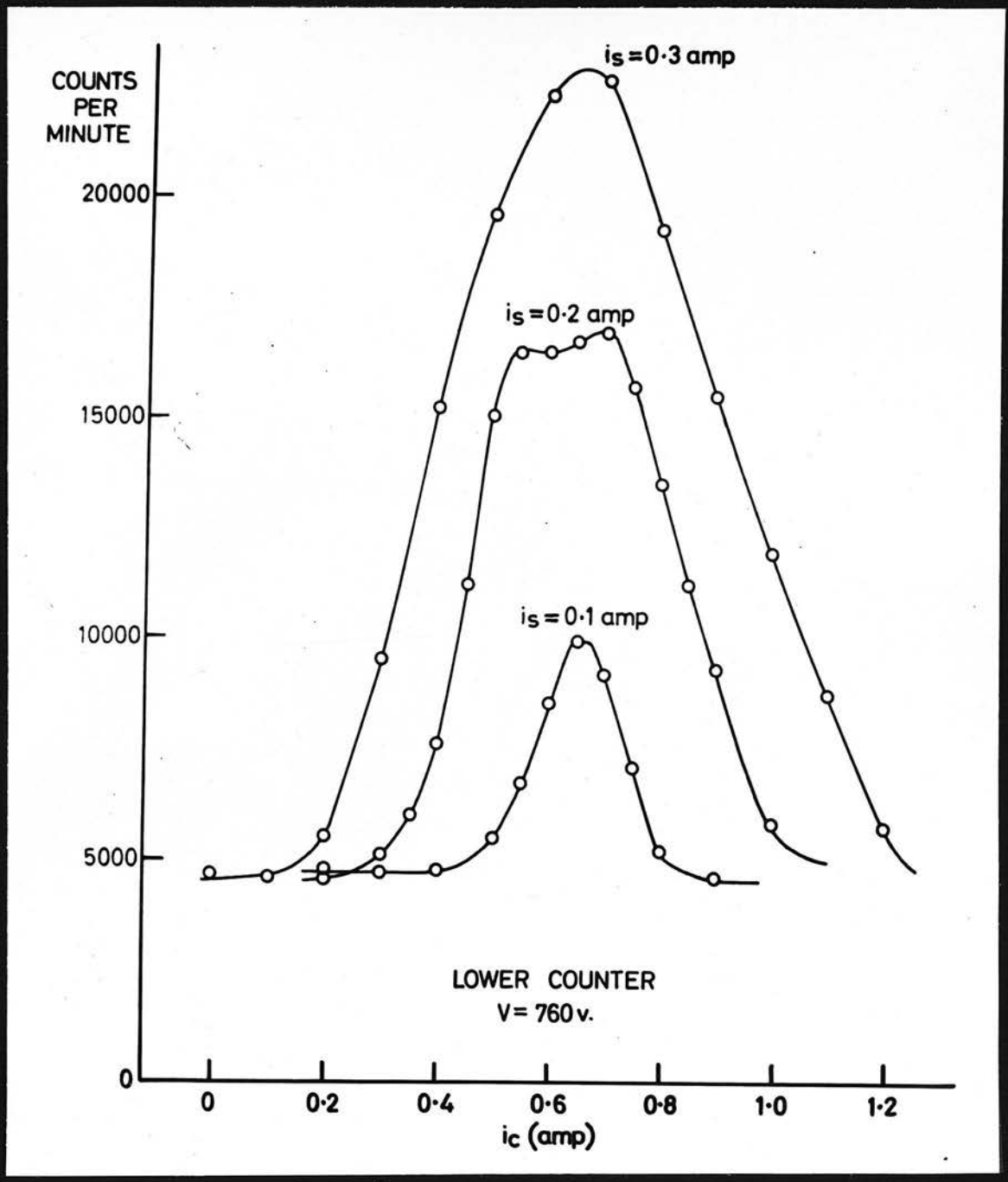

FIG. (V.1.4) Effect of correcting current, i_c. (V = 760 v.)

For values of i_s between 0.1 Amp. and 0.3 Amp., particularly at lower orbit-numbers, these curves were not always as simple and symmetrical in shape as they are in Fig. (V.1.4). In some cases sharp peaks in the counting-rate were observed in one or the other of the two counters. It is possible, but difficult to prove, that these peaks were due to focussing effects. In any case, it was considered desirable, for the purpose of measuring asymmetries, to raise the shimming current to a value sufficient to damp out any such abnormalities. A shimming current of 0.4 Amp. was found to be adequate to render all the curves similar in shape to that for i_s = 0.3 Amp. in Figure (V.1.4). An encouraging feature was that the peak of the curve occurred at nearly the same value of i_c over a wide range of voltage.

At lower voltages, however, there was a fairly marked shift in the position of the curves as i_s was changed. This is illustrated in Figure (V.1.5), which includes the curves for both counters. It would appear that a small shift of the horizontal magnetic symmetry plane was introduced by the shimming coils. In measuring scattering asymmetries one keeps i_s constant and varies the orbit-number so that, strictly speaking, one should reset i_c for each asymmetry measurement. This refinement has not been thought worthwhile at the present stage. In a final form of the apparatus, more care would be taken to avoid any structural asymmetry in the shimming coils.

It was possible, using the type A scintillation heads,

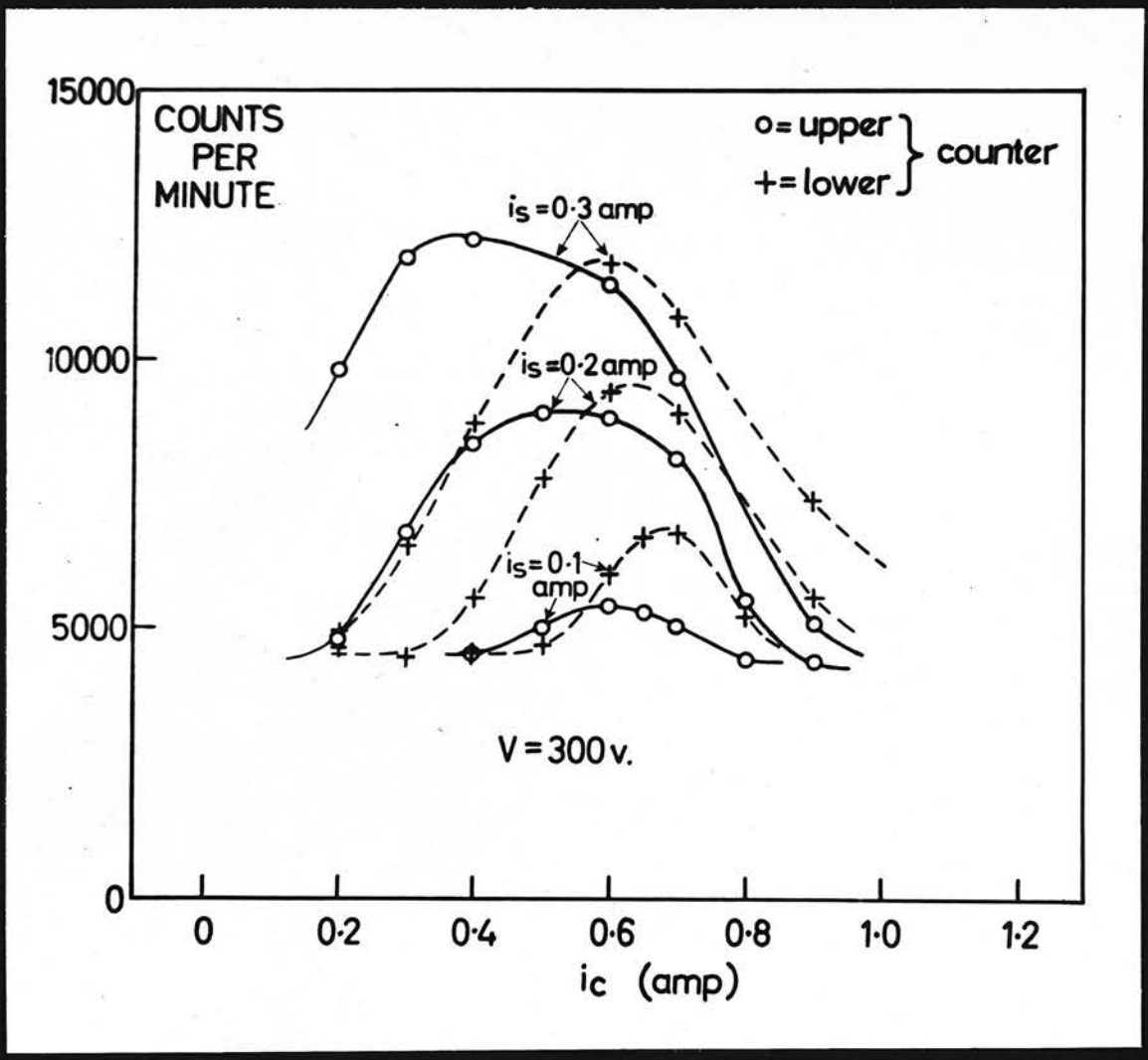

FIG. (V.1.5) Effect of Shimming current, i_s, on beam distribution (V = 300 v.)

to make a direct check on the validity of the equation

$$k = eD_2B_z^2/2\pi m_o \gamma E_y \qquad \text{(III.1.1)}$$

which gives the orbit-number in terms of the field-strengths. For this purpose a line-source was used and observations were made of counting-rate as a function of E_y or, in practice, as a function of the voltage-setting on the potentiometer which was used to monitor the output of the R.F. Voltage Generator. D_2 and B_z were kept constant, implying a nearly constant value of γ (but see later). The source and scintillator widths (about 0.4 mm. and 0.6 mm. respectively) were sufficiently narrow that the individual orbits could be resolved quite easily. The results are shown on Figure (V.1.6). It is clear, first of all, that the 360° focussing property was well-maintained over the whole range of orbit-number examined. The beam intensity falls off fairly rapidly, since only 0.1 Amp. shimming current was applied. The abscissae, v and v', represent the potentiometer readings on two different output ranges of the voltage generator; in both cases, however, they wwere proportional to electric field strength. The numbers attached to the individual peaks represent the number of orbits executed by the beam between source and scintillator at that particular voltage setting. These numbers were obtained from the following analysis, based on Equation (III.1.1).

From the form of that equation we see that, if the

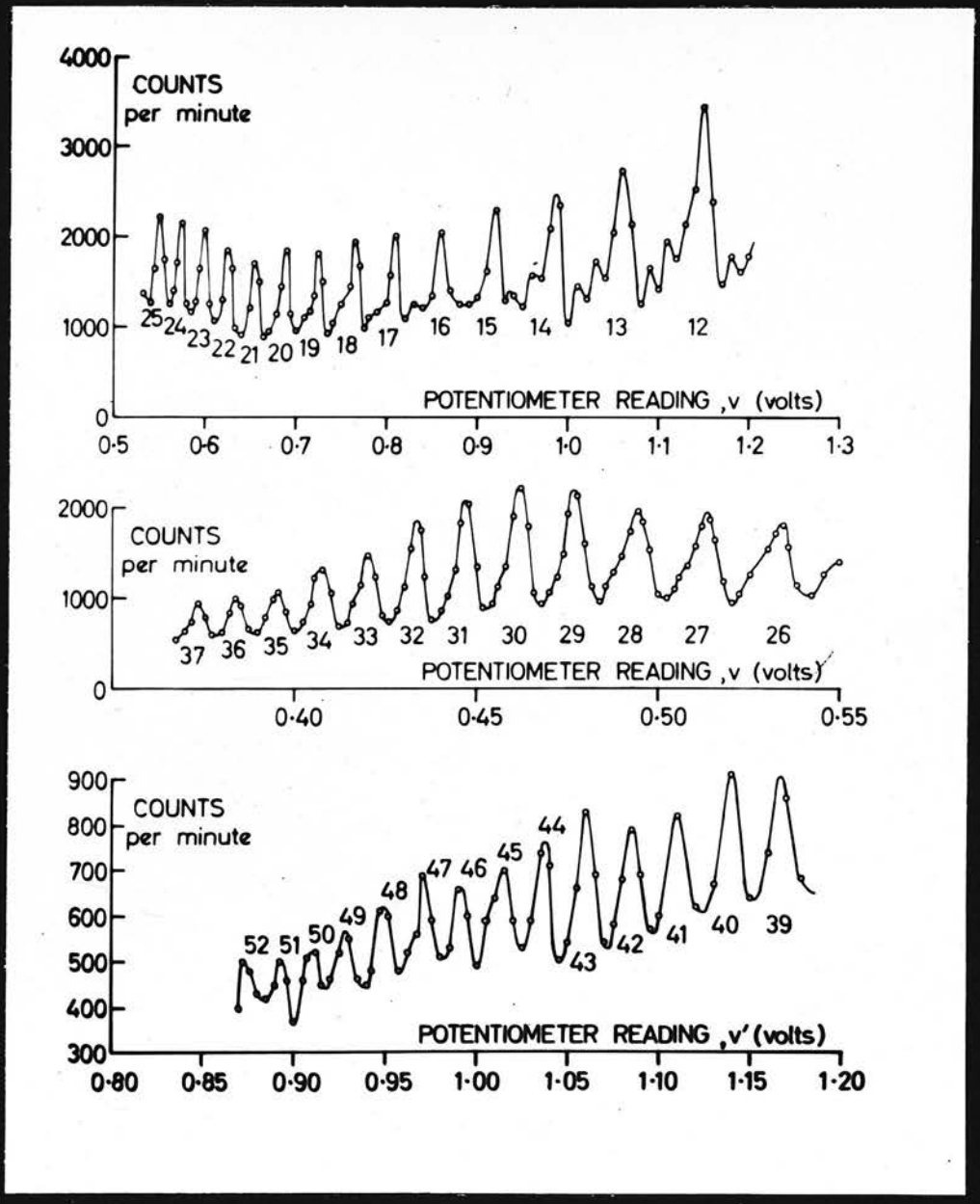

FIG. (V.1.6) Successive orbits from k = 12 to k = 52.

reciprocals of the voltages corresponding to successive peaks in the counting rate are plotted against a series of consecutive integers n, the points should lie on a straight line of gradient $(eD_2B_z^2/2\pi m_o\gamma)^{-1} = M$, say. Further, if the intercept made by this straight line on the axis of n = 0 is denoted by C_o, then

$$k = n + C_o/M,$$

where k is the orbit-number associated with that peak to which the number n has been arbitrarily allocated. It follows then that, if Equation (III.1.1) was actually obeyed, then not only should the points conform to a straight line but also C_o/M should be an integer. The reciprocal-voltage plots corresponding to the observations of Figure (V.1.6) are shown in Figure (V.1.7). There was no significant departure from the linear law. Analysis of the straight line plots gave the following results: see Table (V.1.1).

The mean value of the gradient was 7.57×10^{-7} $(V/m)^{-1}$. This ought to agree with the value calculated from the expression

$$M = 2\pi\gamma m_o/eD_2B_z^2$$

given above. Using the values of γ, D_2 and B_z appropriate to the conditions of the experiment one finds

$$M \text{ (calc)} = (7.7 \pm 0.1) \times 10^{-7} \text{ } (V/m)^{-1} .$$

Most of the uncertainty in this value arises from uncertainty in D_2, and, to some extent, in γ. The observed and calculated results are not in disagreement.

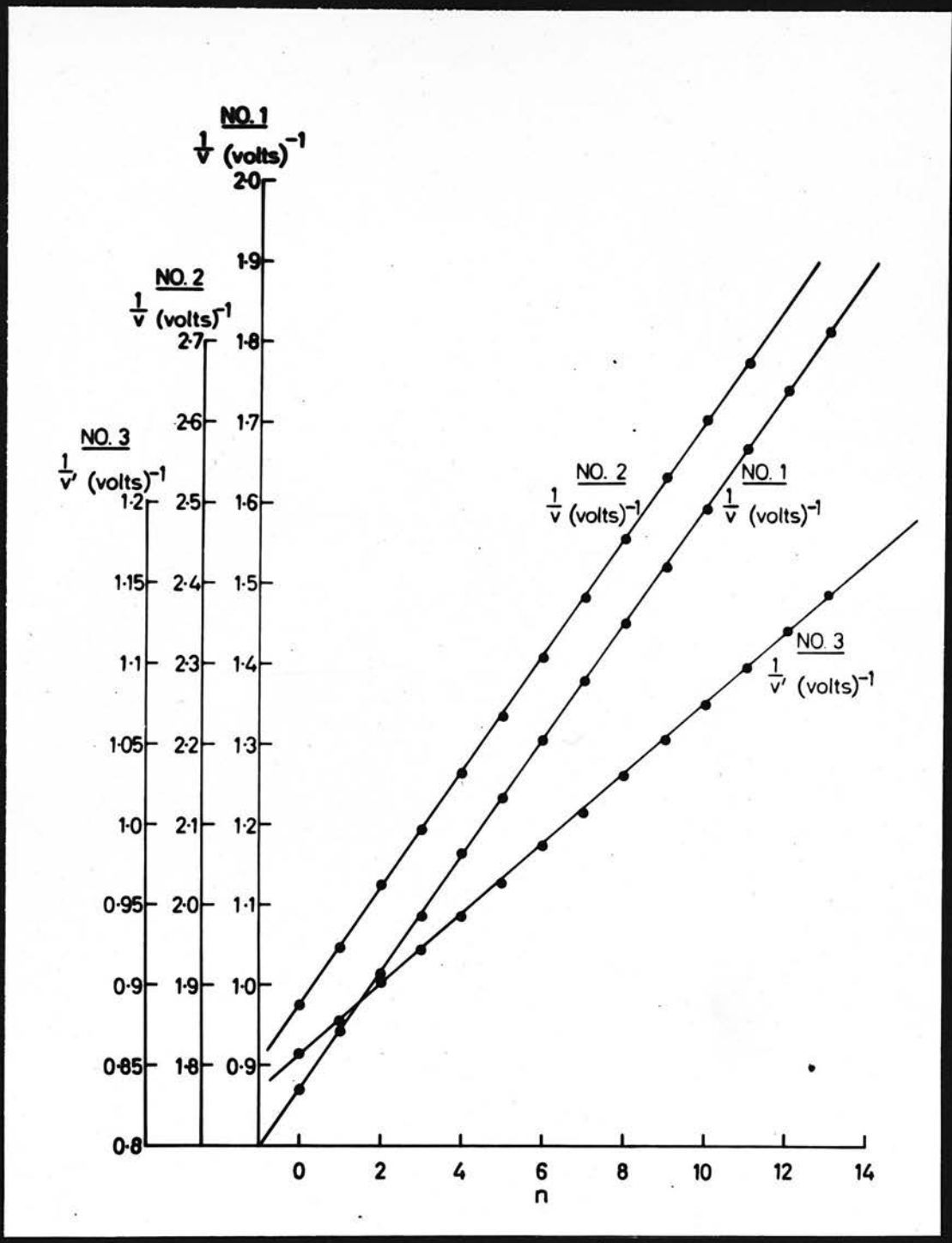

FIG. (V.1.7) Reciprocal-voltage plots of data of Figure (V.1.6).

TABLE (V.1.1)

ANALYSIS OF RECIPROCAL-VOLTAGE PLOTS

k	Gradient, $M(v)^{-1}$	Intercept, $C_o,(v)^{-1}$	C_o/M	Gradient, $(V/m)^{-1}$
12-25	0.0723 ± 0.0001	0.870 ± 0.001	12.03 ± 0.03	$(7.56 \pm 0.02) \times 10^{-7}$
26.37	0.0726 ± 0.0002	1.876 ± 0.001	25.8 ± 0.1	$(7.60 \pm 0.04) \times 10^{-7}$
39-52	$0.0220 \pm .001$	0.878 ± 0.001	39.9 ± 0.2	$(7.53 \pm 0.04) \times 10^{-7}$

One of the conclusions that can be drawn from these observations concerns the type of magnetic field asymmetry discussed at the end of Section (III.6). If such an asymmetrywas actually present, then, in view of the integral values obtained for the orbit numbers, its contribution to the drift-rate of the orbits probably did not amount to more than one part in 200 up to the 50th orbit. Unfortunately since the error, Δk, in orbit-number due to this cause is proportional to k^2, one cannot usefully extrapolate this result up to orbit-numbers of the order of 1000.

Finally, the uncertainties in the values of D_2 and Υ mentioned above call for some comment. In the case of D_2, the source-to-target distance, the uncertainty can be reduced to negligible proportions by taking sufficient trouble over the distance measurement, by using a travelling microscope for instance. The appropriate value of Υ, however, has to be calculated from a knowledge of the effective aperture $D_1 - L_2$ (Section (III.3), p. 13) in conjunction with the shape of the β-spectrum over the momentum range transmitted. The effective aperture can be measured accurately, but the shape of the β-spectrum must be assumed. However, at energies of 100 keV, the β-spectrum cannot be seriously distorted by source absorption and back-scattering and, in any case, Υ is a very slowly varying function of momentum. Thus, neither of the uncertainties mentioned need be a permanent feature of the experiment.

(V.2) Observations of the Scattering Asymmetry

Several attempts were made to detect the spin-dependent scattering asymmetry using Geiger-Muller counters, but none were successful. As has been indicated already (Section (IV.5)), this was not wholly attributable to the properties of the counters. The main reasons, in fact, were first and foremost a lack of adequate beam intensity and, secondly, insufficient care in eliminating instrumental asymmetries. Scattered electrons were actually detected with Geiger-Muller counters at low orbit-numbers, the ratio of scattered electrons to background electrons being about 1:3. This would have been a very favourable ratio had all the scattered electrons been elastically scattered. But, because of the lack of energy resolution of the counters, this could not have been so and the signal-to-noise ratio just mentioned certainly gives a falsely optimistic picture vis-a-vis elastic scattering.

More recently a considerable degree of success has been achieved in obtaining an adequate and properly formed electron beam and renewed efforts have been directed towards the measurement of scattering asymmetry. Scintillation counting has been adopted for this purpose because of the better energy resolution obtainable and because of the much greater solid angle which can be subtended by the counter "window" at the scatterer. The system with which the observations to be reported below were obtained was

that illustrated in Figure (IV.5.2) and described in Section (IV.5). Type B light guides were employed (Fig. (V.1.2)). The principal experimental problems which arose in the use of scintillation counters were three in number. First, it was desirable that the counting efficiencies of the upper and lower units should be equalised as far as possible. To achieve this, the magnetic field was reversed and a pulse-height spectrum taken for the approximately monoenergetic beam falling on the scintillators. The H.T. supplies to the photomultipliers, the gains of the respective amplifiers and the discriminator biases were then set so that as nearly as possible the same numbers of electrons were being counted in each counter. With the semicircular electron-beam the counting rates were such as to swamp the photomultiplier background noise, which could therefore be ignored for this purpose. These same settings were maintained constant during the scattering measurements when, in fact, the photomultiplier noise formed an appreciable fraction of the total counting-rate. The actual pulse-height curves obtained with the type B heads were closely similar to those shown in Figure (IV.5.3) so it was clearly necessary to sacrifice a good deal of the counting efficiency in order to keep the background level down. Under conditions giving curves similar to those of Fig. (IV.5.3), the discriminator biases were set at from 20v. to 25v. The electron energy

chosen for the scattering measurements was 100 keV, so that the counting efficiencies for elastically scattered electrons were probably in the range 50-70%.

The second experimental problem mentioned above was that of eliminating the background counts contributed by photomultiplier noise pulses. To do this it was necessary to set up an interchangeable foil-holder so that counts could be taken with foil and without. The foil-holder is illustrated in Figure (IV.5.2), the centre space being blank and provision being made for fitting two different foils. The control rod for the foil-holder passed through a vacuum seal of the same kind as was used for the light-guides and emerged through a light-tight orifice at the rear of the photomultiplier housing.

Subtraction of the counting-rates with and without foil should give the genuine scattering rate provided, of course, that the noise-level remains constant throughout For the most part this would appear to be a valid assumption but, in any case, slow drifts in noise level may be eliminated by breaking up the full counting periods into short sections and carrying out the subtraction over the individual sections. This was the procedure actually used. Another advantage of this procedure is that any sudden change in background counting rate can be detected at once. Such a change has been noticed on one or two occasions, and because of this it was unfortunately not possible to leave the apparatus counting for long periods unattended,

thus limiting the quantity of data obtainable.

The third problem requiring careful attention was that of eliminating instrumental asymmetries. It is orthodox practice to use an aluminium scattering foil for comparison purposes, since there is only a small spin-dependent contribution to the elastic scattering from light elements. This has been tried in the present case both with 1 mg./cm.^{2} and with 2 mg./cm.^{2} aluminium foils but the scattering-rate has always been found to be so low that an adequate signal-to-noise ratio has not been achieved. In principle, taking account of the different densities and scattering cross-sections, a 2 mg./cm.^{2} aluminium foil should give the same scattering at backward angles near 90° as a 0.4 mg./cm.^{2} gold foil. In practice, however, the scattering rates from such foils were in the ratio of 1:5 approximately, a point which will be further discussed below.

Although it is possible that this difficulty may be overcome by the use of, say, a 10 mg./cm.^{2} foil there are reasons (see below) for thinking that the scattering rate may be much less than proportional to the thickness.

A less well-known method has, therefore, been attempted. This method makes use of the fact, discussed in Section (III.3), p. 10, that the spin-dependent asymmetry for thick gold foils is much reduced compared with that for the thinnest foils. An analysis can be given (see Section (V.3)) which suggests that the difference between the asymmetries measured with a thin and a thick gold foil should be proportional to the spin-

dependent asymmetry and independent of the instrumental asymmetry, provided the latter is not too large. Further discussion of this general problem will be postponed to the next section.

The gold foils used in the observations were of thickness 0.4 mg./cm.^{2} and 2 mg./cm.^{2} respectively, and the data are given in Table (V.2.1). Because of the very time-consuming nature of the operation these were more limited in number than was desirable. They were obtained by the subtraction procedure described above. Each count lasted for 30 minutes; a complete set of three therefore occupied 1½ hours, over which period there was assumed to have been only a negligible drift in the various parameters. Seven such sets of values for the scattering rates from the thin and thick foils at each orbit-number, k, were taken. These were averaged and the standard deviations calculated from the residuals. Any observation lying at more than four times the standard deviation from the mean was rejected (4 actual counts out of 150 were involved), and a new mean and standard deviation were calculated.

The asymmetries are shown graphically in Figure (V.2.1) with their standard deviations. Comment will be reserved for the next section.

Since these observations were taken a new pair of light-guides have been installed in an attempt to improve the signal-to-noise ratio. These were the Type C light-guides of Figure (V.1.2) and they were designed to give better shielding of the scintillator against electrons from

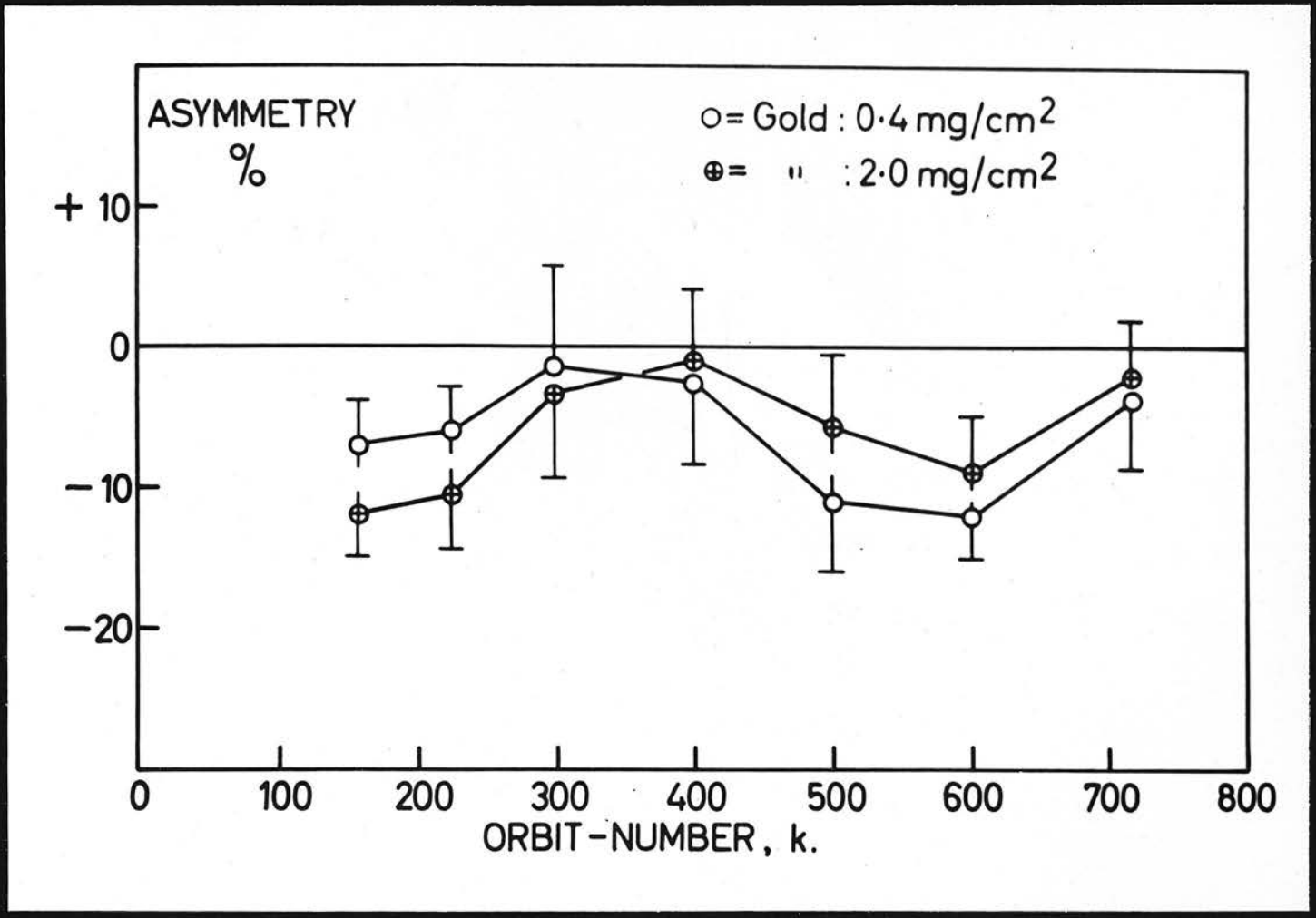

FIG. (V.2.1) Asymmetry observations with gold targets.

TABLE (V.2.1)

Observations on Scattering from Thin and Thick Gold Targets

Orbit Number, k	Thin			Thick			$A_{thin} - A_{thick}$
	Upper cts./30 mins.	Lower cts./30 mins.	Asymm.% $(\frac{u-L}{u+L})$	Upper cts./30 mins.	Lower cts./30 mins.	Asymm.% $(\frac{u-L}{u+L})$	
160	915 ± 47	1056 ± 37	-7 ± 3	1155 ± 70	1477 ± 24	-12 ± 3	+5
225	820 ± 36	920 ± 30	-6 ± 3	1020 ± 80	1260 ± 21	-10.5 ± 4	+4.5
300	715 ± 36	735 ± 93	-1.4 ± 7	1104 ± 67	1179 ± 116	-3.3 ± 6	+2
400	693 ± 66	727 ± 57	-2.4 ± 6	1022 ± 95	1042 ± 35	-1.0 ± 5	-1.5
525	616 ± 50	767 ± 55	-11 ± 5	842 ± 59	940 ± 58	-5.5 ± 5	-5.5
640	513 ± 28	657 ± 26	-12 ± 3	772 ± 62	925 ± 36	- 9 ± 4	-3
715	517 ± 58	557 ± 10	-3.7 ± 5	842 ± 59	876 ± 32	- 2 ± 4	-1.5

the electron beam itself. These have been found to improve the signal-to-noise ratio by a factor of two. A 0.4 mg./cm.^{2} gold foil and a 2 mg./cm.^{2} aluminium foil have been used with these but, as has been explained above, the aluminium gave a very low scattering rate and no valid comparison would have been possible in a reasonable counting-time. The results obtained are given in Table (V.2.2). The asymmetries for the gold foil were all shifted upwards compared with the previous case because the discriminator biases were changed to suit the new light-guides.

It should be remarked, in connection with the considerations of Section (III.3), that it has been found best in practice to observe backward scattering because it is easier to protect the scintillator from the main beam and so to obtain the best signal-to-noise ratio.

TABLE (V.2.2)

Observations of Scattering from Gold (0.4 mg./cm.^{2} and Aluminium (2.0 mg./cm.^{2})

Orbit Number, k	Gold			Aluminium		
	Upper cts./min.	Lower cts./min.	Asymm. % $(\frac{u-L}{u+L})$	Upper cts./min.	Lower cts./min.	Asymm. % $(\frac{u-L}{u+L})$
160	26.0 ± 1.0	24.9 ± 0.8	2.1 ± 2.5	6.0 ± 1	4.3 ± 0.8	17 ± 12
400	21.9 ± 1.1	16.8 ± 0.9	13.2 ± 3.5	3.3 ± 0.9	4.5 ± 0.8	-16 ± 15
525	17.6 ± 1	16.3 ± 0.9	3.8 ± 4	4.8 ± 0.9	2.9 ± 0.8	25 ± 16
715	19.6 ± 0.9	16.6 ± 0.7	8.3 ± 3.2	4.5 ± 0.9	0.0 ± 0.7	100 ± 25
890	15.8 ± 0.9	17.5 ± 0.8	-4.9 ± 3.5	2.1 ± 0.9	1.6 ± 0.8	15.5 ± 34

(V.3) Interpretation of the Observations

We give first an analysis of the problem of instrumental asymmetries. In the experiment of Schupp, Pidd and Crane (1961) these were ignored on the tacit assumption that they were at most slowly-varying functions of the trapping time, as indeed they appeared to be. In the present experiment, however, where at most two full periods of the relative spin precession may be expected to be observed, one cannot assume that the instrumental asymmetries will not seriously affect the measurement of the period.

Let us assume that we use two foils to measure asymmetry, one of thin gold (thickness = t mg./cm.^{2}) and one of thick gold (thickness = T mg./cm.^{2}). Let the counting rates in the upper and lower counters after subtraction of background be N_t^u, N_t^L for the thin foil and N_T^u, N_T^L for the thick foil. Then

$$N_t^u = N(k)\{1 + a(k,t)\}\{1 + \varepsilon(k)\}$$

$$N_t^L = N(k)\{1 - a(k,t)\}\{1 - \varepsilon(k)\}$$

with similar expressions for the thick foil. Here $N(k)$ is some number depending on the orbit-number, k, while $\varepsilon(k)$ expresses the instrumental asymmetry which comprises all asymmetries other than the spin-dependent asymmetry $a(k,t)$. The latter is assumed to be a function of foil thickness as well as of orbit-number, but $\varepsilon(k)$ is assumed

not to be different for the two foils. Then, writing A_t, A_T, for the asymmetries, we have

$$A_t = \frac{\{1 + \alpha(k,t)\}\{1 + \varepsilon(k)\} - \{1 - \alpha(k,t)\}\{1 - \varepsilon(k)\}}{\{1 + \alpha(k,t)\}\{1 + \varepsilon(k)\} + \{1 - \alpha(k,t)\}\{1 - \varepsilon(k)\}}$$

$$= \frac{\alpha(k,t) + \varepsilon(k)}{1 + \alpha(k,t)\varepsilon(k)} \quad ,$$

and $$A_T = \frac{\alpha(k,T) + \varepsilon(k)}{1 + \alpha(k,t)\varepsilon(k)} \quad .$$

Now in the present experiment $\alpha(k,t)$ cannot be appreciably greater than 0.15 even for the thinnest foil, and it is reasonable to assume that $\varepsilon(k) < 0.3$ (according to the results given in the previous section it was probably less than 0.2). Thus the denominators of these expressions are very nearly unity. The spin-dependent term is expected to be periodic in k and so, therefore, should be the measured asymmetries, provided $\varepsilon(k)$ is a slowly-varying function of k. However, $\varepsilon(k)$ may be eliminated in the approximation where

$$1 + \alpha(k,t)\varepsilon(k) \simeq 1 + \alpha(k,T)\varepsilon(k) \simeq 1 \quad .$$

Subtraction of the two asymmetries gives

$$A_t - A_T = \alpha(k,t) - \alpha(k,T)$$

If an aluminium comparison scatterer were used instead of thick gold, the same analysis would apply but now $\alpha(kT) \simeq 0$ and the elimination of $\varepsilon(k)$ is rather more exact. On the other hand the fundamental assumption upon which the whole method is built, namely that $\varepsilon(k)$ is

independent of the type of foil, cannot be so convincingly sustained as in the case where both foils are of gold. Returning to the latter case, we remark that $\alpha(k,t)$ must be of the form $\alpha(k)f(t)$, where $\alpha(k) = \alpha_o \sin(2\pi k/k_o)$ (Section (III.2)) and $f(t)$ is some function of the foil thickness. Hence

$$A_t - A_T = \alpha(k)\{f(t) - f(T)\}.$$

The observations reported in the last section were made at scattering angles over the range 100° - 120° with the foil at right angles to the incident beam. Thus the results of Murray, discussed in Section (III.3), should be relevant. His expression for the effect of foil thickness may be written

$$f(t) = 1 - Ct$$

where $C = 0.35$ per mg./cm.^{2}.

Hence $A_t - A_T = \alpha(k)\, C(T - t)$.

For the case where $t = 0.4$ mg./cm.^{2}, $T = 2.0$ mg./cm.^{2} we have

$$A_t - A_T = 0.6\, \alpha_o \sin(2\pi k/k_o)$$

However, it is probably better, when dealing with thicknesses as large as 2 mg./cm.^{2}, to use the reciprocal law given by Cavanagh et al. (1957) (Section (III.3)), with the parameters derived from Murray's results. Taking

$$f(t) = 1/(1 + Ct)$$

and using Murray's data (Figure (III.3.3)), we find

$$A_t - A_T = 0.34\ a_o \sin(2\pi k/k_o).$$

The maximum available value of a_o would, in theory, be $\beta S(\theta)$, in the notation of Section (III.3), which would give

$$a_o \simeq 0.35 \times 0.55 = 19\ \%\ .$$

However, on account of depolarisation by backscattering in the source-holder and by other causes, it is unlikely that the actual value of a_o was greater than 15 % and it may have been as low as 12 % . Thus the amplitude of the difference curve would be about 4 - 5 % . In the case of the individual asymmetry curves, the application of the law

$$f(t) = 1/(1 + Ct)$$

in conjunction with Murray's data, as above, yields

$$A_t = 0.10 \sin(2\pi k/k_o) + \varepsilon(k)$$

$$A_T = 0.06 \sin(2\pi k/k_o) + \varepsilon(k)\ .$$

Turning now to the observations with the two gold foils (Figure (V.2.1)), the first remark to be made is, of course, that the statistical errors are rather large and that one should therefore refrain from attempting to draw definite conclusions from them regarding the value of the g-factor anomaly. Rather one should ask whether they are compatible with the expected curves, remembering that the period, k_o, is expected to be in the neighbourhood of 700.

Actually one expects

$$k_o = 1/(\gamma a) \simeq 1/(1.2 \times 0.00116) = 720.$$

The values of the differences, $A_t - A_T$, are certainly compatible with the expected results. The values of the individual asymmetries need more consideration. It is arguable that $\varepsilon(k)$ may be slowly varying for orbit-numbers greater than 350 but may become increasingly negative at lower orbit-numbers, in which case the observations would be compatible with expectation for $k > 350$ and possibly also for $k < 350$.

From experience in working with the beam it is thought to be quite probable that the vertical distribution of electron intensity in the beam may have changed quite markedly at the higher voltages. Of course, if the distribution of electron-beam intensity over the scattering foil changed asymmetrically, then quite large spurious asymmetries in counting-rate could have occurred because the scintillators were positioned close to the ends of the foil.

On the other hand, one may assume that $\varepsilon(k)$ is slowly varying for all k. To gain some experience in the fitting of periodic curves to observed data (with a view to the future), the definite assumption was made that $\varepsilon(k)$ was of the form $a + bk$ where a, b are constants and an equation of the form

$$A_t = a + bk + c_1 \sin(2\pi k/k_o) + c_2 \cos(2\pi k/k_o)$$

was fitted to the thin foil data using a digital computer.

The results of this exercise which was carried out for several values of k_o are quoted in Table (V.3.1).

TABLE (V.3.1)

Least-squares fit to A_t for various k_o

k_o	a %	b %	c_1 %	c_2 %	Standard devn. squared. σ^2 $(\%)^2$
575	-10.2	-0.011	-7.3	-7.4	179
600	-9.1	+0.0076	-4.5	-6.0	113
625	-8.3	+0.0053	-2.6	-5.0	85
650	-7.9	+0.0038	-1.36	-4.25	75
675	-7.6	+0.0029	-0.47	-3.64	71
700	-7.5	+0.0023	+0.17	-3.1	70
725	-7.3	+0.0019	+0.64	-2.6	70.6
750	-7.2	+0.0016	+1.0	-2.2	71

The squares of the standard deviations show a shallow minimum near $k_o = 700$, so that one might say that the curve was periodic with period 700 ± 100, giving an estimate of the g-factor anomaly to within the order of 15 % . However, closer examination shows that the actual curve fitted was very nearly an inverted cosine curve. Unfortunately, it is very difficult to think of any physical reason for the presence of a large constant phase shift in the present experiment. In other words it is unlikely that

$\varepsilon(k)$ is periodic with period k_o. Periodic curves of the same type were fitted at a few values of k_o to the thick gold data. It was interesting that, if the best-fitting curve to the thick-gold data for $k_o = 725$ was subtracted from the corresponding curve for the thin gold data, one obtained

$$(A_t - A_T)_{725} = (-0.29 - 0.0003\,k + 5.3 \sin \frac{2\pi k}{k_o} - 0.13 \cos \frac{2\pi k}{k_o})\ \%$$

showing that the difference curve was quite compatible with the expected form.

Glancing now at the second set of observations (Table (V.2.2)) we note first of all that the aluminium data are not meaningful by any standards. It is encouraging to note, however, that the asymmetries for the 0.4 mg./cm.^{2} target in so far as they are comparable with the previous data behave in the same way with respect to variation of k, and this, despite the scintillators and light-guides having been replaced and the gold foil changed in the interval.

In view of all the above considerations, it is the opinion of the writer that one should accept the possibility that $\varepsilon(k)$ may vary quite rapidly over some range of k (probably $k < 300$) and accordingly should attempt to eliminate it. This brings us to a consideration of the actual counting-rates observed. One of the curious features which has appeared has been the lack of

proportionality between foil thickness and scattering rate for the gold targets. Some observations of Dougal (private communication) on the scattering of 200 keV electrons from gold foils at angles near 70° have confirmed this effect. The most likely explanation is that, as the foil thickness increases, the inelastic scattering becomes more important and a large proportion of the scattered electrons have their energies so far reduced that they are no longer detected by the scintillation counter. Various observations by the present writer on foils of 0.2 mg./cm.^{2}, 0.4 mg./cm.^{2}, 1.0 mg./cm.^{2} and 2.0 mg./cm.^{2} suggest that, while the thicknesses are in the ratios 1 : 2 : 5 : 10, the scattering rates are in the ratios 1 : 2 : 3 : 3, very approximately. If the same applies to aluminium, then it sets an upper limit on the signal-to-noise ratio which can be obtained with an aluminium foil in the present apparatus A 2 mg./cm.^{2} aluminium foil ought to be equivalent to a 0.4 mg./cm.^{2} gold foil, but in practice gives only one fifth of the scattering. It is, therefore, not clear without further experiment where it should be placed in the sequence.

(V.4) Conclusions

The situation at the time of writing may be summed up as follows. In the first place the problem of obtaining an adequate beam intensity has been solved and, although a more intense beam would be useful in reducing the counting times, it is believed that the limitations on intensity which exist at present are mainly those inherent in the use of radio-active sources as opposed to electron guns. An improvement of a factor of two may be expected from increasing the source strength and from more careful setting up of the field configurations.

The problem of the detection of asymmetries has been brought to the point where there is some evidence that a genuine spin-dependent asymmetry has been observed and where further progress depends mainly on reducing the statistical errors by counting for long periods. It is believed that the instrumental asymmetries can be eliminated by the use of a suitable comparison foil.

Alternatively, if it is confirmed that $\varepsilon(k)$ is slowly varying for $k > 300$, the observations could be carried out only for $k > 300$ and a periodic curve fitted by least squares computation as indicated in the last Section.

Substantial improvement could be expected in signal-to-noise ratio if the scintillation counters were replaced by solid-state detectors, such as lithium ion drift

detectors, which would give much better energy resolution and lower intrinsic background.

Finally, a more thorough examination of the technical details of setting up the field configurations needs to be undertaken so that the distribution of intensity in the beam can be controlled at all orbit-numbers.

Given all these improvements, there appears to be no fundamental reason why the experiment should not achieve the 1 - 2% accuracy for which it was originally designed.

ACKNOWLEDGEMENTS

I wish to offer my sincere thanks to Professor N. Feather, F.R.S., for giving me the opportunity of working on this project and for his unfailing support throughout.

I am most grateful to Dr. P.S. Farago for his guidance and advice and for the unflagging enthusiasm and skill with which he has supervised the work from the beginning.

My thanks go to Mr. Headridge and to all his staff for their skilful co-operation in the construction of apparatus. I would particularly like to thank Mr. McAnna for maintaining the electronic apparatus so well.

I am indebted to Mr. R.B. Gardiner for numerous friendly discussions and to Mr. R.C. Dougal for some observations on electron scattering undertaken with his apparatus.

My thanks are due to Dr. G.M. Thomas for preparing the programme for some numerical computations.

Finally, I wish to thank my wife for mounting the photographs and for her constant support and encouragement.

APPENDIX A

CLASSICAL CALCULATION OF RELATIVE SPIN PRECESSION RATE IN MOVING FRAME OF REFERENCE

Let a frame of reference S' move with velocity $V = (V_x, 0, 0)$ with respect to the laboratory frame, S. Let the velocities of the electron in the two frames be $\underline{v}'$, $\underline{v}$, respectively, where $v_z = v_z' = 0$. Then the electron experiences, in its instantaneous rest-frame, a magnetic field $B_z'' = \gamma(v')B_z' \equiv \gamma' B_z'$ where B_z' is the magnetic field in the moving frame, S', corresponding to the field $B_z \equiv (0, 0, B_z)$ in S.

In these circumstances

$$\omega_s' = \omega_L'' + \omega_T'$$

where

ω_s' is the spin precession rate in S',

ω_L'' is the spin precession rate in the electron's rest frame,

ω_T' is the Thomas precession of the electron's rest frame relative to S'.

Hence $\omega_s' = (\underline{\omega}_s')_z = (\underline{\omega}_L'' + \underline{\omega}_T')_z$

$$= \frac{ge}{2m_o} \gamma' B_z' + \frac{(\gamma' - 1)}{v'^2} \left(\underline{v}' \times \frac{d\underline{v}'}{dt'}\right)_z$$

But $\frac{d\gamma'}{dt'} = 0$, since the electron sees a pure magnetic field in S'.

$$\therefore \quad \omega'_s = \frac{e}{m_o}\left[\frac{g}{2}\gamma' B'_z + \frac{(\gamma'-1)}{v'^2}\left(\underline{v}' \times \frac{1}{m_o}\frac{d\underline{p}'}{dt'}\right)_z\right]$$

($\underline{p}'$ = electron momentum in S')

$$= \frac{e}{m_o}\left\{\frac{g}{2}\gamma' B'_z + (\gamma'-1)\left[\hat{\underline{v}}' \times (\hat{\underline{v}}' \times \underline{B}')\right]_z\right\}$$

$$= \frac{eB'_z}{m_o}\left\{\frac{g}{2}\gamma' - \gamma' + 1\right\} \qquad \text{since } \hat{\underline{v}}.\underline{B}' = 0.$$

$$= \omega'_c\left\{1 + \left(\frac{g}{2} - 1\right)\gamma'\right\}$$

where ω'_c = cyclotron frequency in S'.

$$\therefore \quad \frac{\omega'_s - \omega'_c}{\omega'_c} = \gamma'\left(\frac{g}{2} - 1\right) \quad .$$

APPENDIX B

TRANSFORMATION FROM MOVING FRAME, S', TO LABORATORY FRAME, S, WITH A NOTE ON THE PRESERVATION OF THE 360° FOCUSSING PROPERTY.

Defining the symbols as in Section (II.4) we have

$$u_\mu \equiv \gamma(v) \left\{ \underline{v},\ ic \right\} \qquad \text{in the frame S.}$$

That is $\begin{cases} u_k = \gamma(v)\, v_k & (k = 1, 2, 3) \\ u_4 = ic\, \gamma(v) . \end{cases}$

Correspondingly

$$u'_4 = ic\, \gamma(v') \qquad \text{in S', which moves with}$$

velocity V relative to S.

If the Lorentz transformation matrix between S and S' is $A_{\mu\nu}(V)$ $(\mu, \nu = 1, \ldots, 4)$,

then $\begin{cases} A_{4k}(V) = -\frac{i}{c}\, \gamma(V)\, V_k \\ A_{44}(V) = \gamma(V) \end{cases}$ (see, for example, Rose, 1961)

Hence $u'_4 = \sum_k A_{4k}\, u_k + a_{44}\, u_4$

$\therefore\ ic\gamma(v') = -\frac{i}{c}\gamma(V)\, \gamma(v) \sum_k V_k v_k + ic\, \gamma(V)\gamma(v)$

$\therefore\ \gamma(v') = \gamma(V)\gamma(v) \left\{ 1 - \underline{V}.\underline{v}/c^2 \right\}$

Replacing $\underline{V}$ by $-\underline{V}$ and $\underline{v}$ by $\underline{v}'$ yields the required result.

The transformation of velocities (Section (III.2)p.2) in the special case where the motion is along the x-axis is given in all the text-books of Special Relativity, but we give here the algebraic derivation using the remaining terms of the Lorentz matrix, namely

$$A_{ik} = \delta_{ik} + \left\{\gamma(V) - 1\right\} \hat{V}_k \hat{V}_i$$

This gives, in the present case,

$$u'_i = \sum_k A_{ik} u_k + A_{i4} u_4$$

$$= u_i + \gamma(v) \left\{\gamma(V) - 1\right\} \hat{V}_i (\hat{\underline{V}}.\underline{v}) - \gamma(v)\gamma(V)\, V_i$$

Therefore

$$u'_x = u_x + \gamma(v) \left\{\gamma(V) - 1\right\} v_x - \gamma(v)\gamma(V)\, V_x \ .$$

That is

$$\gamma(v')v'_x = \gamma(v) \left\{v_x + \gamma(V)\, v_x - v_x - \gamma(V)V\right\}$$

$$= \gamma(v)\gamma(V)(v_x - V)$$

$$\therefore\ v'_x = (v_x - V)/(1 - \underline{V}.\underline{v}/c^2)$$

Also $\gamma(v')v'_y = \gamma(v)v_y$ since $V_y = 0$

$\therefore\ v'_y = v_y/\gamma(V)(1 - \underline{V}.\underline{v}/c^2)$

and $v'_z = v_z = 0$ in the present experiment.

Finally we note that the 360° focussing property which exists in S' is preserved in S. For let us suppose that, in S', two electrons start from a point P' in the source at an instant $t'_1 = t_1 = 0$. Their orbits in S' are circles and they again coincide at P' at some later instant t'_2.

At the beginning and end of this motion the interval (in the relativistic sense) between them is identically zero, and is therefore zero in all inertial frames including S. Let us suppose that they start from a point P_1 in S at $t_1 = 0$ and let P' have coordinates $x' = y' = z' = 0$. Then because the two frames are in relative motion in the x direction only we have $x = y = z = 0$ at $t_1 = 0$ for the coordinates of P_1. The interval between them will next be zero at the point P_2 in S corresponding to P' at time t_2' in S'. Clearly this point P_2 must lie on the x-axis.

APPENDIX C

DERIVATION OF EQUATION (III.1.1)

If the drift-distance per orbit is δ , we have

$$E_y/B_z = V_x = \delta . \omega_c \qquad (\omega_c = \text{cyclotron frequency})$$

$$= \frac{eB_z . \delta}{2\pi m_o \gamma}$$

$$\therefore \qquad \delta = \frac{2\pi m_o \gamma E_y}{eB_z^2}$$

Now $k = D_2/\delta$ (Section (III.1))

$$= \frac{eD_2 B_z^2}{2\pi m_o \gamma E_y} \quad .$$

APPENDIX D

LEAST SQUARES ANALYSIS OF DATA

Given a set of observations y_j ($j = 1, 2, \ldots, s$) corresponding to values x_j of the independent variable, it is sometimes useful to be able to give a criterion by which to decide whether a best-fitting 2nd order (parabolic) curve is a significantly better fit to the points than a straight line. The following technique is useful for this purpose.

Define $X_j = x_j - \bar{x}$ $\qquad (\bar{x} = \frac{1}{s}\sum_j x_j)$

$Y_j = y_j - \bar{y}$ $\qquad (\bar{y} = \frac{1}{s}\sum_j y_j)$

(weighted means may be used if desired)

Then $\sum_j X_j = \sum_j Y_j = 0.$

Let a curve $Y = F(X)$ be fitted to the data

where $F(X) = \mu_1 X + \mu_2 P_2(X)$

with $P_2(X) = M_o + M_1 X + M_2 X^2$

such that

$$\sum_j P_2(X_j) = 0$$

$$\sum_j X_j P_2(X_j) = 0$$

$$\sum_j P_2^2(X_j) = 0$$

Then the constant coefficients M_o, M_1, M_2 are given by

$$M_1/M_o = s \sum_j X_j^3 / \left(\sum_j X_j^2 \right)^2$$

$$M_2/M_o = -s / \sum_j X_j^2$$

$$1/M_o = s \sqrt{\frac{\left(\sum X_j^4\right)}{\left(\sum_j X_j^2\right)^2} - \frac{\left(\sum X_j^3\right)^2}{\left(\sum_j X_j^2\right)^3} - \frac{1}{s}}$$

Note that the M's are not subject to error. To determine the μ_1 and μ_2 coefficients we make

$$\sigma^2 = \sum_j \left[F(X_j) - Y_j \right]^2 \quad \text{a minimum.}$$

Putting $\frac{d(\sigma^2)}{d\mu_1}$ and $\frac{d(\sigma^2)}{d\mu_2}$ equal to zero

gives $\mu_1 = \left(\sum_j X_j Y_j\right) / \sum_j X_j^2$

$$\mu_2 = \sum_j Y_j P_2(X_j) = M_1 \sum_j X_j Y_j + M_2 \sum_j X_j^2 Y_j$$

Now it can be claimed that the 2nd order fitting is significantly better than the 1st order fitting if and only if

$$\left(\frac{\delta \mu_2}{\mu_2}\right)^2 \ll 1, \quad \text{say} \quad \delta\mu_2 < \tfrac{1}{3} \mu_2 ,$$

where $\delta\mu_2$ is obtained from the assigned standard deviations of the individual data.

Thus

$$(\delta \mu_2)^2 = \sum_j \left(\frac{\partial \mu_2}{\partial Y_j}\right)^2 (\delta Y_j)^2$$

$$= \sum_j P_2^2(X_j) \, (\delta Y_j)^2 ,$$

and $(\delta Y_j)^2 = \sum_k \left(\frac{\partial Y_j}{\partial y_k}\right)^2 (\partial y_k)^2$

$\simeq \delta y_j$ in most practical cases, where δy_j are the assigned standard deviations of the data.

Similarly, we find

$$(\delta\mu_1)^2 = \sum_j X_j^2 (\delta Y_j)^2 / (\sum_j X_j^2)^2 .$$

Finally we note that the error of the fitting is given by

$$(\delta Y)^2 = \frac{1}{s} \sum_j \left[F(X_j) - Y_j\right]^2$$

and thus the error of the 2nd order fitting is

$$(\delta_2 Y)^2 = \frac{1}{s}\left(\sum_j Y_j^2 - \mu_j^2 \sum_j X_j^2 - \mu_2^2\right)$$

while the error of the first order fitting is

$$(\delta_1 Y)^2 = \frac{1}{s}\left(\sum_j Y_j^2 - \mu_1^2 \sum_j X_j^2\right)$$

Thus

$$\frac{(\delta_1 Y)^2 - (\delta_2 Y)^2}{(\delta_1 Y)^2} = \mu_2^2 / \left(\sum_j Y_j^2 - \mu_1^2 \sum X_j^2\right)$$

which is another way of expressing the criterion mentioned above.

This technique was applied to the results of Schupp, Pidd and Crane (1961). The outcome was that

$$\mu_1 = 0.452 \times 10^{-3} .$$

$$\mu_2 = 59 \times 10^{-18} .$$

$$(\delta\mu_1)^2/\mu_1^2 = 0.16$$

$$(\delta\mu_2)^2/\mu_2^2 = 0.9$$

$$\frac{(\delta_1 Y)^2 - (\delta_2 Y)^2}{(\delta Y)^2} = 1.2 \times 10^{-21}$$

Hence the conclusion stated in the text:Section (I.4), p. 10.

The great advantage of the above method of analysis is that the 1st and 2nd order fittings are carried out completely independently of one another, so that the statistical comparison is made quite explicit.

The method could equally well be applied to other types of function, such as sine curves.

BIBLIOGRAPHY

Baker & Burd, 1957, Rev. Sci. Instr. 28, 313.

Bargmann, Michel & Telegdi, 1959, Phys. Rev. Letters 2, 435.

Bartlett & Watson, 1940, Proc. Am. Acad. Arts. Sci. 74, 53.

Bartlett & Welton, 1951, Phys. Rev. 59, 281.

Beringer & Heald, 1954, Phys. Rev. 95, 1474.

Bernardini, Brovetto & Ferroni, 1958, Nucl. Phys. 8, 294.

Bethe, 1947, Phys. Rev. 72, 339.

Bethe & Salpeter, 1958, Quantum Mechanics of the One and Two Electron Systems; Vienna; Springer Verlag; Addendum to 21.

Bloch, 1953, Physica 19, 821. See also Rabi (1928).

Bohr, 1928, quoted by Mott & Massey (1949).

Bothe, 1949, Z. Naturf. 4a, 542.

Breit, 1928, Nature 122, 649.

Breit, 1930, Phys. Rev. 35, 1447.

Breit, 1947, Phys. Rev. 72, 984.

Carrassi, 1958, Nuovo Cimento 7, 524.

Cavanagh, Turner, Coleman, Gard & Ridley, 1957, Phil. Mag. 2, 1105.

Charpak, Farley, Garwin, Muller, Sens, Telegdi & Zichichi, 1961, Phys. Rev. Letters 6, 128.

Charpak, Lederman, Sens & Zichichi, 1960, Nuovo Cimento 17, 288.

Cohen & Dumond, 1958, Phys. Rev. Letters 1, 291.

Connor & Fairweather, 1957, Proc. Phys. Soc. Lond. A70, 769. see also p. 909.

Darwin, C.G., 1928, Proc. Roy. Soc. Lond. A120, 621.

Dayhoff, Triebwasser & Lamb, 1953, Phys. Rev. 89, 98.

Dehmelt, 1958, Phys. Rev. 109, 381.

BIBLIOGRAPHY (Contd.)

Doggett & Spencer, 1956, Phys. Rev. 103, 1597.

DuMond, 1959, Ann. Phys. 7, 365.

DuMond & Cohen, 1955, Rev. Mod. Phys. 27, 363.

Einstein, P.A., 1951, Brit. J. Appl. Phys. 2, 49.

Fano, 1957, Revs. Mod. Phys. 29, 74.

Farago, 1958, Proc. Phys. Soc. 72, 891.

Farago, 1961, Proc. Roy. Soc. Edin., to be published.

Fradkin & Good, 1961, Rev. Mod. Phys. 33, 343.

Franken & Liebes, 1956, Phys. Rev. 104, 1197.

* Gardner, 1951, Phys. Rev. 83, 996.

Gardner & Purcell, 1949, Phys. Rev. 76, 1262.

Geiger, Hughes & Radford, 1957, Phys. Rev. 105, 183.

Grodzins, 1959, Prog. Nucl. Phys. 7, 163

Hardy & Purcell, 1959, Bull. Am. Phys. Soc. (Ser. II) 4, 37.

Houston & Hsieh, 1934, Phys. Rev. 45, 263.

Karplus & Kroll, 1950, Phys. Rev. 77, 536.

Kemp & Barber, 1957, Nature 180, 1116.

Kennedy & Kent, 1956, Rev. Sci. Instr. 27, 916.

Koenig, Prodell & Kusch, 1952, Phys. Rev. 88, 191.

Kramers, 1957, Quantum Mechanics; North Holland Publ. Co., (Chap. 6.)

Kusch, 1955, Phys. Rev. 100, 1188.

Kusch & Foley, 1948, Phys. Rev. 74, 250.

Lamb & Retherford, 1947, Phys. Rev. 72, 241.
1950, Phys. Rev. 79, 549.
1951, Phys. Rev. 81, 222.
1952, Phys. Rev. 86, 1014.

Landau, 1957, Nucl. Phys. 3, 127.

* Gardiner, R.B., 1961, Ph.D. thesis, University of Edinburgh.

BIBLIOGRAPHY (Contd.)

Lande, 1923, Z. Phys. 15, 189.

Lee & Yang, 1957, Phys. Rev. 105, 1671.

Louisell, Pidd & Crane, 1954, Phys. Rev. 94, 7.

Mendlowitz & Case, 1955, Phys. Rev. 97, 33.

Mohr & Tassie, 1954, Proc. Phys. Soc. Lond. A67, 711.

Moljk & Curran, 1954, Phys. Rev. 96, 395.

Mott, 1929, Proc. Roy. Soc. A124, 425.

Mott & Massey, 1949, Theory of Atomic Collisions, (Clarendon Press, Oxford) 2nd Ed., p. 63.

Muhlschlegel & Koppe, 1958, Z. Phys. 150, 474.

Murray, 1960, Ph.D. Thesis, University of Edinburgh.

Nafe & Nelson, 1948, Phys. Rev. 73, 718.

Nafe & Nelson & Rabi, 1947, Phys. Rev. 71, 914.

Nelson, 1958, Ph.D. Thesis, University of Michigan.

Nelson & Pidd, 1959, Phys. Rev. 114, 728.

Panofsky & Phillips, 1955, Classical Electricity & Magnetism (Addison-Wesley).

Paul & Steinwedel, 1955, Beta & Gamma Ray Spectroscopy. Ed. Siegbahn (North Holland Publ. Co.) Chapter 1.

Pauli, 1927, Z. Phys. 43, 601.

Pauli, 1958, Handbuch der Physik (Berlin, Springer Verlag) Vol. 5/1, p. 157.

Petermann, 1958, Nucl. Phys. 5, 677.

Pound, 1952, Prog. Nucl. Phys. 2, 21.

Prodell & Kusch, 1952, Phys. Rev. 88, 184.

Rabi, 1928, Z. Phys. 49, 507.

Ramsey, 1950, Phys. Rev. 77, 567,
see also Phys. Rev. 78, 699,
and 1952, Phys. Rev. 86, 243.

BIBLIOGRAPHY (Contd.)

Rose, 1961, Relativistic Electron Theory (John Wiley & Sons, Inc.)

Salam, 1957, Nuovo Cimento 5, 299.

Saxon, 1951, Phys. Rev. 81, 639.

Schupp, Pidd & Crane, 1961, Phys. Rev. 121, 1.

Series, 1957, Spectrum of Atomic Hydrogen (Oxford University Press).

Sherman, 1956, Phys. Rev. 103, 1601.

Sherman & Nelson, 1959, Phys. Rev. 114, 1541.

Slatis, 1955, Beta & Gamma Ray Spectroscopy. Ed. Siegbahn (North Holland Publ. Co.) p. 259.

Sommerfield, 1957, Phys. Rev. 107, 328.
See also Ann. Phys. 5, 26 (1958).

Sternheimer, 1959, Adv. in Electronics & Electron Physics 11, 31.

Telegdi & Winston, 1959, Proc. Phys. Soc. 74, 782.

Thomas, 1926, Nature 117, 514.
See also Phil. Mag. 3, 1 (1927).

Tolhoek, 1956, Rev. Mod. Phys. 28, 277.

Uhlenbeck & Goudsmit, 1925, Naturwiss., 13, 953.
See also Nature 117, 264 (1926).

Watkins & Pound, 1951, Phys. Rev. 82, 343.

Williams, R.C., 1938, Phys. Rev. 54, 558.

Wittke & Dicke, 1956, Phys.Rev. 103, 625.